QATAR UNIVERSITY

COLLEGE OF ENGINEERING

DRAINED RESIDUAL SHEAR STRENGTH OF FINE-GRAINED SOILS AND SOIL-SOLID INTERFACES AT LOW TO MEDIUM EFFECTIVE NORMAL STRESSES: ANALYSES AND APPLICATIONS

BY

KHALED HASSAN RABIE

A Thesis Submitted to the Faculty of

College of Engineering

in Partial Fulfillment of the Requirements

for the Degree of

Master of Science

February 2016

COMMITTEE PAGE

The members of the Committee approve the thesis of Khaled Hassan Rabie defended on February, 8, 2016.

Prof. Hisham T. Eid
Thesis Supervisor

Prof. Osman A. Elnawawy
Committee Member

Dr. Riyadh I. Al Raoush
Committee Member

Prof. Mohamad O. Al Hariri
Committee Member

Approved:

Dr. Rashid Alammari, Dean, College of Engineering

Abstract

A laboratory research program was undertaken to study the large-strain shear strength characteristics of fine-grained soils under low effective normal stresses (~3 to 6 kPa). Soils that cover a wide range of plasticity and composition were utilized in the program. The interface shear strength of these soils against a number of solid surfaces having different roughness was also investigated at similar low effective normal stress levels. The findings contribute to advancing the knowledge on the parameters needed for the design of pipelines placed on sea beds and the stability analysis of shallow soil slopes. A Bromhead-type torsional ring shear apparatus was modified to suit measuring soil-soil and soil-solid interface drained residual shear strengths at the low effective normal stresses. In consideration of increasing the accuracy of assessment and depicting the full-scale field behavior, the interface residual shear strengths measured using the modified ring shear apparatus were compared with those measured by research collaborators for similar interfaces using a macro-scale interface direct shear device with a plan interface shear area of approximately 3.0 m^2. Correlations are developed to estimate the soil-soil and soil-solid interface residual shear strengths at low effective normal stresses. The correlations are compared with soil-soil and soil-solid interface drained residual shear strengths and correlations presented in the literature.

Data of torsional ring shear tests at a wide range of effective normal stress (10 to 700 kPa) for soils, mudstones and shales of different plasticity and gradation were analyzed. The data were made available for this research to study

the effects of the change in nonlinearity of shear strength envelope over the normal stress ranges relevant to soil slope stability analyses. Using this data set, new empirical residual shear strength correlations were developed as a function of soil index parameters and wide range of effective normal stresses. In essence, the correlations are presented as revised versions of those previously developed for a limited number of normal stresses utilizing the same soil index parameters. Comparisons were made with a considerable amount of back-calculated shear strength data reported in the literature for reactivated landslides as well as results predicted from existing shear strength correlations to verify the increased suitability of the new correlations for use in slope stability analyses. A numerical expression was also introduced to express the residual shear strength correlations for direct incorporation in slope stability software.

Table of Contents

List of Tables

List of Figures

Acknowledgements

This Thesis has been prepared under the direct supervision of Hisham T. Eid, Professor of Civil Engineering, to whom the author is indebted for his valuable support, guidance and encouragement during the experimental work, analysis of the results, and the preparation of the manuscript. Without his assistance and patience, this work would not have been possible.

The author acknowledges the funding provided by Qatar National Research Fund (QNRF), Qatar, under Projects No: NPRP 08–203–2–064, and NPRP 5-488-2-194 for a major part of this research. He also appreciates the two year Graduate assistantship granted by Qatar University.

Help received from Mr. Abdul Azeez Kilayil, Lab Engineer at Qatar University and technicians of the mechanical workshop at Qatar University, and the commercial organization specialized in epoxy coating in British Columbia, Canada is acknowledged.

Providing the macro-scale interface direct shear device results by the research collaborators at the University of British Columbia Ruslan Amarasinghe and Dharma Wijewickreme as well as the torsional ring shear test results by Dr. Hisham Eid is also acknowledged.

The author would like to thank his parents and his brother Mohammed and sister Sara for their love and support throughout his graduate work. Finally, the author would like to thank his wife Rania for her understanding, and care throughout this work.

Chapter 1. Introduction

1.1. Statement of the Problem.

Measurement of the residual shear strength of soils at low to medium effective normal stresses has direct application on the stability analysis of shallow soil slopes. Advanced knowledge on soil-solid interface shear strength characteristics at such stresses is also particularly crucial for the offshore and near shore pipeline construction industry in relation to assessing, (i) the stability of pipelines placed on sloping sea floors; and (ii) the potential of pipeline walking. However, soil-soil and soil-solid interface shear strength studies have been commonly conducted at effective normal stress levels greater than 15 kPa and typically ranging between 50 and 700 kPa.

The drained residual and large-strain strength of fine-grained soils have been often assessed using the direct shear box and the torsional ring shear devices by many researchers (e.g., Bishop et al. 1971; Lupini et al. 1981; Skempton 1985; Stark and Eid 1994). The same devices have been used extensively to study the shear strength at the interface between fine-grained soils and solid material surfaces (e.g., Tika-Vassilikos 1991; Lehane and Jardine 1992; Lemos and Vaughan 2000). Because of the relatively small area available for shear combined with friction associated with the mechanical system, the commonly used design of these devices are not able to deliver low shear stresses to the soil specimen at a suitable accuracy. In addition, the low soil-soil and soil-solid interface shear strengths expected under small confining stress levels would be small and may lead to less reliable estimates of strength parameters (Fang et al. 2004). Clearly, the current understanding of the

residual shear and interface strength of fine-grained soils at low to medium effective normal stress levels is limited, and it is mainly based on data originating from purpose-designed devices. As a result, a study of the laboratory measurement techniques, magnitude, effect of soil index properties, and solid interface roughness on those drained shear strengths was initiated.

Several empirical correlations of soil shear strengths with index properties are available in the literature (e.g., Skempton 1964; Voight 1973; Kanji 1974; Mitchel 1976; Cancelli 1977; Lupini et al. 1981; Lambe 1985; Skempton 1985; Mesri and Cepeda-Diaz (1986); Collotta et al. 1989; Nelson 1992; Stark and Eid 1994; Mesri and Shahien 2003; Wesley 2003; Sridharan and Raghuveer Rao 2004; Stark et al. 2005; Stark and Hussain 2013). The correlations are particularly useful for preliminary designs and when soil samples and funding resources are not readily available for advanced soil testing. Such correlations have been developed based on tests conducted at a relatively high effective normal stresses (50 to 700 kPa).

Several expressions are also presented in the literature for estimating the residual friction angles as a function of the soil index properties without considering the effective normal stress to yield linear shear strength envelopes (e.g., Kanji 1974; Cancelli 1977; Nelson 1992; Sridharan and Raghuveer Rao 2004) or at specific high normal stresses to develop tri-linear or quad-linear shear strength envelopes (e.g., Stark and Hussain 2013). In conducting analyses using slope stability software, utilizing smooth nonlinear envelopes leads to an accurate determination of the shear strength that corresponds to the effective normal stress acting on the base of each slice of the proposed failure wedge.

1.2. Objectives of the Study

This study has two main objectives. The first is to study the residual shear and soil-solid interface shear strength-deformation characteristics of fine-grained soils at effective normal stresses between 3 and 6 kPa. The goal is achieved through an extensive experimental program involving measurement of soil-soil and soil-solid interface drained residual shear strengths on the element scale, using a modified ring shear apparatus (MRSA) to conduct soil-soil and soil-solid interface shear tests. The results were compared with those yielded from testing similar interfaces using a macro-scale interface direct shear device (MDSD) fabricated at the University of British Columbia (UBC), Canada. The MDSD tests were conducted at UBC as a part of a research project collaboration with Qatar University funded by Qatar Foundation.

The second objective of this thesis is to: (i) revise and update the drained residual shear strength correlations that have been developed by Stark and Eid 1994; Mesri and Shahien 2003; Stark et al. 2005; and Stark and Hussain 2013 based on soil residual shear strength data at effective normal stresses of 10, 25, 50, 100, 200, 300, 400, and 700 kPa made available by Eid (2014); (ii) to verify the increased suitability of the new correlations for use in slope stability analyses thorough comparison with a considerable amount of back-calculated shear strength data reported in the literature for reactivated landslides as well as results predicted from existing shear strength correlations; and (iii) to introduce a numerical expression of the residual shear strength correlations for direct incorporation in slope stability software.

To accomplish the first objectives, the study involved the following major tasks:

(1) Evaluation of the existing literature of the fine-grained soils and interface drained residual shear strength at low to medium effective normal stresses.

(2) Modification of a Bromhead-type torsional ring shear apparatus to suit measuring soil-soil and soil-solid interface residual shear strengths at the low effective normal stresses (3 to 6 kPa).

(3) Measurement of soil-soil and soil-solid interface drained residual shear strengths using the modified ring shear apparatus (MRSA).

(4) Comparison of the soil-solid interface shear strength measured using a modified ring shear apparatus with those measured for similar interfaces using a macro-scale interface direct shear device with a plan interface shear area of approximately 3.0 m^2 specially fabricated for this comparison.

(5) Development of correlations to estimate the soil-soil and soil-solid interface residual shear strengths at low effective normal stresses.

(6) Comparison of the developed correlations with soil-soil and soil-solid interface drained residual shear strengths and correlations presented in the literature.

To accomplish the second objectives, the study also involved the following major tasks:

(1) Evaluation of the existing empirical correlations for estimating the soil drained residual shear strength.

(2) Investigating the degrees of nonlinearity of the shear strength envelope over the normal stress ranges relevant to soil slope stability analyses.

(3) Development of new empirical residual correlations as function of soil index parameters and wide range of effective normal stresses based on shear strength

data provided by Eid (2014) as a revised versions of those previously developed for a limited number of normal stresses.

(4) Evaluating statistically the performance of the new empirical residual shear strength correlations thorough comparison with a considerable amount of back-calculated shear strength data reported in the literature for different case histories of reactivated landslides as well as results predicted from existing shear strength correlations.

(5) Development of a numerical expression that would account for the dependence of residual friction angle on the effective normal stress for direct incorporation in slope stability software.

1.3. Scope

This thesis is divided into five chapters. Chapter 1 is the introduction. Chapter 2 presents a literature review on the drained residual interface strength of fine-grained soils at low effective normal stress levels based on data originating from purpose-designed devices. Review on the existing literature of the soil drained residual shear strength at effective normal stresses relevant to soil slope stability as well as the existing empirical correlations for estimating such a strength is also presented.

Descriptions of the modified ring shear apparatus (MRSA) and the experimental procedure used in this research to measure soil-soil and soil-solid interface drained residual shear strengths at low effective normal stresses are presented in Chapter 3. Comparison of the soil-solid interface shear strengths measured on the element scale using the MRSA with those measured for similar

interfaces measured at UBC using a macro-scale interface direct shear device is also presented in this chapter. The data of the MRSA was used to develop a correlation for estimating the soil-soil and soil-solid interface drained residual shear strengths at low effective normal stresses. Comparisons of the developed correlations with the similar correlations presented in the literature are also introduced.

Chapter 4 provides torsional ring shear testing data which were made available by Eid (2014) at a wide range of effective normal stress (10 to 700 kPa). This chapter presents a new empirical correlation for soil drained residual strength as a revised version of those previously developed for a limited number of normal stress levels. The reliability of using the developed correlations is examined in this chapter through comparisons with a considerable amount of back-calculated shear strength data reported in the literature for reactivated landslides as well as results predicted from existing correlations. Finally, a new numerical expression was introduced in this chapter for direct incorporation in slope stability software. Chapter 5 presents the summary and the conclusions of the research.

Chapter 2. Literature Review and Discussion

2.1. The Use of Interface Residual Shear Strength at Low Effective Normal Stresses

Understanding the interface residual shear strength is crucial for offshore pipeline construction industry in relation to assessing, (i) the stability of pipelines placed on sloping sea floors; and (ii) the potential of pipeline walking. Seabed pipelines are typically subjected to differential movements with large strains at the pipe-soil interface. Such movements are due to thermal expansion or contraction under successive start up and shut down cycles. The developed large strains can significantly mobilize the interface strength to the residual value. There are considerable limitations that arise when testing interfaces under stress conditions commonly encountered in offshore environments. Primarily, the limitations arise as a result of the need to shear interfaces at very low effective normal stresses to relatively large strains. As a result, the typical shear testing devices do not produce reliable data. Attempts have been made to develop novel devices that are specifically used to experimentally measure residual shear and interface strength of fine-grained soils at low effective normal stress.

2.2. Existing Devices for Measuring Interface Residual Strength at Low Effective Normal Stresses.

The current understanding of the residual shear and interface strength of fine-grained soils at low effective normal stress levels is mainly based on data originating from purpose-designed devices. A description of these devices and their use is provided in the following subsections.

2.2.1. Tilt Table Device

Utilizing a custom tilt table device, large-strain soil and interface shear strengths have been measured at effective normal stresses of 2.9 and 4.1 kPa by Najjar et al. (2003) and from 1.7 to 5.8 kPa by Najjar et al. (2007). These tilt table tests used gravity to apply the normal and shear stresses, and the normal stress was applied on a specimen measuring 152 x 152 mm in plan (Fig. 2.1). In order to mobilize the residual strength, the table was successively lowered and raised until at least 100 mm of shear displacement was attained and constant shear strength was developed.

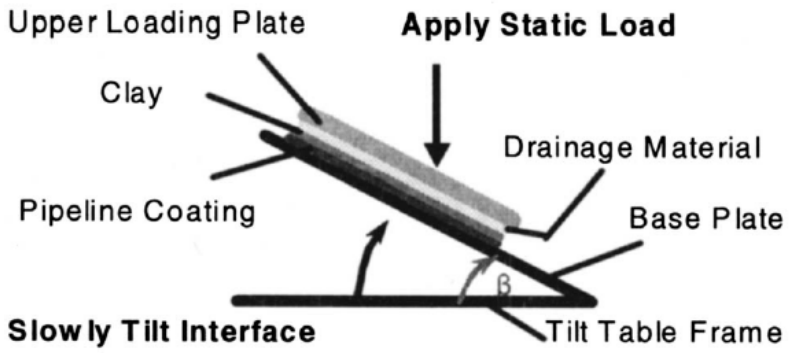

Figure 2.1. Schematic diagram of tilt-table device (after Najjar et al. 2003)

2.2.2. Cam-Shear Device

A custom-made shear box called the "Cam-shear" device, designed to minimize mechanical friction of the device and to allow the simulation of axial pipe-soil interaction behavior through dragging a 75 mm-diameter soil sample over a flat sheet of pipe coating material was utilized by Kuo et al. (2010) to measure interface strength at normal stresses between 2 and 6 kPa. Although a total stroke length of 190 mm can be achieved in this apparatus, the residual shear strength was measured at shear displacement of approximately 50 mm. The shearing rates used

were relatively fast providing limited freedom to develop fully drained shearing conditions (Colliat et al. 2011, Kuo and Bolton 2014). The Cam-shear device was also used by Ganesan et al. (2014) to measure the drained large-displacement interface shear strength of a single soil against a smooth and rough pipe coating materials at normal stresses ranging from 1 to 4.5 kPa (Fig. 2.2). The shear displacements for the interface testing were between 60 and 120 mm. Concurrently, soil-soil drained shear tests were also conducted but to a displacement limited to 12 mm.

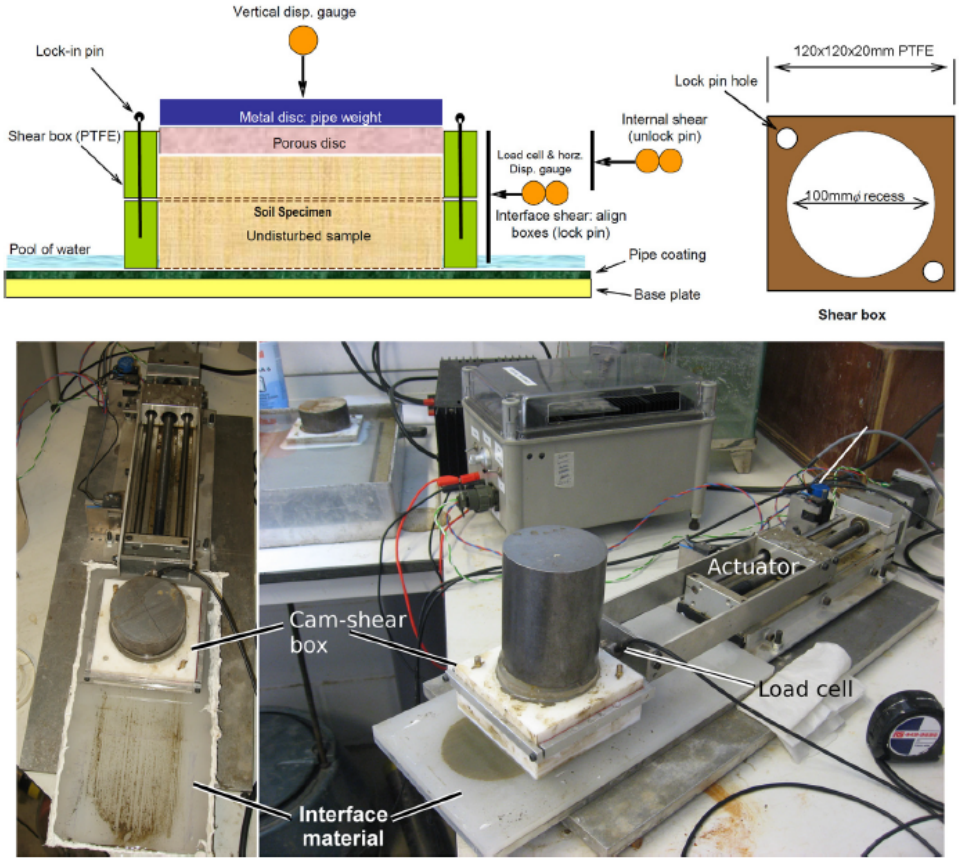

Figure 2.2. Main features of the Cam-shear box (after Ganesan et al. 2014).

2.2.3. UWA Small-Scale Direct Shear Box

A small-scale direct shear box modified at the University of Western Australia (UWA) to operate at the low stress levels relevant to pipeline geotechnics was used by White and Cathie (2011) and White et al. (2012) in measuring the partially drained interface shear strength at a normal stress of 2.5 kPa for rough steel surface against kaolin clay and carbonate soils, respectively. In the UWA low-stress shear box, the lower half of the shear box is placed with a coated or uncoated plate (Fig. 2.3). Reversal of shearing direction is possible with a maximum shear displacement of 10 mm in one direction. Interface residual resistances recorded at the end of the first shearing cycle in low-stress shear box tests were presented by Hill et al. (2012). In such tests, marine clay was sheared against smooth and rough surfaces at normal stress ranging from 2 to 8 kPa using different shearing displacement rates.

Figure 2.3. UWA small-scale direct shear box (after White et al. 2012)

2.2.4. Other Devices

In a more practical approach, axial sliding of a pipe model over soil surface has also been used to estimate the drained residual interface shear strength at low effective normal stresses. Utilizing such a technique, White and Randolph (2007) and Bruton et al. (2009) presented interface shear strengths measured at effective normal stresses between 2 and 4 kPa. The tests used full-size rough-coated pipe sheared axially in bins containing 3 m^3 of reconsolidated clay (Fig. 2.4).

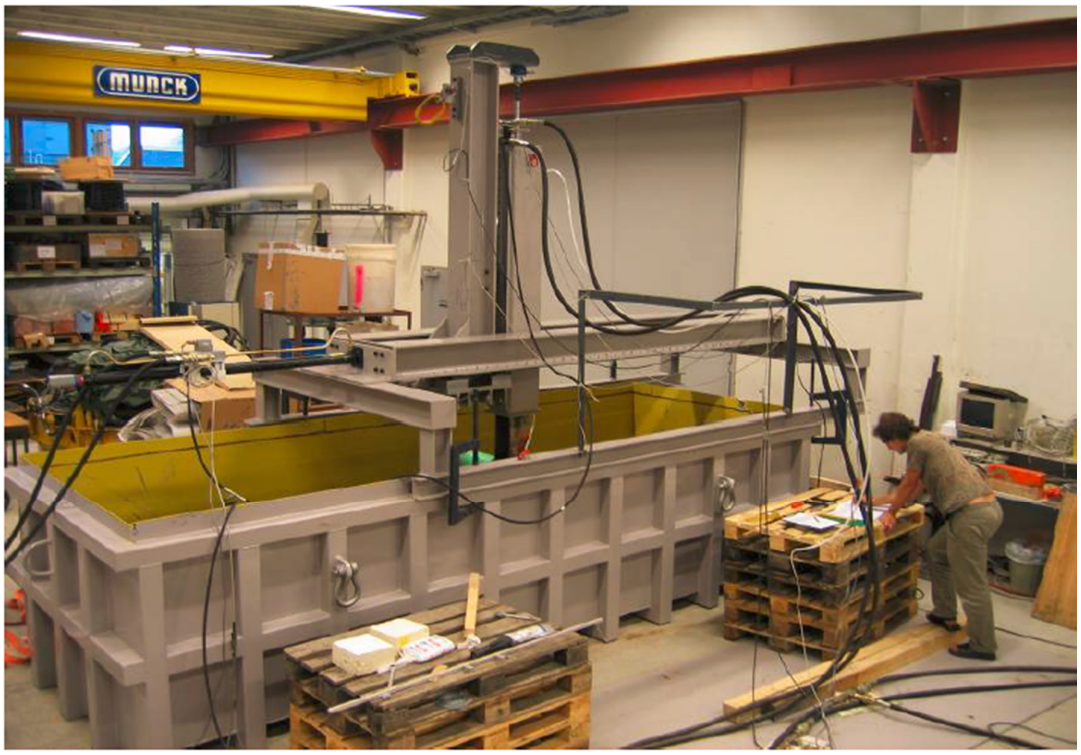

Figure 2.4. Pipe-soil model testing at large scale (after Bruton et al. 2009)

2.3. Measurement of Soil Drained Residual Shear Strength

It is recognized that a prudent approach for obtaining reliable shear strength parameters would be to use data derived from tests conducted on different soils. Direct shear and torsional ring shear apparatus are commonly used to measure the

drained residual shear strength of soils (τ_r). The suitability of each apparatus is discussed in the following sections.

2.3.1. Ring Shear Apparatus

There are different types of torsional ring shear devices. One of the widely accepted torsional ring shear device is the Bishop-type ring shear apparatus suggested by Bishop et al. (1971) in which the specimen is sheared at a mid-depth. A more commonly used device is the Bromhead ring shear apparatus suggested by Bromhead (1979) in which shearing occurs at the top of specimen. In measuring the residual shear strength, the torsional ring-shear apparatus has several advantages including: (i) shearing the specimen continuously in one direction for any magnitude of displacement; (ii) having a constant cross-sectional area of shear surface during shear; and (iii) utilizing a relatively thin test specimen and consequently allowing relatively faster displacement rates to be used without affecting drainage conditions

2.3.1.1. Bishop-Type Ring Shear Apparatus

Bishop et al. (1971) developed a torsional ring shear apparatus to measure the residual strength of soils. The apparatus uses an annular specimen with 152 mm and 101 mm outer and inner diameters, respectively, and a specimen height of 19 mm. The specimen is sheared near the mid-height and shearing occurs only in one direction. Thus, the specimen can be sheared to an unlimited continuous shear displacement without changing the direction of shear. The specimen is confined radially by upper and lower confining rings.

2.3.1.2. Bromhead Ring Shear Apparatus

Bromhead (1979) presented another type of torsional ring shear device in which shearing occurs at the top of soil specimen. This device uses 5 mm-thick with inside and outside diameters of 70 and 100 mm, respectively. Stark and Eid (1993 and 1994) suggested modification to the Bromhead ring shear specimen container to allow the raise of the specimen after consolidation to be flush with the top of the specimen container. Such raising minimizes the effect of wall friction on the test results. Stark and Eid (1994) showed that the Modifed Bromhead ring shear apparatus yields values of residual shear strengths that are in agreement with those calculated from case histories of reactivated landslides.

2.3.2. Direct Shear Apparatus

Direct shear box is the most common used apparatus for measuring the shear strength of a soils. The Casagrande shear box with bottom and top halves having dimensions of 60 mm x 60 mm x 25 mm (2.36 in. x 2.36 in. x 1 in.) is frequently used around the world. Skempton (1964) suggested a reversal direct shear test procedure to measure the drained residual shear strength of soils. The direct shear box can be displaced in one direction to a limited shear displacement of only about 6 mm. Larger shear displacement in one direction is usually required to orient the clay particles parallel to the direction of shear and develop the residual shear strength condition.

2.4. Existing Residual Shear Strength Correlations

This section presents the available empirical correlations for residual shear strength of soils. The correlations are listed herein based on their way of presentation

(Graphical or Numerical) as well as the parameters used in their development. All of the graphical correlations are shown in Appendix A.

2.4.1. Graphical Correlations

2.4.1.1. Correlations Based on Clay-Size Fraction

2.4.1.1.1 Skempton (1964)

Skempton (1964) considered it appropriate to correlate the drained residual friction angle (ϕ_r') with clay-size fraction (*CF*). The clay-size fraction is defined as the quantity of particles – by weight - smaller than 0.002 mm. Skempton (1964) used direct shear test results of nine natural soils and three clay minerals to establish his correlation. Skempton (1964) concluded that drained residual friction angle decreases with increasing the *CF*.

2.4.1.1.2 Skempton (1985)

Skempton (1985) also showed a relationship between *CF* and ϕ_r' for different soils with limited values of activity between 0.5 and 0.9. The activity (*A*) is defined as the plasticity index divided by the clay-size fraction (*PI*/*CF*). Skempton (1985) concluded that clay-size fraction (as an indication of particle size) has little effect on residual strength when the *CF* is less than 20%, and greater than or equal to 50%. The correlation still shows a considerable scatter in ϕ_r'.

2.4.1.2. Correlations Based on Liquid Limit

2.4.1.2.1 Mitchell (1976)

Mitchell (1976) presented empirical correlation between residual friction angle and liquid limit (*LL*). Mitchell (1976) cited personal communication with Deere (1974)

as the source for his correlation. The drained residual friction angle decreases with an increase in the liquid limit. However, no test data points were presented in the correlation.

2.4.1.2.2 Mesri and Cepeda-Diaz (1986)

Mesri and Cepeda-Diaz (1986) presented a relationship between ϕ_r' and *LL* based on direct shear tests on 24 shale specimens and data from Kenney (1967). The residual friction angle decreases with an increase in the liquid limit. However, Mesri and Cepeda-Diaz (1986) do not include effective normal stress at which the direct shear tests were performed in their correlations.

2.4.1.2.3 Stark and Eid (1994)

Stark and Eid (1994) presented empirical correlation for drained residual angle of cohesive soils based on ring shear tests of 32 clays and shales. Stark and Eid (1994) concluded that the shear strength envelope is nonlinear and incorporated the effect of liquid limit, clay-size fraction, and effective normal stress (σ_n') in the empirical correlation. Stark and Eid (1994) showed three different values of residual friction angle corresponding to *LL* and *CF* for three different effective normal stresses, i.e., 100, 400, and 700 kPa.

Stark and Eid (1994) used samples processed through the Number 200 sieve for highly overconsolidated clays. The soil is ball milled prior to reduce the aggregation of the overconsolidated clay particles so they can be processed through the Number 200 sieve. ASTM D4318 and D422 test methods were used to estimate *LL* and CF, respectively, for the material processed through the Number 200 sieve. If the clay is not highly overconsolidated, i.e., without significant induration (aggregation), the samples are only processed through the Number 40 sieve and

thus not ball milled. The method for sample preparation using ball milling of highly overconsolidated clays was proposed by Mesri and Cepeda-Diaz (1986) and used to measure *LL* and *CF* because most of the highly overconsolidated clays, mudstones, claystones, and shales possess varying degrees of induration. Because the empirical correlations presented by Stark and Eid (1994) were developed using *LL*, *CF*, and σ_n', the correlation showed good agreement with the back-calculated drained residual friction angles calculated from case histories of reactivated landslides.

2.4.1.2.4 Stark et al. (2005)

Stark et al. (2005) introduced a revisited residual strength correlation through adding test results of an additional 34 soils for Stark and Eid (1994) correlation. Stark et al. (2005) miss plotted some of the Stark and Eid (1994) data points, utilized index parameters of claystones and shales derived from different sample preparation procedures, and used some results collected from commercial sources. Kaya (2009) noted that the revised correlation by Stark et al. (2005) shows a larger data scatter up to *LL* of 100%.

2.4.1.2.5 Stark and Hussain (2013)

Stark and Hussain (2013) extended the correlation of Stark et al. (2005) through adding data and trend line for an effective normal stresses of 50 kPa. Extending the covered level of effective normal stress down to 50 kPa was done to capture the curvature and nonlinearity of the residual failure envelope. The ring shear data for an effective normal stress of 50 kPa was collected from Eid (1996).

2.4.1.3. Correlations Based on Plasticity Index

2.4.1.3.1 Voight (1973)

Voight (1973) presented a relationship between plasticity index and residual strength coefficient ($\tan(\phi_r')$). The relationship was developed using data from other researchers. Voight (1973) presented an argument that the scatter in his correlation may be caused by the low plasticity measured for some of the soils, such as Cucaracha shale. Voight (1973) attributed it to either flocculation or to insufficient breakdown of particle aggregates. Voight (1973) concluded that the plasticity index appears to be a useful guide to residual strength of natural relationship between ϕ_r' and *PI*.

2.4.1.3.2 Kanji (1974)

Kanji (1974) plotted the friction angles versus the plasticity index. Kanji (1974) endorsed the Voight (1973) findings that the index property of a soil can be correlated to the residual friction angle.

2.4.1.3.3 Mitchell (1976)

Mitchell also presented a relationship between ϕ_r' and *PI* derived from Deere (1974). The drained residual friction angle decreases with an increase in the plasticity index. However, no test data points were presented in the correlation.

2.4.1.3.4 Lupini et al. (1981)

Lupini et al. (1981) presented ring shear test results for a number of natural soils. The test results for 52 different soils were compiled and plotted by Lupini et al. (1981) to develop a relationship between ϕ_r' and plasticity index. Lupini et al. (1981) showed that a number of test results fall outside any reasonable correlation

band and conclude that some of the degradable mudstone and shale materials show a typically low residual friction angles when they are correlated with plasticity index. Thus, Lupini et al. (1981) suggested that simple correlations with index properties are inadequate for the prediction of residual strength.

2.4.1.3.5 Lambe (1985)

Lambe (1985) developed a correlation as a function of the plasticity index based on a relatively few number of direct shear tests on Amuay soils only. Lambe (1985) considered the stress dependency of the failure envelope, and presented trend lines that represent effective normal stresses as low as 19.6 kPa.

2.4.1.4. Mesri and Shahien (2003)

Mesri and Shahien (2003) used the data of Stark and Eid (1994 and 1997) and Eid (1996) to develop a correlation between friction angles and plasticity index. Mesri and Shahien (2003) showed three different plots for each effective normal stress , i.e., 50, 100, and 400 kPa. Lower and upper bounds with an average curve are presented for friction angles versus plasticity index. The scatter in his correlation for residual friction angle values especially for the $PI < 50\%$ is still greater than 7°.

2.4.1.5. Correlations Based on Other Parameters

Some other researchers present empirical correlations for drained residual friction angle based on different parameters besides *LL*, *CF*, *PI*, *A*, and/or σ_n', which are discussed below.

2.4.1.5.1 Collotta et al. (1989)

To include the influence of both the clay-size fraction and soil plasticity, Collotta et al. (1989) used one parameter called as *CALIP* (Equation 2.1) that combines the

CF, *LL*, and *PI* to present residual strength correlations that contain less scattering. The correlations were developed based on direct shear or ring shear testing at effective normal stress ranged between 100 and 700 kPa. However, the effect of the normal stress level was not shown in the correlations.

$$CALIP = (CF^2 \times LL \times PI \times 10^{-5}) \tag{2.1}$$

2.4.1.5.2 Wesley (2003)

Using results of residual shear strength testing on volcanic ash clays and sedimentary soils with *LL* > 50%, Wesley (2003) introduced a correlation based on the position in relation to the A-line (i.e., utilizing the *PI* and *LL*) which is given in Equation 2.2 . The effect of normal stress was not considered. In spite of showing a clear trend, the correlation contains a considerable data scattering.

$$\Delta PI = PI - 0.73(LL - 20) \tag{2.2}$$

2.4.2. Numerical Correlations

2.4.2.1. Kanji (1974)

Kanji (1974) also presented the following expression for the residual friction angle as a function of the plasticity index without considering the effective normal stress:

$$\phi_r' = \frac{46.6}{PI^{0.466}} \tag{2.3}$$

2.4.2.2. Cancelli (1977)

Cancelli (1977) obtained the following expression for the residual friction angle in terms of the liquidity limit (W_L) with a coefficient of determination (R^2) of 0.76.

$$\phi_r' = \frac{453.1}{W_L^{0.85}} \tag{2.4}$$

However, there was no information on the type of the test device utilized to develop his correlation.

2.4.2.3. Nelson 1992

Nelson (1992) developed three correlations between the residual strength coefficient $\tan(\phi_r')$, and *LL*, *PI*, and *CF* based on direct shear testing of 13 fabricated specimens . Least square regression was performed and a third order equation was developed as shown below. Nelson (1992) indicated an R^2 regression of 0.9, 0.796, and 0.795 for the correlations based on liquid limit, plasticity index, and clay-size fraction, respectively.

$$\tan(\phi_r') = 1.6 - 3.6\times10^{-2}\times(LL) + 2.2\times10^{-4}\times(LL)^2 + 2.5\times10^{-8}\times(LL)^3 \quad (2.5)$$

$$\tan(\phi_r') = 1.1 - 4.6\times10^{-2}\times(PI) + 7.2\times10^{-4}\times(PI)^2 - 3.8\times10^{-6}\times(PI)^3 \quad (2.6)$$

$$\tan(\phi_r') = 1.1 - 4.9\times10^{-2}\times(CF) + 8.8\times10^{-4}\times(CF)^2 - 5.6\times10^{-6}\times(CF)^3 \quad (2.7)$$

2.4.2.4. Mesri and Shahien (2003)

The nonlinear relationship between the residual shear strength and the effective normal stress is presented in Mesri and Shahien (2003) by the following expression:

$$s(r) = \sigma_n' \tan[\phi_r']_s^{100}\left[\frac{100}{\sigma_n'}\right]^{1-m_r} \quad (2.8)$$

Where *s(r)* is the residual shear strength, $[\phi_r']_s^{100}$ is the secant residual friction angle at σ_n' = 100 kPa, and m_r is a parameter with values in the range of 0.85 to 1.0. However, no relationship between the soil index parameters and the power parameter (m_r) is presented in Mesri and Shahien (2003) expression.

2.4.2.5. Sridharan and Raghuveer Rao (2004)

In response to the correlation presented by Wesley (2003), Sridharan and Raghuveer Rao (2004) utilized Wesley (2003) testing results, and presented a relationship between ϕ_r' and liquid limit, clay-size fraction, and $(W_L \pm \Delta\text{PI})$ for soils other than volcanic ash which are given below.

$$\phi_r' = \frac{257.44}{W_L^{0.745}} \tag{2.9}$$

$$\phi_r' = \frac{336.97}{CF^{0.893}} \tag{2.10}$$

$$\phi_r' = \frac{322.04}{(W_L \pm \Delta\text{PI})^{0.782}} \tag{2.11}$$

Sridharan and Raghuveer Rao (2004) indicated an R^2 regression of 0.462, 0.58, and 0.486 for the correlations based on W_L, CF, and $(W_L \pm \Delta\text{PI})$, respectively.

2.4.2.6. Wright (2005)

Wright (2005) utilized the correlation of Stark et al. (2005) to develop an equation for the secant residual friction angle in terms of the liquid limit and the ratio between the effective stress and the atmospheric pressure "P_a" (i.e., 100 kPa) (Equation 2.12) . The Equation were derived for clay-size fraction greater than or equal to 50% and liquid limit of less than 150.

$$\phi_r' = 52.5 - 21.3 \log(W_L) - 3\log\left(\frac{\sigma_f'}{P_a}\right) \tag{2.12}$$

2.4.2.7. White and Randolph (2007)

White and Randolph (2007) presented the following equation –developed based on a data from ring shear tests at normal stress levels of 50 to 300 kPa- to estimate the residual friction angle of soil as a function of the effective normal stress only.

$$\tan(\phi_r') = 0.25 - 0.3 \log (\sigma_n' / P_a) \quad (2.13)$$

2.4.2.8. Stark and Hussain (2013)

Stark and Hussain (2013) developed mathematical equations for each trend line in the three *CF* groups and each effective normal stress. A set of four equations was developed for each *CF* group and each effective normal stress as shown below:

For $CF \leq 20\%$

$$\left[\phi_r'\right]_{\sigma_n' = 50\,\text{kPa}} = 39.71 - 0.29(LL) + 6.63\times10^{-4}(LL)^2 \quad (2.14a)$$

$$\left[\phi_r'\right]_{\sigma_n' = 100\,\text{kPa}} = 39.41 - 0.298(LL) + 6.81\times10^{-4}(LL)^2 \quad (2.14b)$$

$$\left[\phi_r'\right]_{\sigma_n' = 400\,\text{kPa}} = 40.24 - 0.375(LL) + 1.36\times10^{-3}(LL)^2 \quad (2.14c)$$

$$\left[\phi_r'\right]_{\sigma_n' = 700\,\text{kPa}} = 40.34 - 0.412(LL) + 1.683\times10^{-3}(LL)^2 \quad (2.14d)$$

For $25\% \leq CF \leq 45\%$

$$\left[\phi_r'\right]_{\sigma_n' = 50\,\text{kPa}} = 31.4 - 6.79\times10^{-3}(LL) + 3.61\times10^{-3}(LL)^2 + 1.86\times10^{-5}(LL)^3 \quad (2.15a)$$

$$\left[\phi_r'\right]_{\sigma_n' = 100\,\text{kPa}} = 29.8 - 3.62\times10^{-4}(LL) - 3.58\times10^{-3}(LL)^2 + 1.85\times10^{-5}(LL)^3 \quad (2.15b)$$

$$\left[\phi_r'\right]_{\sigma_n' = 400\,\text{kPa}} = 28.4 - 5.62\times10^{-2}(LL) - 2.95\times10^{-3}(LL)^2 + 1.72\times10^{-5}(LL)^3 \quad (2.15c)$$

$$\left[\phi_r^{'}\right]_{\sigma_n^{'}=700\,\text{kPa}} = 28.05 - 0.2083(LL) - 8.18\times10^{-4}(LL)^2 + 9.372\times10^{-6}(LL)^3 \quad (2.15d)$$

For $CF \geq 50\%$ and $30\% \leq LL < 120\%$

$$\left[\phi_r^{'}\right]_{\sigma_n^{'}=50\,\text{kPa}} = 33.5 - 0.31(LL) + 3.9\times10^{-4}(LL)^2 + 4.4\times10^{-6}(LL)^3 \quad (2.16a)$$

$$\left[\phi_r^{'}\right]_{\sigma_n^{'}=100\,\text{kPa}} = 30.7 - 0.25(LL) + 4.2\times10^{-4}(LL)^2 + 8.04\times10^{-6}(LL)^3 \quad (2.16b)$$

$$\left[\phi_r^{'}\right]_{\sigma_n^{'}=400\,\text{kPa}} = 29.4 - 0.262(LL) + 4.01\times10^{-4}(LL)^2 + 8.71\times10^{-6}(LL)^3 \quad (2.16c)$$

$$\left[\phi_r^{'}\right]_{\sigma_n^{'}=700\,\text{kPa}} = 27.7 - 0.323(LL) + 2.89\times10^{-4}(LL)^2 + 7.11\times10^{-6}(LL)^3 \quad (2.16d)$$

For $CF \geq 50\%$ and $120\% \leq LL \leq 300\%$

$$\left[\phi_r^{'}\right]_{\sigma_n^{'}=50\,\text{kPa}} = 12.03 - 0.0215(LL) \quad (2.17a)$$

$$\left[\phi_r^{'}\right]_{\sigma_n^{'}=100\,kPa} = 10.64 - 0.0183(LL) \quad (2.17b)$$

$$\left[\phi_r^{'}\right]_{\sigma_n^{'}=400\,\text{kPa}} = 8.32 - 0.0114(LL) \quad (2.17c)$$

$$\left[\phi_r^{'}\right]_{\sigma_n^{'}=700\,\text{kPa}} = 5.84 - 0.0049(LL) \quad (2.17d)$$

Chapter 3. Residual Shear Strength of Soils and Soil-Solid Interfaces at Low Effective Normal Stresses

3.1. Introduction

It has been recognized that the drained residual shear strength envelope of fine-grained soils is nonlinear. This stress dependency is more pronounced for plastic soils especially at low effective normal stress ranges (Skempton 1985). A similar conclusion can be drawn from test results presented for the residual and large-strain shear strength of fine-grained soils sheared against solid interfaces (e.g., Tsubakihara and Kishida 1993) and polymeric geosynthetics (e.g., Esterhuizen et al. 2001). Due to such nonlinearity, soil-soil and soil-solid interface residual frictional resistance at low effective normal stresses as applicable to offshore pipeline design can be significantly underestimated when data developed from shear tests conducted at relatively high effective normal stress ranges are used to generate soil friction parameters.

Testing soil-solid interfaces under very low effective normal stresses stems from the need to quantify the shear strength at the pipe-soil interface for offshore oil and gas pipeline design applications where the effective normal at the pipe-soil interface is within the range of 3 kPa to 6 kPa. The following sections provide details of the soil-soil and soil-solid interface shear testing using the modified ring shear apparatus (MRSA).

3.2. Test Materials

Nine soils were used in this program of soil-soil and soil-solid interface shear testing. The basic physical properties and grain-size distribution of these soils are

presented in Table 3.1 and Fig. 3.1, respectively. The grain diameter corresponding to 50% passing on gradation curve (D_{50}) of each soil is also listed in Table 3.1. The particle-size distributions were determined using the standard test method for particle-size analysis, ASTM D422 (1999). This method was appropriate since the marine soils utilized in the current testing program do not contain palletized material such as that described in Kuo and Bolton (2013). As shown in Table 3.1, the chosen soils cover a wide range of plasticity and clay-size fraction. Fraser-River silt (FS) and Gray silt (GS) are materials that originate from natural soil deposits in the Province of British Columbia, Canada. The Kaolinite (K) was purchased in the form of a commercially available powder. The Gulf-deposit (GD) and Nile-deposit (ND) samples were obtained from different locations along the Gulf shore of Doha, Qatar and the Nile Delta of Egypt, respectively.

Table 3.1 Properties of the soils used

Soil description	*LL* (%)	*PL* (%)	*PI* (%)	*CF* (%)	D_{50} *(mm)*	c_v[a] *(m^2/yr)*
Fraser-River silt (FS)	21	18	3	9	0.024	17.19
Gray silt (GS)	34	17	17	28	0.0096	2.98
Nile deposit 1 (ND1)	36	24	12	18	0.017	2.61
Kaolinite (K)	48	26	22	32	0.0027	1.95
Gulf deposit 1 (GD1)	53	34	19	19	0.035	1.16
Gulf deposit 2 (GD2)	54	22	32	51	0.0019	0.84
Nile deposit 2 (ND2)	69	35	34	50	0.002	0.51
Nile deposit 3 (ND3)	77	28	49	39	0.005	0.53
Gulf deposit 3 (GD3)	89	33	56	57	<0.001	0.32

[a] Evaluated for remoulded soil from oedometer tests at normal stress of 6 kPa.

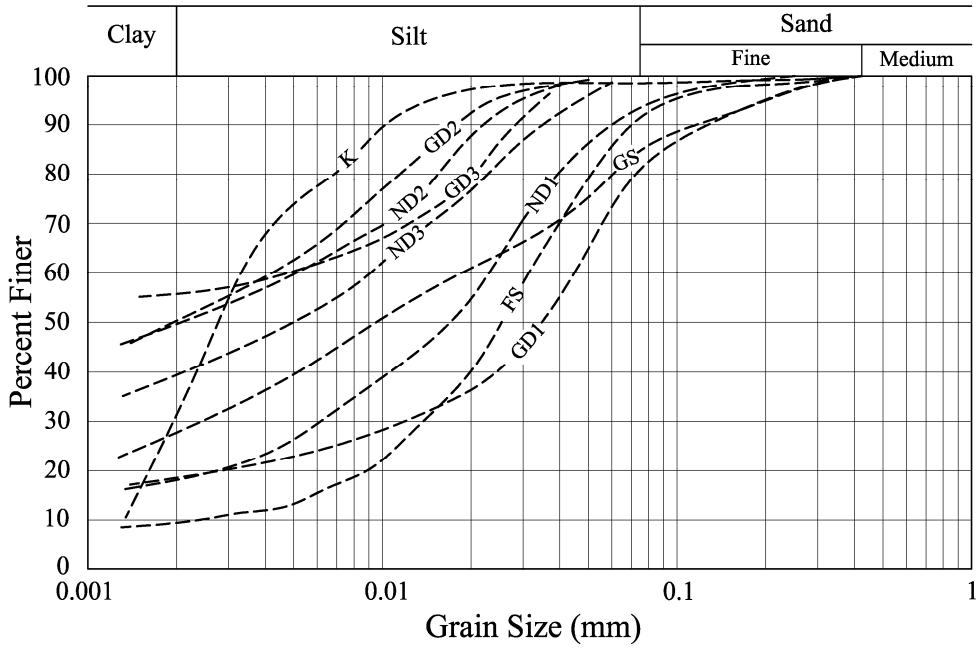

Figure 3.1 Gradation curves of test soils.

The natural water content of typical marine soils is close to the liquid limit. As a result, soil specimens for shear testing were prepared by adding water to air-dried soil to produce a homogenous mixture or slurry having moisture contents slightly above their liquid limits. The coefficient of consolidation (c_v) evaluated for these remoulded soil samples from oedometer tests at normal stress of 6 kPa are also listed in Table 3.1. In the soil-solid interface testing program, the selected test soils were sheared against: (i) bare-steel; and (ii) epoxy-coated steel surfaces. In this regard, miniature disks cut from 7 mm-thick hot-rolled mild steel sheets were utilized in the element-scale ring shear testing. The bare-steel surfaces were cleaned with a de-greasing agent, washed with water and then dried well prior to each interface shear test. The surfaces for soil/coated-solid interface testing were prepared by spraying selected liquid epoxy materials on the test surface of the steel disks used in the element-scale ring shear device. Two epoxy materials were used

as coatings for this test program: (i) a 100% solids epoxy of green color; and (ii) a liquid epoxy three coat system of gray color. Spraying of the epoxy on the surfaces of the disks was conducted by professionally qualified personnel of a commercial organization specialized in epoxy coating in British Columbia, Canada. This has resulted in a uniform coating layer with an average thickness of 1.5 mm. The test surfaces used in the interface shear tests along with their average roughness (R_a) are listed in Table 3.2.

Table 3.2 Interface materials and surface roughness

Material	Surface finish	Average roughness, R_a (μm)
Green epoxy (I1)	Sprayed on steel	0.16
Gray epoxy (I2)	Sprayed on steel	0.8
Mild steel (I3)	As supplied	2.3

The average roughness is the most universally used parameter for describing the surface asperity height (Dangall 1986). It is defined as the arithmetic mean of the departure of the profile from the mean line of a surface profile. The average roughness was measured using a Mitutoyo-SJ210 type portable roughness tester in accordance with ISO standard 4287 (ISO/TC5 1997).

3.3. Element-Scale Testing

A torsional ring shear apparatus was modified to examine the shearing behavior of the interface between soils and solid surfaces. The apparatus was also used to determine the residual shear strengths of the test soils (soil-soil shearing) for comparison with those of the associated soil-solid interface tests. The soil-soil and soil-solid interface tests were conducted at effective normal stresses of 3 and 6 kPa. The low normal stresses used in this study, result in very low shear forces measured during the soil-soil, and soil-solid interface shear tests at element scale.

Therefore, modifications to specific parts of the original ring-shear apparatus were made to minimize potential experimental errors. The original apparatus and the modifications made are discussed in the following subsections.

3.3.1. Orignial Bromhead Ring Shear Apparatus

The original apparatus is described by Bromhead (1979). The ring-shear specimen is annular with inside and outside diameters of 70 and 100 mm, respectively. Double vertical drainage is provided through two annular bronze porous stones; one secured to the bottom of the specimen container, and the other to the loading platen. The specimen is confined radially by the hollow cylindrical specimen container, which is 5 mm deep. The normal stress is applied to the loading platen (and then to the specimen) through a vertical steel rod that is connected to a 10:1 lever loading system. This vertical rod comes in contact with the platen when sufficient weight is placed on the lever. The torque transmitted through the specimen is developed by a pair of proving rings or load cells bearing on a cross arm and located at a constant radial distance from the central axis of the specimen to generate a circumferential force-couple. The bearing point of each proving ring or load cell has two positions so that the effective length of the torque arm can be changed.

3.3.2. Limitations of the Original Design in Measuring Soil and Interface Strengths at Low Normal Stresses

Several problems are encountered in conducting soil-soil, and soil-solid interface tests at normal stresses equal to or less than 6 kPa using the original design of the ring shear apparatus. These problems are related to: (i) the application of normal stress; (ii) the sensitivity of measuring low shear forces; and (iii) the effect of side-

wall friction on measured shear strength. The loading platen alone imposes a normal stress of about 2.5 kPa on specimen in the original Bromhead design. As a result, placement of very small weights would be needed to apply a normal stress of 6 kPa or lower through the lever loading system. This does not secure the contact required between the vertical steel rod and the loading platen and leads to failure in normal stress application during shear. Proving rings and load cells with capacities of 0.5 kN or higher that have been commonly utilized in measuring the residual shear strength of soils are not sensitive enough to accurately sense the low shear forces mobilized in this testing program. Because of the low magnitude of these forces, they can be significantly overestimated due to having side-wall friction during shear (Stark and Eid 1993; Meehan et al. 2007). These problems were rectified by modifying the original design of the ring shear apparatus.

3.3.3. Modified Ring Shear Apparatus

The problems described above were overcome by several modifications made to the loading assembly, shear measuring devices, and specimen container. A general view of the modified apparatus is shown in Fig. 3.2. It can be seen that sensitive digital dial gauges (with maximum capacity and resolution of 0.1 kN and 0.01 N, respectively) were utilized for measuring the low shear forces. The lever loading system was also replaced by a light-weight hanger for direct normal stress application. In addition, a light-weight loading assembly is used to help in applying small normal stresses.

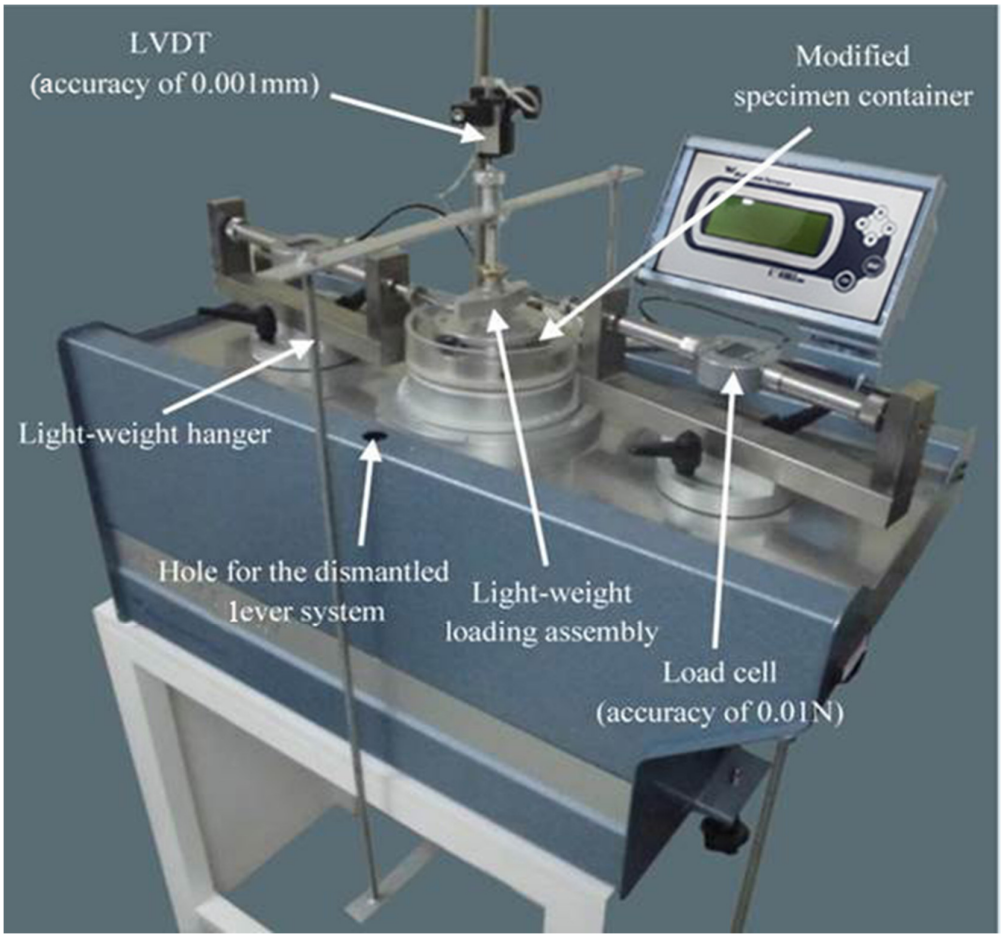

Figure 3.2 General view of the ring shear apparatus showing the components utilized to apply low normal stresses and measure the corresponding shear forces

The differences between the original loading assembly and the modified version are shown in Fig. 3.3a (end elevation) and Fig. 3.3b (perspective view). It can be seen that the long steel torque arm and the thick top platen of the original design are replaced by a short aluminum torque arm and a thin top platen in the modified loading assembly. The use of a short torque arm was advantageous since it reduced the weight of the loading assembly and enhanced the readings of the load cells measuring the force-couple. A horizontal hole was made in the loading platen to release any potential air pressure generated between the platen and the centralizing pin around which the specimen container rotates during shear (Fig.

3.3a). It should also be noted that for soil-solid interface testing, the porous stone that is fixed to the original top platen using fully penetrated screws was replaced by a steel disk attached to the top platen using partially penetrated screws (Fig. 3.3b). This secures the flatness of the steel disk surface needed for the soil-solid interface testing. As shown in Fig. 3.3a, the edges of the steel disks are beveled to avoid coating the disk outer perimeter (edges). Coating the edges may result in a significant error in shear force reading due to friction between such coated edges and the inner walls of the specimen container. To eliminate the effects of side-wall friction during shear, the original one-piece specimen container was replaced by a three-piece system (Fig. 3.4) and the procedure described in Stark and Eid (1993) for eliminating such effects was followed.

(a)

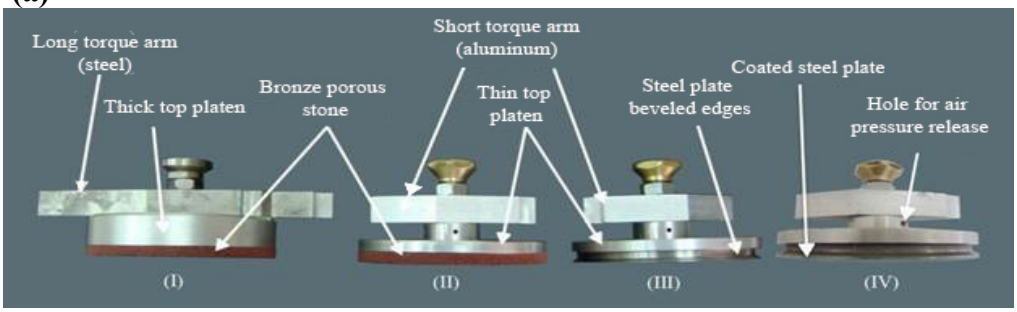

(b)

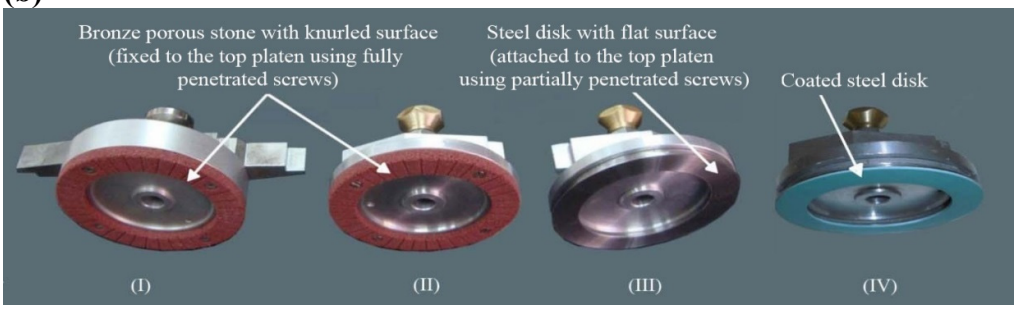

Figure 3.3 Views showing the different loading assemblies of the ring shear apparatus: (I) the original assembly; (II) assembly modified for soil/soil testing; (III) assembly modified for interface testing; (IV) modified assembly with coated disk

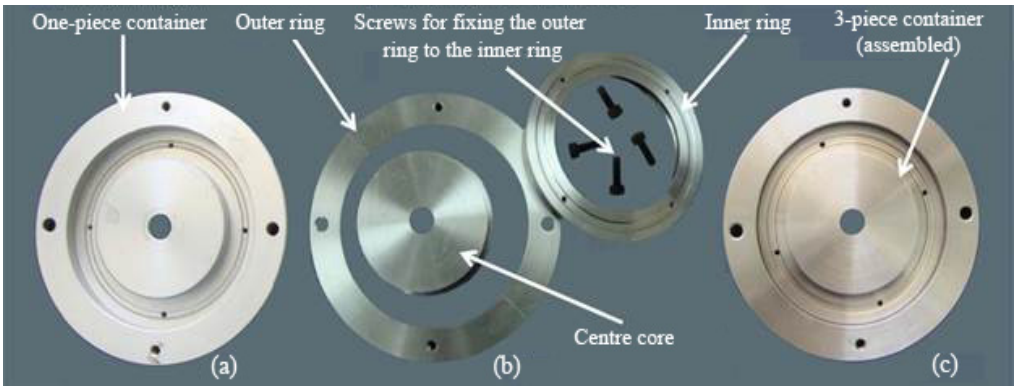

Figure 3.4 Top view shows the specimen containers of the torsional ring shear apparatus: (a) original container; (b) components of the modified container; (c) assembled modified container

3.3.4. Testing Procedure

3.3.4.1. Sample Preparation

Before each soil-soil and soil-solid interface shearing test, the soil samples were air-dried and material passing through the # 40 sieve was selected for testing. Except for the Gray silt, gradations of the natural soils used in the current testing program were not changed by this sieving process. The natural Gray silt has about 7% of its particles coarser than # 40 sieve (i.e., 0.425 mm). The Gray silt grain-size distribution shown in Fig. 3.1 is for the material processed through # 40 sieve. The properties of the processed material that are shown in Table 3.1 were used in all of the analyses presented in the subsequent section. As mentioned earlier, water was added to the processed soil until a liquidity index of about 1.0 was obtained. The sample was then allowed to rehydrate for 24 hours. A spatula was used to place the remolded soil paste into the modified annular specimen container. The top of the specimen was then planed flush with the top of the specimen container using a razor blade.

The loading assembly –with a secured porous stone (in the case of soil-soil testing), or a bare steel or coated steel disk (in the case of soil-solid interface testing) - was placed on top of the specimen. The normal stress was then gradually increased to 3 or 6 kPa by loading the specimen through the light-weight hanger. After completion of consolidation, the specimen was unloaded and the settlement of the loading platen into the specimen container was eliminated using the procedure described in Stark and Eid (1993). The specimen was then reloaded to the consolidation pressure and sheared until a shear displacement of 400 mm was achieved.

3.3.4.2. Selection of the Appropriate Rate of Shear

Gibson and Henkel (1954) have presented Eq. 3.1 that relates the time to failure, t_f, that corresponds to a given degree of pore-water pressure dissipation, U_f, of a normally consolidated clay specimen with a drainage distance of H:

$$t_f = \frac{H^2}{2(1-U_f)c_v} \tag{3.1}$$

To calculate the shear displacement rate that provides a drained residual shear condition (defined for ring shear tests of the current study by having $U_f \geq 0.99$), the time to failure is selected to be the time to achieve a shear displacement of 400 mm. This magnitude of displacement is considered sufficient to mobilize the drained residual shear strength in all of the soil-soil and soil-solid interface ring shear tests conducted in this study. Shearing interfaces against the most plastic soil used in the current investigation (i.e., having H = 5 mm and c_v = 0.32 m^2/yr) would need the slowest rate to mobilized such condition. Utilizing these values, as well as a U_f = 0.99 in Eq. 3.1 results in a t_f of 2050 min. This suggests a shear displacement

rate of 0.2 mm/min to produce a drained residual shear strength condition. A much slower displacement rate of 0.05 mm/min was used in all of the soil-soil and soil-solid interface ring shear tests to ensure fully drained residual strength mobilization. Larger displacement rates could have been used in shearing some of the soils utilized in this study. Considering the short displacement needed to mobilize the soil and interface peak shear strength, the used shearing rate may produce a partially drained condition for such strengths especially in cases of testing plastic soil-solid interfaces. Studying peak strengths is outside the scope of the current research.

3.3.5. Test Results

Fig. 3.5 shows typical stress ratio-shear displacement relationships yielded from the soil-soil and soil-solid interface tests at an effective normal stress of 6 kPa. The stress ratio is defined as the shear stress (τ) divided by the effective normal stress. In both of the soil-soil and soil-solid interface tests, a peak shear strength was reached at a displacement less than 5 mm before experiencing a strength reduction that is more pronounced in soil-soil tests. A shear displacement of about 200 mm was needed to reach the residual shear strength of the soils. A similar trend was also noticed in testing soils and interfaces at an effective normal stress of 3 kPa. The displacement to the residual strength decreases with decreasing soil plasticity and/or the roughness of the tested surface. Comparatively, less displacement is needed to reach the interface residual shear strength. A similar behavior has been reported by several researchers (e.g., Lemos and Vaughan 2000).

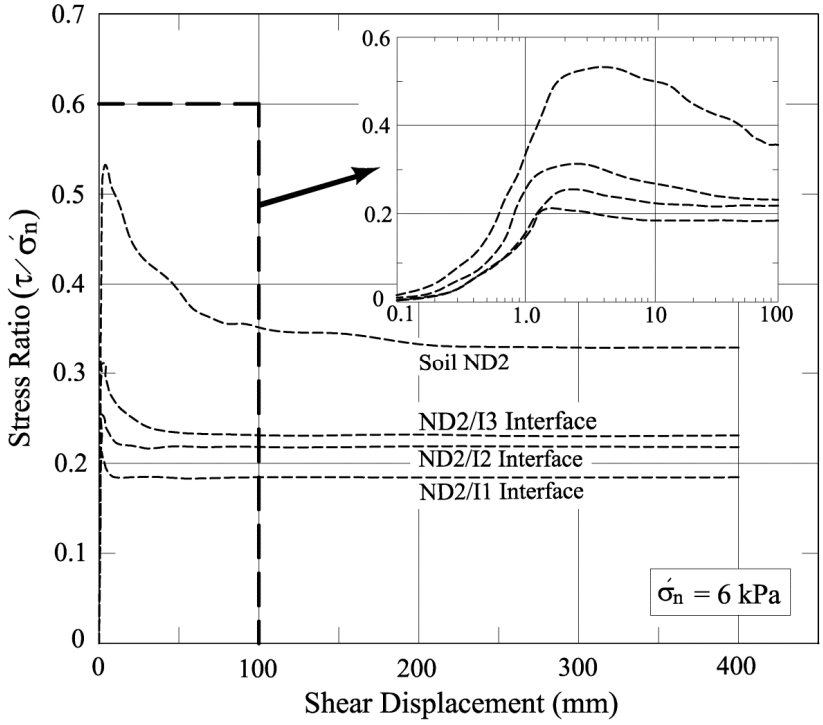

Figure 3.5 Representative stress ratio-shear displacement relationships for soils and interfaces tested using the modified ring shear apparatus

Tables 3.3 and 3.4 present a summary of the soil secant residual friction angles, ϕ_r', and interface secant residual friction angles, δ_r', measured in the element-scale testing at effective normal stresses of 3 and 6 kPa, respectively. The secant residual friction angle is defined as the angle between the effective normal stress axis and the line formed from the origin to the residual shear strength at a particular effective normal stress. It should be noted that the modified ring shear apparatus showed a limitation in accurately measuring shear stresses less than approximately 1.1 kPa. This is due to the unbalanced readings of the two load cells, especially prominent at large shear displacement. As a result, soil-soil and soil-solid interface shear tests that mobilized shear stresses less than 1.1 kPa were stopped. These tests are designated in Tables 3.3 and 3.4 as not available (NA).

Table 3.3 Secant drained residual friction angles measured in soil-soil and soil-solid interface testing using MRSA

		Interface δ_r' (deg.)		
Soil	Soil ϕ_r' (deg.)	I1	I2	I3
FS	32.88	21.82	22.71	26.55
GS	27.05	NA	NA	20.63
ND1	28.12	NA	NA	22.98
K	25.19	NA	NA	23.21
GD1	25.76	NA	NA	20.54

Note: σ_n' = 3 kPa. NA, not available

Table 3.4 Secant drained residual friction angles measured in soil-soil and soil-solid interface testing using MRSA

		Interface δ_r' (deg.)		
Soil	Soil ϕ_r' (deg.)	I1	I2	I3
FS	32.97	21.65	22.48	26.47
GS	26.71	16.50	17.19	19.76
ND1	28.73	18.10	19.32	23.81
K	25.02	14.64	15.75	22.50
GD1	25.59	14.94	17.98	20.17
GD2	20.75	12.88	14.55	16.72
ND2	18.33	10.47	12.30	13.18
ND3	19.12	NA	12.18	15.18
GD3	15.43	NA	NA	11.94

Note: σ_n' = 6 kPa. NA, not available

3.4. Macro-Scale testing

In order to justify the modifications made in the torsional ring shear apparatus and depicting the full-scale field behavior to estimate interface residual shear strengths, a macro-scale interface direct-shear test device (MDSD) was custom designed and manufactured by research collaborators at the University of British Columbia, Canada to assess the drained residual interface shear strength at low effective normal stresses. The detailed design of the apparatus is described in Wijewickreme et al. (2014). The results of the macro-scale interface shear tests conducted by the collaborators on three soils (FS, GS, and K) were utilized for comparison with the

element-scale testing of this study. The following subsections provide details of the device.

3.4.1. Overview of Macro-Scale Interface Direct-Shear Device

The macro-scale interface direct-shear device is fundamentally similar to the conventional small-scale direct shear box device except for its large footprint that provides a plan interface shear area of approximately 3.0 m^2. Fig. 3.6 shows a schematic diagram and photograph of the device. The device was designed to impart displacement-controlled interface shearing with the ability to reach a maximum interface shear displacement of 1.2 m. The desired normal stress at the soil-solid interface is obtained using surcharge loads externally applied by means of bulk sand or water masses, or both. The device is instrumented with transducers mounted flush with the top surface of the solid surface for the measurement of pore water pressure at the shear interface. As a result, the device allows for accurate determination of the effective normal stress at the soil-solid interface during shear testing.

(a)

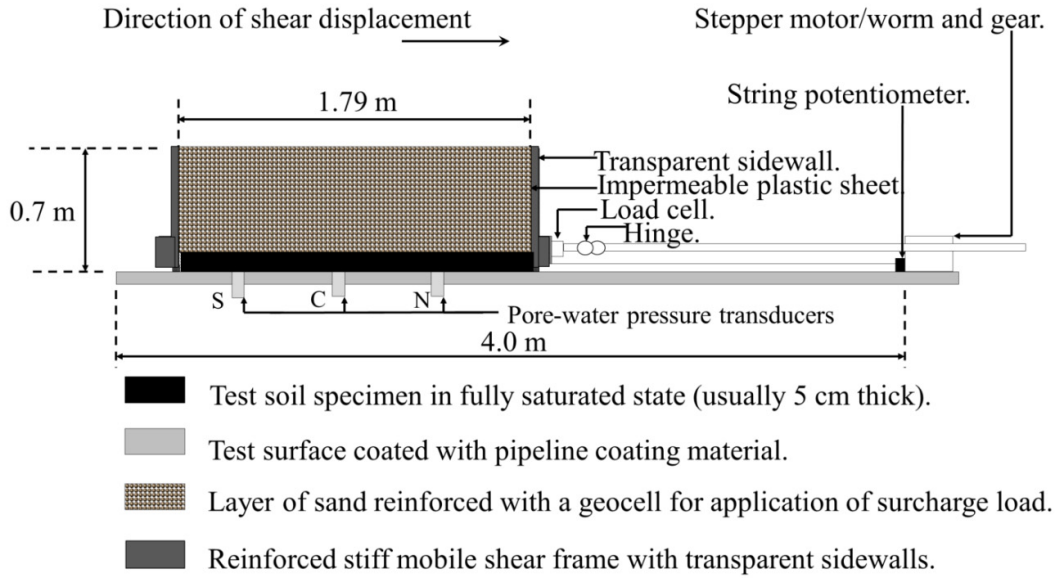

(b)

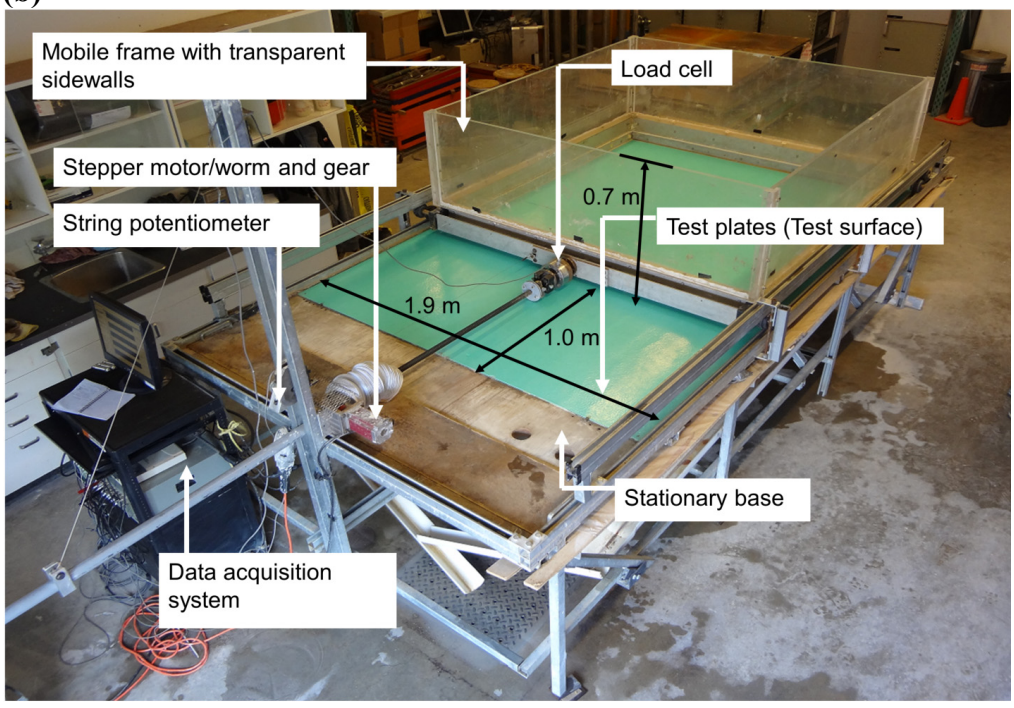

Figure 3.6 The macro-scale interface direct shear device: (a) schematic diagram; (b) perspective photo (after Wijewickreme et al. 2014)

3.4.2. Measurement of Pore-water Pressure

The presence of the porous stone that surrounds the pore-water-pressure transducers can affect the measured excess pore-water pressure at the interface. However, it is important to note the shear-induced excess pore-water pressures are not present when the specimen is sheared to large displacements. The purpose of the macro-scale interface direct shear apparatus is to determine the effective shear strength of an interface under a given low effective normal stress at large interface shear displacement conditions, and the device is not suitable to study the small strain behaviour of the interface at the early stages of a test. As such, the accuracy of the excess pore-water pressure at the soil-solid interface during the initial portion of shear displacement, (where excess pore-water pressure is likely to be present) is considered of less importance. In essence, the device allows for accurate determination of the effective normal stress at the soil-solid interface at large displacement.

The direct experimental pore-water pressure measurements confirm the suitability of this assumption where the data indicates that excess pore-water pressures are indeed developed at the early stages of shearing, and when sufficient time (and displacement) has elapsed, these excess pore-water pressures subside and return to their original static values. Once this happens, upon continued shearing, the pore-water pressure remains constant throughout the remainder of the test. While it is observed that different soils take different amounts of time to dissipate the excess pore-water pressure generated as expected, the end-of-the-test static pore water pressure measured compares well with initial static pore water pressures.

3.4.3. Determination of the Appropriate Rate of Shear

Determination of the appropriate rate of shear displacement requires an estimate of the time required for pore-water pressure equalization and amount of deformation required to reach shear failure. The theoretical equation proposed by Gibson and Henkel (1954), as given by Eq 3.1, was also used by the collaborators (Amarasinghe 2013) to calculate the time to failure, t_f, that would correspond to a given degree of pore-water pressure equalization at failure.

3.4.4. Interface Shear Tests

Three (FS, GS, and K) of the nine soils utilized in the element-scale ring shear testing were sheared by the collaborators (Amarasinghe 2013) against bare steel or coated steel plates in the macro-scale interface direct-shear test device. The steel plates have dimensions of 1.52 m by 1.93 m in plan. For each test, slurry of the test soil with a liquidity index of 1.0 is allowed to flow over the face of the test plate under gravity into the mobile frame to fill the 1.72 m by 1.75 m footprint until a soil specimen thickness of 10 cm is achieved. The slurry is then allowed to consolidate under its own weight. The surface of the consolidated slurry is covered with a non-woven geotextile layer in preparation for surcharge loading. The desired surcharge load – that results in a normal stress of approximately 3 or 6 kPa - is then applied and the soil specimen is allowed to consolidate. The specimen is then sheared against the steel plate for displacements ranging between 500 and 800 mm to ensure mobilization of the interface residual shear strength. Typical stress ratio-shear displacement relationships and the corresponding pore-water pressures yielded from the macro-scale interface direct-shear testing are shown in Fig. 3.7(a) and Fig. 3.7(b), respectively. It can be seen that, except for the Fraser-river silt, the

soil-solid interface tests showed a peak shear strength reached at shearing displacement of less than 70 mm followed by a noticeable strength reduction. The relationships shown in Fig. 3.7(a) were drawn using the calculated ratios between the measured shear stress at a given interface displacement, and the effective normal stress at the interface at the same displacement. The effective normal stress is computed by taking the difference between the total normal stress at the interface, and the pore-water pressure measured at the interface at that shear displacement. The relationships of Fig. 3.7(a) have been labeled according to the effective normal stress value at a shear displacement of 800 mm (i.e., σ_n' at 800 mm shear displacement), which corresponds to the large-displacement interface shear strength. In other words, the labels for a given test represent the σ_n' that prevailed at large-strain conditions for that test. The interface residual friction angles measured at different low effective normal stresses are presented in Table 3.5.

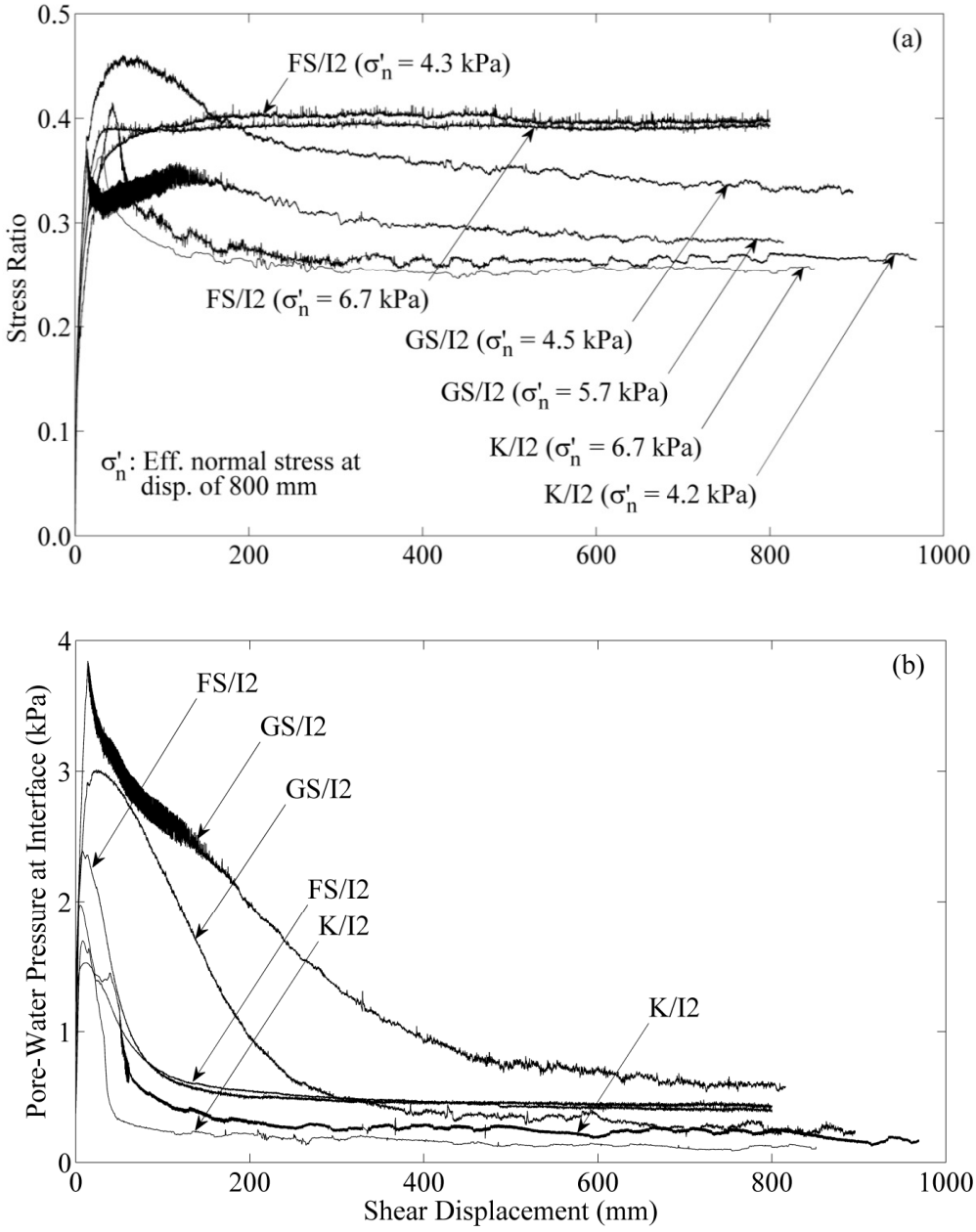

Figure 3.7 Representative relationships yielded from MDSD interface testing: (a) stress ratio-shear displacement; (b) average pore-water pressure-shear displacement (after Amarasinghe 2013)

Table 3.5 . Interface residual friction angles measured in MDSD testing (data from Amarasinghe 2013)

	Interface $\delta_r^{'}$ (deg.)		
Soil	I1	I2	I3
FS	23.3 ($\sigma_n^{'}$ = 3.6 kPa)	21.6 ($\sigma_n^{'}$ = 4.3 kPa)	26.6 ($\sigma_n^{'}$ = 4.3 kPa)
FS	23.3 ($\sigma_n^{'}$ = 6.7 kPa)	21.3 ($\sigma_n^{'}$ = 6.7 kPa)	26.6 ($\sigma_n^{'}$ = 5.9 kPa)
GS	16.7 ($\sigma_n^{'}$ = 3.2 kPa)	18.3 ($\sigma_n^{'}$ = 4.5 kPa)	NA
GS	16.7 ($\sigma_n^{'}$ = 5.1 kPa)	15.6 ($\sigma_n^{'}$ = 5.7 kPa)	NA
K	14.6 ($\sigma_n^{'}$ = 4.1 kPa)	14.6 ($\sigma_n^{'}$ = 4.2 kPa)	27 ($\sigma_n^{'}$ = 4.4 kPa)
K	14.6 ($\sigma_n^{'}$ = 6.3 kPa)	14.0 ($\sigma_n^{'}$ = 6.7 kPa)	NA

Note: σ_n' measured at large shear displacement

3.5. Evaluation of Test Results

The measured soil residual friction angles shown in Tables 3.3 and 3.4, along with the corresponding soil properties presented in Table 3.1 suggest that the secant residual friction angle of soil decreases with increasing liquid limit and clay-size fraction. These soil parameters have a similar effect on the measured interface residual friction angles that are also lower for smoother surfaces (Tables 3.3, and 3.4). A comparison between the interface residual friction angles yielded from tests using the MRSA (This study) and the MDSD is shown in Fig. 3.8. It can be seen that the results measured using the different scale testing devices and procedures are in reasonable agreement. The same conclusion can be drawn from Fig. 3.9(a) that shows a good alignment between the MDSD interface testing results and the corresponding interface residual shear strength envelopes developed based on the MRSA testing. Such a conclusion supports the validity of the MRSA in measuring the interface and soil drained residual shear strength at low effective normal stresses. The change in effective normal stresses within the range utilized in this

study did not show a considerable effect on the measured residual friction angles of soils and soil-solid interfaces. This has led to having approximately linear residual shear strength failure envelopes for most of the tested soils and interfaces (Fig. 3.9).

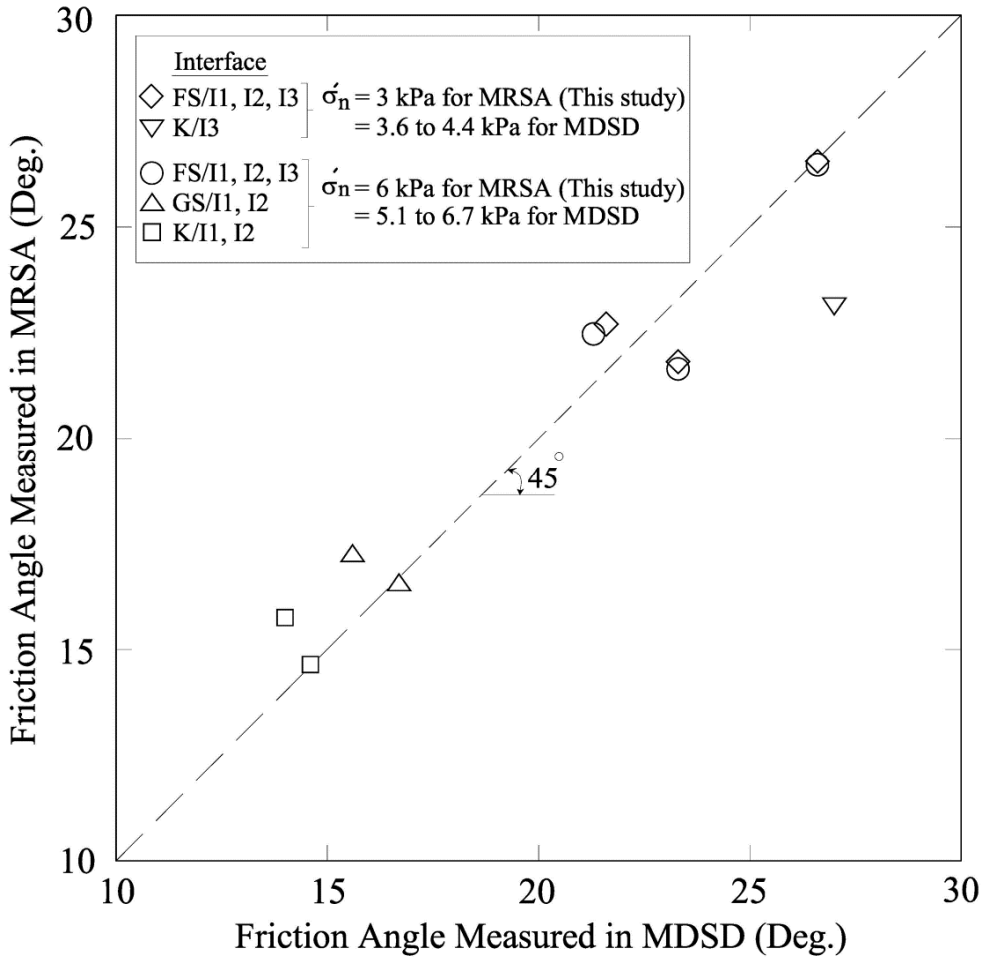

Figure 3.8 . Comparison between interface secant residual friction angles measured by the MRSA (this study) and MDSD.

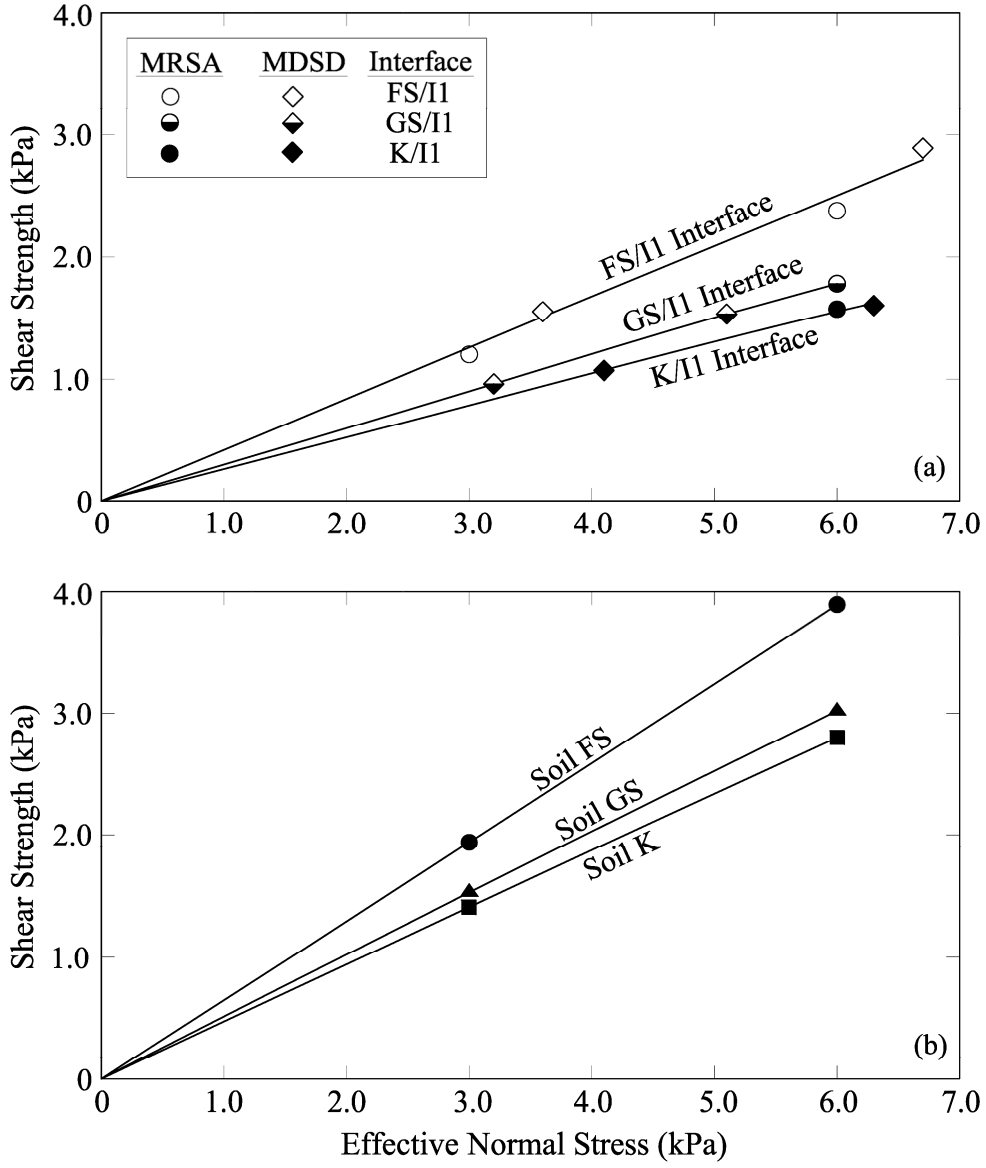

Figure 3.9 Typical drained residual shear strength envelopes developed from testing: (a) interfaces using the MRSA (this study) and MDSD; (b) soils using the MRSA (this study).

Secant residual friction angles of soils tested in the MRSA at an effective normal stress of 6 kPa are plotted as a function of soil liquid limit and clay-size fraction in Fig. 3.10. This plotting format was first introduced by Stark and Eid (1994) to develop a correlation for residual friction angles measured at 100, 400,

and 700 kPa. It can be seen that the residual shear strength correlation based on the value of liquid limit magnitude and clay-size fraction grouping is evident even at effective normal stresses as low as 6 kPa. The secant residual friction angles measured at this effective normal stress range is considerably higher than those reported by Stark and Eid (1994) for soils with similar liquid limits and clay fractions tested at effective normal stress of 100 kPa. This seems to be especially true for soils with high clay-size fraction. For such soil types, the drained residual shear strength envelopes are considerably curved at low effective normal stresses, becoming less stress dependent as the effective normal stress increases.

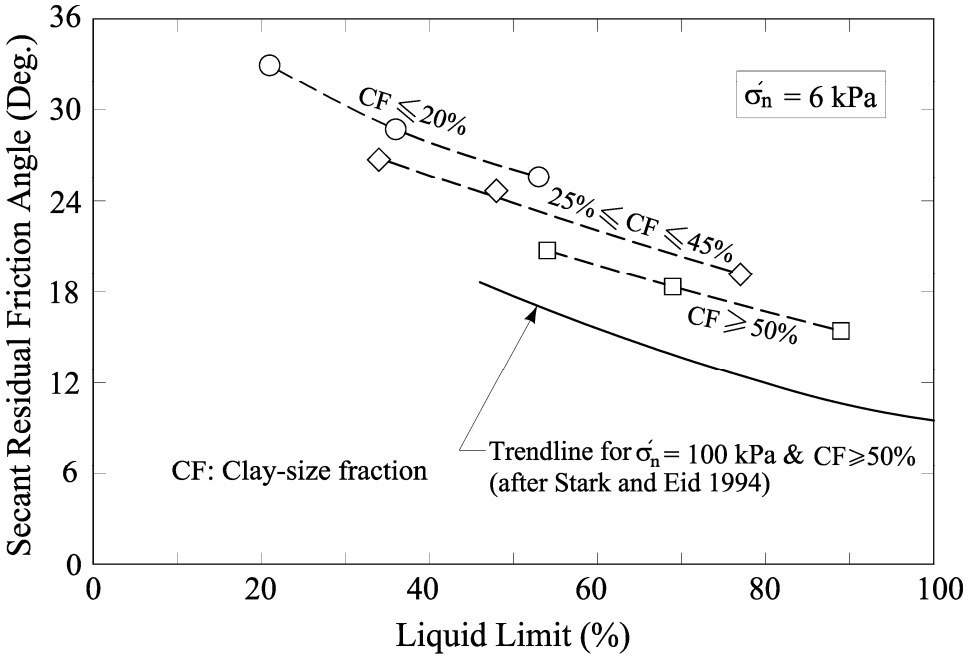

Figure 3.10 Soil secant drained residual friction angle relationships with liquid limit and clay-size fraction.

At the low effective normal stress range considered in this study, the clay-size fraction, as an indication of particle size and shearing mode (Lupini et al. 1981), has less influence on the measured residual friction angle than the influence of the

liquid limit that indicates the clay mineralogy and particle shape. This is indicated by the nearness of the clay-fraction trend lines shown in Fig. 3.10. Such a conclusion agrees with the data presented by Stark and Eid (1994) and shown in Fig. 3.11 in terms of the difference in residual friction angles ($\Delta\phi_r$) predicted for soils with liquid limits between 54 and 77% and clay-size fractions that yield mobilization of translational shearing mode (25% ≤ CF≤ 45%) and sliding mode (CF≥ 50%). This specific liquid-limit range was considered because it represents the liquid-limit overlap between the trend lines of these two clay-size-fraction groups shown in Fig. 3.10. It should be noted that the distinguished effect of clay-size fraction on developing different residual shear strength modes and in turn on the measured friction angles was presented by Lupini et al (1981), Skempton (1985), Stark and Eid (1994) for effective normal stresses of 350, 100 and 50 to 700 kPa, respectively.

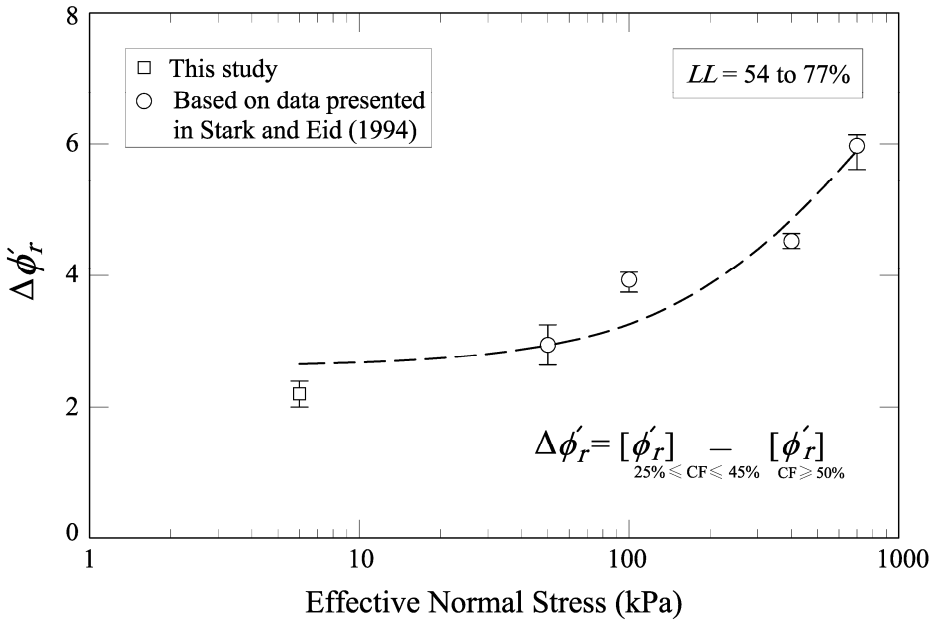

Figure 3.11 Effect of clay-size fraction grouping on the soil secant residual friction angle as a function of the applied effective normal stress.

Secant residual friction angles of soils measured at low effective normal stresses using the MRSA were plotted against the plasticity index. The relationship is shown in Fig. 3.12 indicating a good correlation that can be well described by the following equation for the ranges of effective normal stress and plasticity index considered in this study.

$$\phi_r' = 34^\circ \, e^{-0.014\,PI} \tag{3.2}$$

This good correlation can be attributed to the possible encapsulation of information on both plasticity and clay-size fraction by the plasticity index (Nelson 1992; Mesri and Shahien 2003) as well as the small influence of the clay-size fraction on residual friction angles measured at low effective normal stresses. Another factor that also contributes to having little scattering of data in Fig. 3.12 is the narrow range of low effective normal stress used. Considerable data scattering can be noticed when correlating the plasticity index to soil-soil drained residual shear strength (e.g., Voight 1973) and soil-steel interface residual strength (e.g., Ramsey et al. 1998; Jardine et al. 2005) using data developed at wide range of high effective normal stress for which changing the clay-size fraction as well as the effective normal stress considerably affect the measured secant residual friction angle. It should be noted that, the correlations presented in Figs. 3.10 and 3.12 are for effective normal stresses that are an order of magnitude smaller than those used to develop the empirical correlations available in the literature.

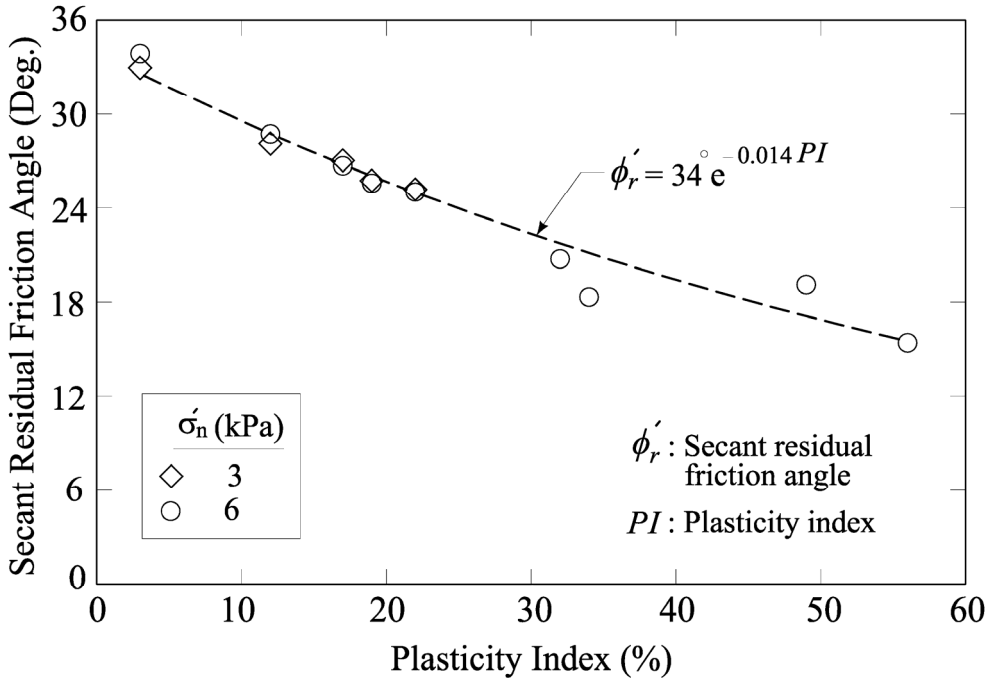

Figure 3.12 Soil secant drained residual friction angle relationship with plasticity index based on the MRSA testing results.

It is of interest to examine the published data that is available in the literature for soil residual friction angles measured at low effective normal stress ranges similar to that utilized in this study. Bishop et al. (1971) measured a drained secant residual friction angle of 13.8 degrees at an effective normal stress of 6.9 kPa for a very stiff Brown London clay with liquid limit, plastic limit, and clay-size fraction of 66%, 24%, and 53%, respectively, The test was conducted using a ring shear apparatus on a 19 mm-thick undisturbed specimen sheared –during the same test- under a series of different higher effective normal stresses. This test result is in good agreement with the correlation presented in Figs. 3.10 and 3.12 provided that the liquid limit of the tested heavily overconsolidated material is adjusted to account for sample preparation problems related to particle induration (Eid 2001

and 2006). It should be noted that such problems were not faced in the current study due to the disaggregated nature of the utilized soil deposits.

It should be noted also that the correlation provided in Fig. 3.12, and consequently Eq. 3.2, would underestimate the secant drained friction angle at low effective normal stresses for marine soils that contain robust faecal pellets (Hill and Jacob 2008; Colliat et al. 2011; Kuo and Bolton 2013 and 2014) or numerous skeletal remains or foraminifera (Mesri et al. 1975; Najjar et al. 2007). This is also the case for carbonate soils (White et al. 2012) and soils composed chiefly of allophane or halloysite that are unlikely to have particle rearrangement towards some preferred orientation (Wesley 1977, 1992). To differentiate them from those tested in the current study, these fine-grained soils are called herein as soils of distinct contents. Even when normally consolidated and plastic, most of these soils exhibit high friction angle and small or no difference between the drained peak shear strength and the drained residual shear strength. Using two different types of ring shear devices, Saldivar and Jardine (2005) measured equal drained peak and residual friction angles of about 36 degrees for Mexico City clay with skeletal fragments of diatoms and a plasticity index of 160%.

The drained residual friction angles at low effective normal stress reported for some soils of distinct contents were plotted against the plasticity index as shown in Fig. 3.13. It can be seen that these angles fall far from the trend line presented in Fig. 3.12 and represented by Eq. 3.2 for soil types similar to those utilized in this study. This can be interpreted in terms of the contents of these soils that yield an exceptionally high drained residual strength that is not significantly affected by the plasticity index (Najjar el al. 2007, White et al. 2012). It should be

noted that, in spite of the increased number of studies conducted in the last decade on evaluating soil-solid interface shear strength at low effective normal stresses, the number of data points in Fig. 3.13 is limited due to the lack of reporting the plasticity indices and the fully drained residual shear strength of the tested soils.

It has been long recognized that the residual shear strength envelopes of plastic soils are nonlinear, especially at low effective normal stress range (Terzaghi and Peck 1948). With this consideration in mind, the use of the correlation presented in this study (Figs 3.10 and 3.12) can help in avoiding a significant underestimation of drained residual shear strength angles predicted for low normal stress ranges when utilizing correlations developed for high effective normal stress ranges. It also avoids overestimating the drained residual friction angles of soils similar to those utilized in the current study when using residual strength expressions, the development of which is influenced by testing soils of distinct contents at low effective normal stresses and consequently do not consider the effect of soil plasticity (e.g., expression suggested by White and Randolph 2007) as shown in Fig. 3.13.

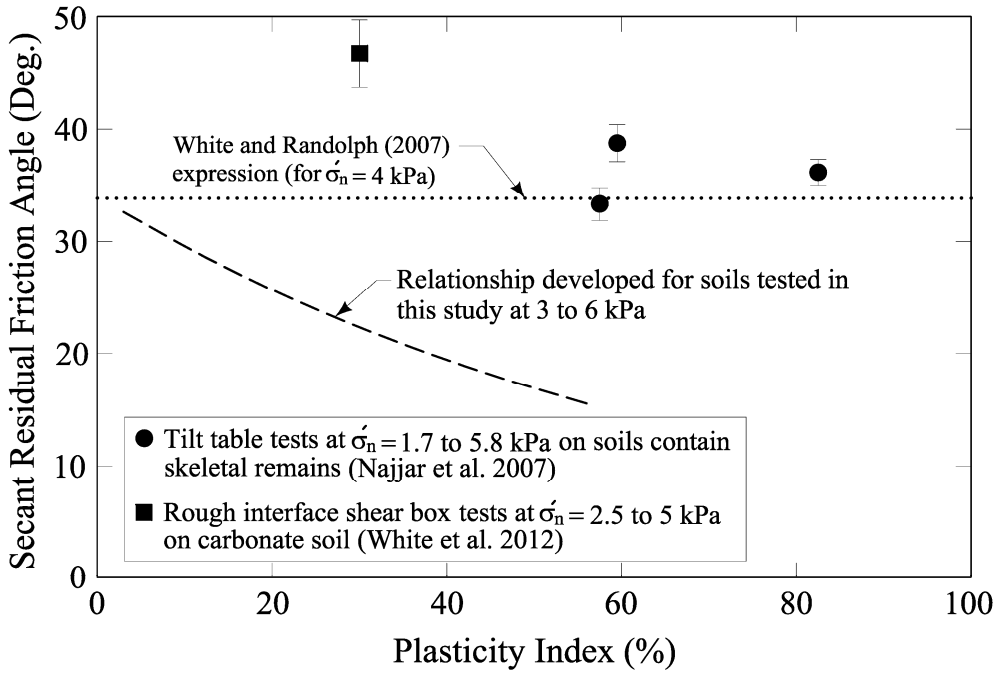

Figure 3.13 Variation of drained residual friction angle with plasticity index for soils having different contents.

As expected based on existing literature, shearing soils against the solid surfaces utilized in this study has led to measuring interface residual friction angles that are less than the residual friction angles of the corresponding soils (Tables 3.3 and 3.4). This is clear from the data shown in Fig. 3.14 that includes the soil-soil residual shear strength trend line developed in Fig. 3.12 along with the soil-solid interface drained residual shear strength results measured using the MRSA at effective normal stresses of 3 and 6 kPa.

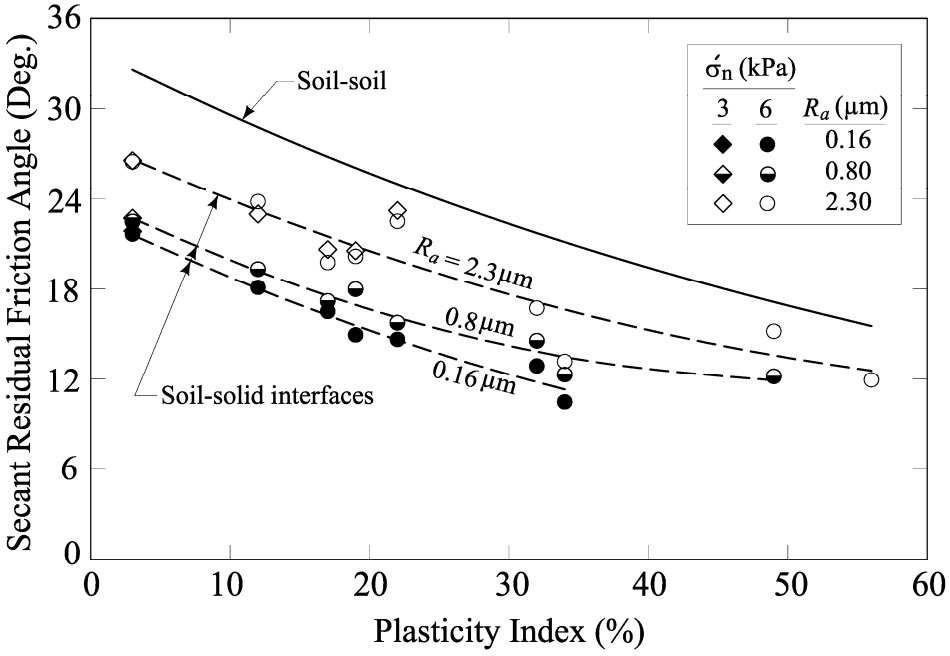

Figure 3.14 Relationship between the plasticity index and soil-soil and soil-solid interface drained residual friction angles measured in the MRSA

It is evident that trend lines can be developed for soil-solid interface strength based on the roughness of each interface solid material. Similar to the soil-soil trend line, the soil-solid interface trend lines show a reduction in drained residual shear strength with increasing soil plasticity. Such reduction in residual shear strength is evaluated as the ratio between the tangents of these soil-soil and soil-solid interface friction angles using the term residual interface efficiency. The average and range of the residual interface efficiency calculated for the three surfaces sheared against soils in the study are plotted against R_a in Fig. 3.15. A single empirical relationship fits the data with a correlation coefficient of 0.8 considering a total of thirty one ring shear interface tests. As shown in Fig. 3.15, the empirical equation obtained is:

$$\frac{\tan \delta_r^{'}}{\tan \phi_r^{'}} = 0.7 R_a^{\,0.12} \qquad (3.3)$$

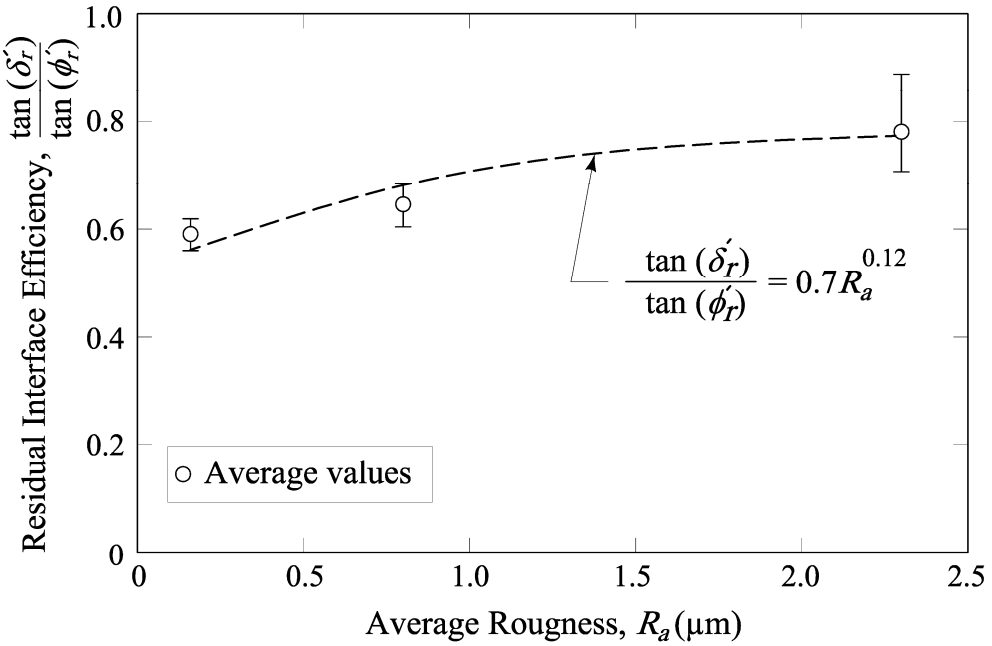

Figure 3.15 Relationship between surface roughness and residual interface efficiency measured for fine-grained soils tested in the MRSA at effective normal stress of 3 and 6 kPa.

For comparison, Eq. 3.3 that is developed based on the results of ring shear testing at 3 and 6 kPa is plotted in Fig. 3.16 along with residual interface efficiency data from the Macro-scale interface direct shear tests conducted by Amarasinghe (2013) at a similar effective stress range. The secant residual friction angles needed to calculate the interface efficiency using the MDSD test results at certain effective normal stresses were taken from the MRSA soil tests conducted at the closest effective normal stress (i.e., either at 3 or 6 kPa). It can be seen that Eq. 3.3 compares well with most of the data developed based on the MDSD test results. Data reported in the literature based on interface testing at higher effective stress ranges were also included in Fig. 3.16 showing an interesting agreement with the relationship developed based on shear strengths measured at low effective normal stresses. Data presented in Fig. 3.16 indicate that the residual interface efficiency

changes from about 0.9 to 0.4 when R_a decreases from 8 to 0.005 μm regardless of the effective normal stress range. Further experimental investigation is required to substantiate this conclusion.

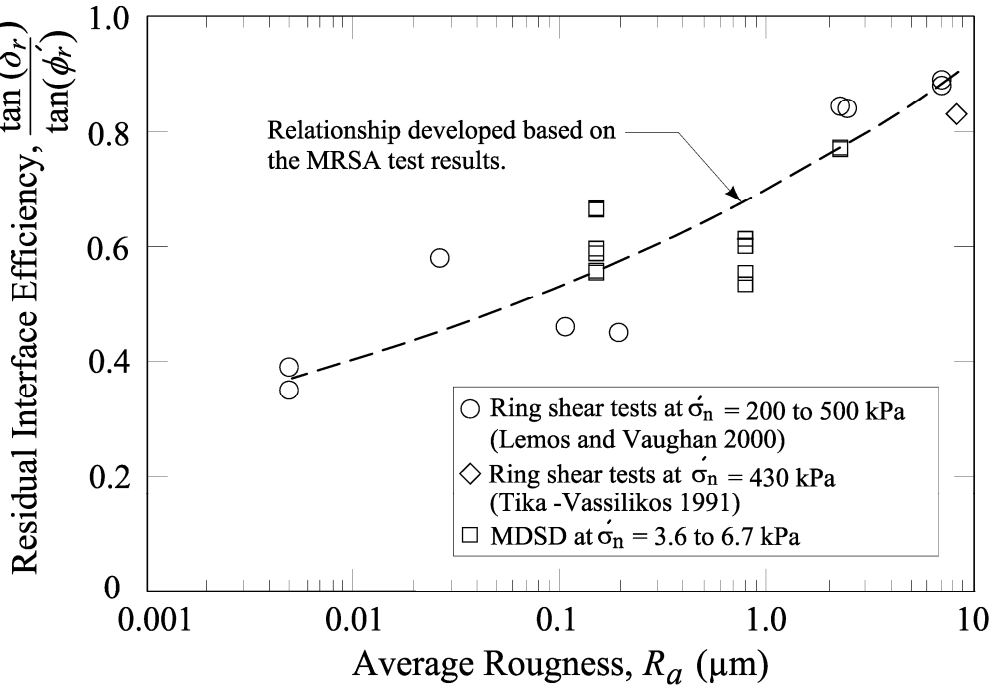

Figure 3.16 Residual interface efficiency for fine-grained soils as a function of surface roughness.

The drained residual strength results of fine-grained interface testing other than those shown in Fig. 3.16 were not considered for the comparison because of one or more of four main reasons: (i) the lack of reporting of R_a for the utilized rigid surfaces (e.g., Najjar et al. 2007) or geomembranes (e.g., Fishman and Pal 1994; Fleming et al. 2006); (ii) not achieving the large shearing displacement needed to mobilize the drained residual soil-soil and soil-solid interface shear strength (e.g., Tsubakihara et al. 1993); (iii) the lack of reporting of the drained residual shear strength of soils at the effective normal stress range used in interface testing (e.g., Lehane and Jardine 1992; Ganesan et al. 2014; Kuo and Bolton 2014);

and (iv) the use of testing techniques that - based on many researchers (e.g., Stark and Eid 1993; Meehan et al. 2007) - may lead to considerable errors in measuring residual shear strength (e.g., Hammoud and Boumekik 2006). Both the first and third points above were also the reasons for not considering results of several soil-solid interface shear strength tests (e.g., Ramsey 1998; Colliat et al. 2011; White and Cathie 2011) in Fig. 3.16.

The relationship shown in Figs. 3.15 and 3.16 and represented by Eq. 3.3 is developed based on values of interface shear strengths measured for soils with different plasticity and clay-size fractions sheared against surfaces with a wide range of average roughness. This range covers roughness of several materials used in geotechnical engineering practice such as pipeline smooth coatings, R_a of 0.04 to 5 μm (Farshad et al. 2001; White et al. 2011; Ganesan et al. 2014; Kuo and Bolton 2014), smooth geomembranes, R_a of less than 2 μm (Dove and Harpring 1999), and stainless and mild steel, R_a of 0.06 to 2.5 μm (Subba Rao et al. 1998; Lemos and Vaughan 2000). Concrete surfaces (Hammoud and Boumekik 2006) and rough pipeline coatings (Najjar et al. 2007; Ganesan et al. 2014; Kuo and Bolton 2014) possess higher R_a values. Based on the data presented in Fig. 3.16 as well as Eq. 3.3, shearing fine-grained soil against concrete surfaces and rough pipeline coatings should lead to a residual interface efficiency that is slightly less than or equal to 1.0. In this case, the shear zone will likely move away from the interface to occur essentially within the soil matrix and the measured interface shear strength will be predominantly governed by the soil properties. The value of R_a above which shearing would occur mostly within the soil (i.e., the critical average roughness for

surface sheared against fine-grained soils) can be estimated using data of Fig. 3.16 or Eq. 3.3 to be about 20 μm.

The present data supports the use of Eq. 3.3 in estimating the interface residual shear strength as a function of the surface roughness that is within the studied range (i.e., R_a between 0.005 and 10 μm) and the soil residual shear strength provided that the soil-soil and soil-solid interface residual strengths are estimated at the same effective normal stress range. While noting the above, It is advocated that the surface roughness alone may not adequately characterize a given surface. The hardness, yield strength, the solid material stress-strain behavior are likely to impact the overall interface frictional response observed at the solid surface. For example, a given material tested at the same normal stress against two solid surfaces having the same roughness but made of two different materials may not produce the same interface friction angle. Having compatibility between the soil particle size and the interface surface roughness can also affect the measured interface residual shear strength (Kuo et al. 2012). Further studies are warranted to explore these aspects.

In an effort to obtain good correlations with the interface yield shear strength, D_{50} and the average diameter (D_{av}) of soils have been used by several researchers (e.g., Uesugi and Kishida 1986; Paikowsky et al. 1995; Subba Rao et al. 1998 and 2000) to normalize measurements of the maximum and average of surface roughness (i.e., calculate the relative roughness R_{max}/D_{50} or R_a/D_{av}). Oliphant and Maconochie (2007) also suggested that D_{50} can be used in place of D_{av} to normalize R_a. This idea was attempted in the current study for fine-grained soil interface residual shear strength using the normalized average roughness (R_a/D_{50}).

This normalized roughness is plotted against the corresponding residual interface efficiency determined based on data yielded from the testing program presented herein and those reported in the literature (Fig. 3.17). A clear trend of reducing the residual interface efficiency with the decrease of the normalized roughness can be noticed. However, using the normalized roughness did not reduce the level of data scattering below that shown in Fig. 3.16.

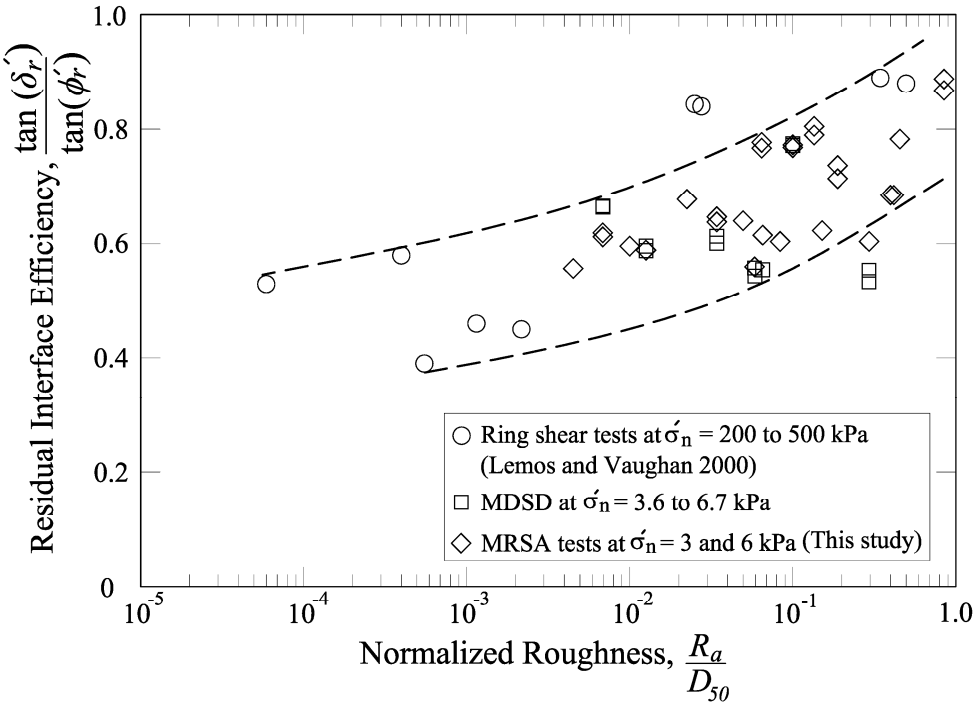

Figure 3.17 Residual interface efficiency for fine-grained soils as a function of the surface normalized average roughness.

Chapter 4. Drained Residual Shear Strength Relevant to Slope Stability Analyses

4.1. Introduction

Shear strength is a key input in any stability analysis of soil slopes. The drained residual shear strength, τ_r, is a crucial parameter in evaluating the stability of slopes that contain a pre-existing shear surface (Skempton 1964 and 1985). It can be also used along with the fully softened shear strength in determining the factor of safety against first-time sliding in stiff plastic clay slopes (James 1970; Bishop 1971; Potts et al. 1997; Stark and Eid 1997; Mesri and Shahien 2003). Significant efforts have been reported in the literature for assessing the residual shear strength through laboratory testing and back analysis of failed case histories. As shown in section 2.4, several empirical correlations have been also presented to estimate such strength as a function of soil index parameters. The performance of most of these correlations have been statistically evaluated in a subsequent section of this chapter.

It is well known that the shear strength envelopes of plastic soils are nonlinear, especially at a low effective normal stress (σ'_n < 50 kPa) range (Terzaghi and Peck 1948; Penman 1953; Bishop et al. 1965 and 1971; Ponce and Bell 1971; Charles and Soares 1984; Atkinson and Farrar 1985; Skempton 1985; Day and Axten 1989; Maksimovic 1989). Such low normal stresses are usually relevant in slope stability analyses at locations where the critical slip surface intersects the face of the slope or passes through shallow depths or zones with high enough pore-water pressures to reduce effective stresses. In spite of this, parameters derived from laboratory shear tests that have been carried out at higher effective normal

stresses are commonly used to represent all zones in slope stability analyses. Even most of the existing residual shear strength correlations that incorporate the effect of the normal stress level (e.g., Stark and Eid 1994; Mesri and Shahien 2003; Stark and Hussain 2013) have also been developed based on testing at a limited number of relatively high effective normal stresses. For example, the currently available correlations do not efficiently cover certain low and moderate ranges of the average effective normal stress ranges (i.e., σ'_n < 50 kPa and 100 kPa < σ'_n < 400 kPa) that have been mobilized in several reported reactivated and long-term first-time landslides in stiff plastic clays. Fig. 4.1 illustrates this limitation for well-documented landslides through English clays (namely; Upper Lias clay, London clay, Oxford clay, Kimmeridge clay, Chalky Boulder clay, Gault clay, Atherfield clay, Etruvia marl, Walton's wood and Jackfield carboniferous mudstone, and Edale shale).

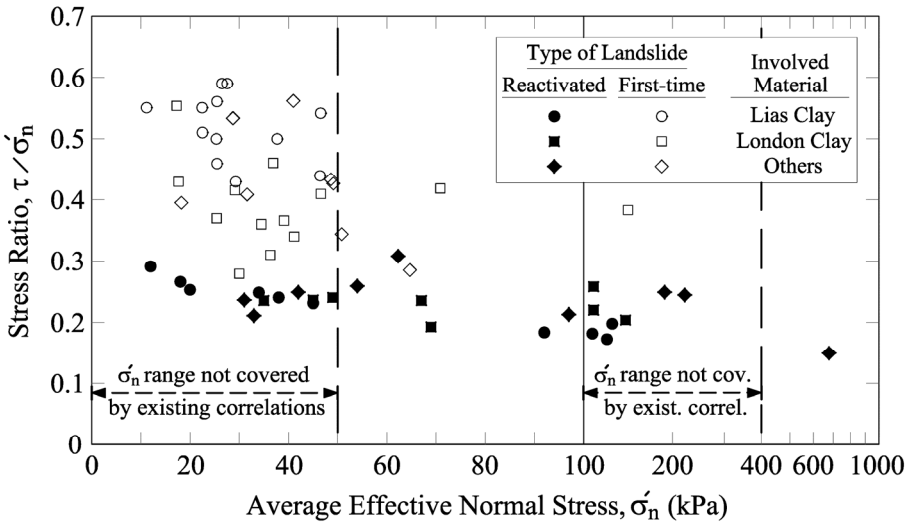

Figure 4.1 Average normal stresses reported for landslides in English soil formations and the normal stress ranges not covered by testing utilized to develop the commonly-used residual strength correlations that incorporate the effect of normal stress (data points from Skempton 1964, 1972, 1977, 1985, James 1970; Chandler 1974, 1976, 1977, 1982, 1984; Chandler and Skempton 1974; Bromhead 1978).

To fill the knowledge gap described above, this chapter mainly presents analysis of residual shear strength tests results which were made available by Eid (2014) at effective normal stresses of 10, 25, 50, 100, 200, 300, 400, and 700 kPa on clays, silts, mudstones, and shales with plasticity and gradation varying over a wide range. The test methods used to get such given data is described in the following section. The data analysis intended to: (i) complement the data set developed through conducting a series of torsional ring shear tests by Eid (1996); and (ii) to consequently revise and update the drained shear strength correlations that have been developed entirely (e.g., Stark and Eid 1994; Mesri and Shahien 2003) or chiefly (e.g., Stark et al. 2005; Stark and Hussain 2013) based on such a data set.

4.2. Testing Method of the Provided Data

The analysis presented in this chapter to develop the revised residual strength correlations utilizes a result of testing a total of 50 clay, silt, mudstone, and shale samples as shown in Table 4.1. The utilized test samples shown in Table 4.1 cover a wide range of liquid limit, plastic limit, plasticity index, clay-size fraction, and activity. Except for the heavily overconsolidated clay, mudstone, and shale samples, Atterberg limits and clay-size fractions were determined in accordance with the particle disaggregation procedure described in ASTM D4318 (1999) and ASTM D422 (1999) or BS 1377 (1990) standards. Most heavily overconsolidated clays, mudstones, and shales possess diagenetic bonding that results in particle aggregation (induration). This aggregation usually survives the standard sample preparation procedure and consequently influences the measured index properties and the accuracy of their correlations to the results of shear strength testing in

which aggregation particles would be battered (La Gatta 1970; Townsend and Banks 1974; AiroFarulla and Rosa 1977; Eid 2001 and 2006). As a result, these materials were disaggregated by ball-milling of representative air-dried samples until all particles passed the standard sieve No. 200. The hydrated ball-milled materials were used in determining the index properties as well as the shear strengths. This sample preparation procedure was adopted from that used by Mesri and Cepeda-Diaz (1986) to determine liquid limit and clay-size fraction that better infer the clay mineralogy and gradation of shales. Updated relationships between index properties of indurated materials disaggregated using the standard and ball-milling sample procedures are given in a subsequent section of this chapter.

Table 4.1 Clay, silt, mudstone, and shale samples used in ring shear tests, the results of which are utilized in the analysis of this study

No.	Soil Name	location	*LL* (%)	*PL* (%)	*CF* [a] (%)	*A (PI/CF)*
1	Fraser-river silt [b, e]	Vancouver, BC, Canada	21	18	9	0.33
2	Glacial till [b,d]	Urbana, IL, USA	24	16	18	0.44
3	Loess [b,d]	Vicksburg, MS, USA	28	18	10	1.00
4	Gray silt [b, e]	Vancouver, BC, Canada	34	17	26	0.65
5	Bootlegger Cove clay [b,d]	Anchorage, AK, USA	35	18	44	0.39
6	Duck Creek shale [c,d]	Fulton, IL, USA	37	25	19	0.63
7	Slide debris [b, e]	San Francisco, CA, USA	37	26	28	0.39
8	Chinle (red) shale [c,d]	Holbrook, AZ, USA	39	20	43	0.44
9	Slopewash material [b, e]	San Luis Dam, CA, USA	42	24	34	0.53
10	Colorado shale [c,d]	Montana, MT, USA	46	25	73	0.29
11	Panoche mudstone [d]	San Francisco, CA, USA	47	27	41	0.40
12	Kaolinite clay [b,e, f]	Hephzibah, GA, USA	48	26	32	0.69
13	Four Fathom shale [c,d]	Durham, England	50	24	33	0.79
14	Mancos shale [d]	Price, UT, USA	52	20	63	0.51
15	Panoche shale [d]	San Francisco, CA, USA	53	29	50	0.48
16	Gulf-bed deposits [b, e]	Doha, Qatar	53	34	18	1.06
17	Red Sea white shale [e]	Alsokhna, Egypt	55	22	50	0.66
18	Comanche shale [c,d]	Proctor Dam, TX, USA	62	32	68	0.44
19	Breccia material [b, e]	Manta, Ecuador	64	41	25	0.92
20	Bearpaw shale [c,d]	Billings, MT, USA	68	24	51	0.86
21	Slide debris [d]	San Francisco, CA, USA	69	22	56	0.84
22	Bay Mud [b,d]	San Francisco, CA, USA	76	41	16	2.19
23	Patapsco shale [c,d]	Washington D.C., USA	77	25	59	0.88
24	Nile deposit [b, e]	Damanhur, Egypt	82	27	58	0.95
25	Pierre shale [c,d]	Limon, CO. USA	82	30	42	1.24
26	Red Sea gray shale [e]	Alsokhna, Egypt	84	27	44	1.30
27	Upper Pepper shale [e]	Waco, TX, USA	89	29	72	0.83
28	Santiago claystone [d]	San Diego, CA, USA	89	44	57	0.79
29	Toshka shale [e]	Toshka, Egypt	91	30	58	1.05
30	Lower Pepper shale [d]	Waco Dam, TX, USA	94	26	77	0.88
31	Altamira Bentonitic tuff [d]	Portuguese Bend, CA, USA	98	37	68	0.90
32	Brown London clay [d]	Bradwell, England	101	35	66	1.00
33	Mokattam yellow shale [e]	Cairo, Egypt	103	33	43	1.63
34	Cucaracha shale [c,d]	Panama Canal	111	42	63	1.10
35	Otay Bentonitic shale [d]	San Diego, CA, USA	112	53	73	0.81
36	Denver shale [c,d]	Denver, CO, USA	121	37	67	1.25
37	Bearpaw shale [c,d]	Saskatchewan, Canada	128	27	43	2.35
38	Mokattam gray shale [e]	Cairo, Egypt	134	37	79	1.23
39	Pierre shale	New Castle, WY, USA	137	32	67	1.57
40	Oahe firm shale [d]	Oahe Dam, SD, USA	138	41	78	1.24
41	Claggett shale [c,d]	Benton, MT, USA	157	31	71	1.78
42	Bentonitic claystone [e]	Fayoum, Egypt	164	55	79	1.38
43	Taylor shale [c,d]	San Antonio, TX, USA	170	39	72	1.82
44	Pierre shale [c,d]	Reliance, SD, USA	184	55	84	1.54
45	Oahe bentonitic shale [d]	Oahe Dam, SD, USA	192	47	65	2.23
46	Panoche clay gouge [d]	San Francisco, CA, USA	219	56	72	2.26
47	Midra gray shale [e]	Sealine, Qatar	231	74	79	1.99
48	Lea Park bentonitic shale [d]	Saskatchewan, Canada	253	48	65	3.15
49	Bearpaw shale [c,d]	Fort Peck Dam, MT, USA	288	44	88	2.77
50	Bentonitic clay [b,e, f]	El Hammam, Egypt	293	46	89	2.78

[a] Quantity of particles < 0.002 mm.

[b] Samples not ball-milled.

[c] Index properties from Mesri and Cepeda-Diaz (1986).

[d] Residual shear strength at normal stress of 50, 100, 400, and 700 kPa from Stark and Eid (1994), and at normal stress of 10, 25, 200, 300 kPa from Eid (2014) were used.

[e] Residual shear strength at normal stress of 10, 25, 50, 100, 200, 300, 400, and 700 kPa from Eid (2014) were used.

[f] Received in the form of powder passed through sieve # 200.

Remolded specimens for ring shear testing were obtained by adding distilled water to the air-dried and processed samples until a liquidity index of 1.5 was obtained. The sample was then allowed to rehydrate for at least one week in a moist room. The modified Bromhead ring shear apparatus described in Stark and Eid (1993) was utilized for measuring the residual shear strength. The modified apparatus allows for eliminating the effect of wall friction during shear which is especially crucial for accurate measurement of low shear stresses developed when testing soils at effective normal stresses as low as 10 kPa.

For each soil presented in Table 4.1, the residual shear strength was determined using a ring shear specimen overconsolidated and presheared at 700 kPa. The multistage shearing process as described in Stark and Eid (1993 and 1994) and ASTM D6467 (1999) was followed for shear testing at normal stresses of 10, 25, 50, 100, 200, 300, 400, and 700 kPa. Multistage shear tests were conducted by Eid (2014) at normal stresses of 10, 25, 200, and 300 only for materials tested in Stark and Eid (1994).

To investigate the degrees of nonlinearity of the residual failure envelopes, the determined residual shear strength values as well as the residual stress ratios (τ_r/σ'_n) are plotted in Fig. 4.2 against the corresponding effective normal stresses. It can be seen that the residual stress ratios are higher at low effective normal stress levels. This clearly indicates the curvature of the residual shear strength envelope. Such curvature or nonlinearity significantly decreases at effective normal stresses higher than 200 kPa. This also shows the importance of having shear strength data at the low and intermediate to high effective normal stresses considered in this study to efficiently describe the shape of the drained residual shear strength failure

envelopes. Details about the degrees of nonlinearity of these envelopes are presented in the subsequent section.

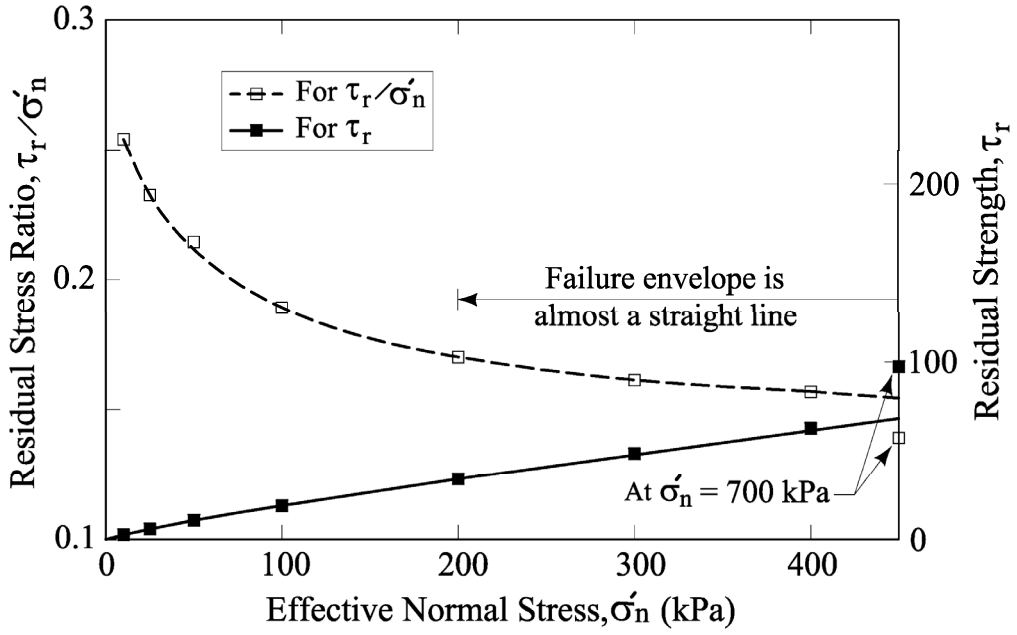

Figure 4.2 Relationship of the residual stress ratio and residual strength to the effective normal stress for Toshka shale.

4.3. Analysis of Residual Strength Results

The soils are sorted into three groups based on their clay-size fraction: less than or equal to 20%, between 25% and 45%, and greater than or equal to 50%. Similar grouping was first introduced by Lupini et al. (1981) to categorize soils that exhibit rolling, translational, and sliding shearing behavior, respectively. This grouping was also adopted by Skempton (1985) for developing his correlation between the residual shear strength friction angle and clay-size fraction. Grouping based on the clay-size fraction (as an indication of particle size) is effective in developing low-scattering correlations between the liquid limit (as an indication of clay mineralogy) and the residual friction angle (Stark and Eid 1994). For soils with

clay-size fractions between 20% and 25%, and 45% and 50%, the friction angle can be estimated by interpolation between the clay-size fraction groups.

4.3.1. Residual Shear Strength Envelope

The provided test results were utilized to study the change in nonlinearity of the shear strength envelope over the effective normal stress ranges occasionally mobilized in slope failures. Fig. 4.3 was developed to present the failure envelope degree of nonlinearity over two effective normal stress ranges of approximately equal spans. The first range is between 10 and 200 kPa while the second is between 200 and 400 kPa. Friction angle ratios were used to represent the degree of nonlinearity in Fig. 4.3. Secant residual friction angles at effective normal stresses of 10, 200, and 400 kPa [i.e., $(ø'_r)_{10}$, $(ø'_r)_{200}$, and $(ø'_r)_{400}$, respectively] were used to calculate these ratios. The secant residual friction angle is defined as the angle between the effective normal stress axis and the line formed from the origin to the residual shear strength at a particular effective normal stress. It can be seen from Fig. 4.3 that the curvature of the envelopes, as represented by the friction angle ratios, is generally more pronounced for soils with moderate to high plasticity and CF $\geq$ 50%. Such curvature is significant at effective normal stresses less than 200 kPa. At the higher effective normal stresses considered in this study, the friction ratios are low and consequently the failure envelope can be assumed as a straight line without significant error (Figs. 4.2 and 4.3). A similar conclusion about the general shape of the residual shear strength envelopes was made by several researchers (e.g., Hawkins and Privett 1985; Maksimovic 1989 and 1996; Tiwari and Marui 2005). Having more curvature at low effective normal stress ranges can be attributed to orienting most of the clay particles in the direction of shear at such

range of stresses. The described general shape of the residual shear strength envelope was considered in presenting the corresponding correlations introduced in the next subsection.

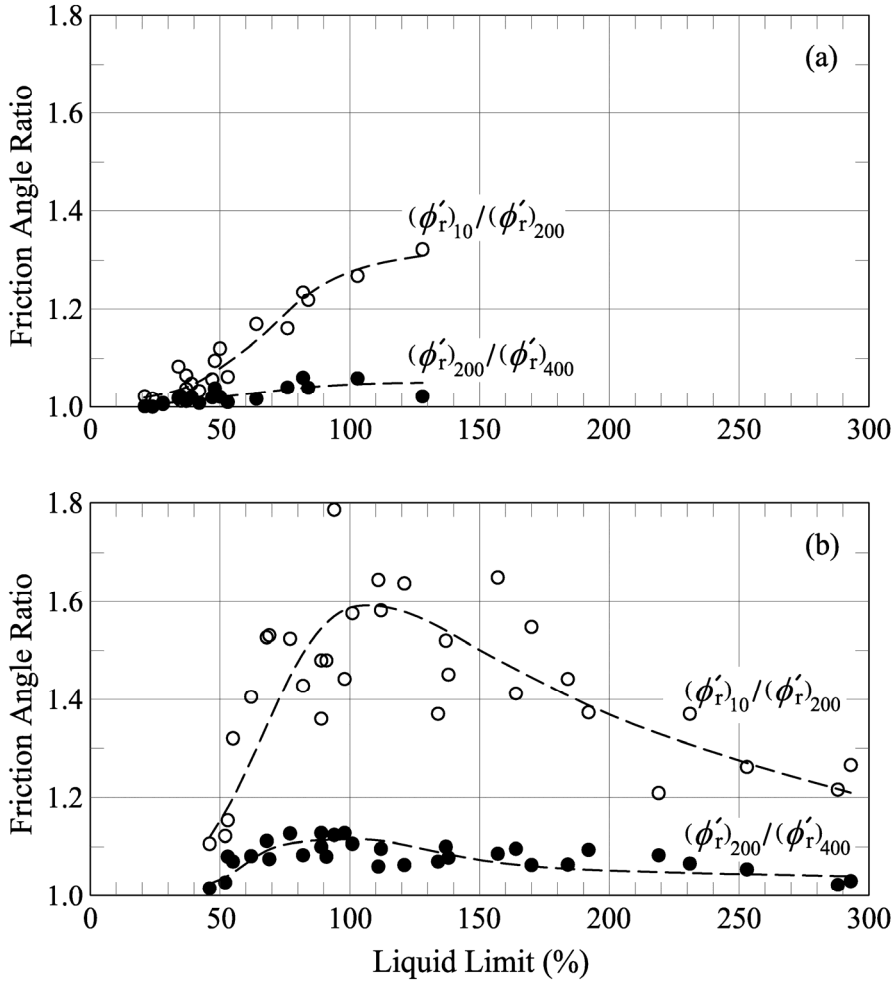

Figure 4.3 Change in the reduction of secant residual friction angle over different ranges of effective normal stress for soils with: (a) CF ≤ 20% and 25% ≤ CF ≤ 45%; (b) CF ≥ 50%.

4.3.2. Empirical Correlations for Estimating Drained Residual Shear Strength

Several empirical correlations of soil shear strengths with index properties are available in the literature (Section 2.4). The correlations are particularly useful for

preliminary designs and when soil samples and funding resources are not readily available for advanced soil testing. Based on the shape of the residual shear strength failure envelope described herein and in the literature, having the shear strength at effective normal stresses of 10, 25, 50, and 100 kPa are needed to more accurately develop the potential significantly-curved initial part of the envelope. The approximately straight-line part of the same envelope that starts at effective normal stress of about 200 kPa can be developed by having the shear strength data at least at a single higher effective normal stress of those occasionally mobilized in slope failures. Consequently, shear strengths measured at effective normal stresses of 10, 25, 50, 100, 200, and 400 kPa were utilized in developing the correlations presented in this chapter. Clearly, the inclusion of data from tests conducted at different effective normal stresses between 10 kPa and 50 kPa as well as between 100 kPa and 400 kPa provides an opportunity to improve the correlations developed by Stark and Eid (1994), Mesri and Shahien (2003), Stark et al. (2005), and Stark and Hussain (2013) for estimating the residual friction angles based on shear testing at effective normal stresses limited to 50, 100, 400, and 700 kPa. For example, drawing a smooth curve by connecting the data from these four effective normal stress levels to the origin of τ versus σ'_n plot to develop the full shear strength failure envelope would lead to underestimating the shear strengths at effective normal stresses lower than 50 kPa as well as the shear strengths at effective normal stresses between 100 and 400 kPa. Fig. 4.4 shows the residual shear strength relationships developed in this study as a function of the liquid limit, clay-size fraction, and effective normal stress. Considering these three parameters combined with the utilization of ball-milled derived index parameters of indurated

materials seems to have resulted in good relationships with less scatter. It is noted that the testing program of this data is limited to sedimentary materials (i.e., material with mostly plate-like clay particles); as such, the relationships shown in Fig. 4.4 can be used to predict the drained residual friction angles of sedimentary fine-grained materials.

Similar to the correlations presented in Chapter 3, the relationships of Fig. 4.4 also exclude soils with distinct contents such as the carbonate soils (White et al. 2012) and soils composed chiefly of allophane or halloysite (i.e., soils with non-platy particles such as volcanic ashes) that are unlikely to have particle rearrangement towards some preferred orientation (Wesley 1977, 1992, and 2003). They also exclude marine soils that contain numerous skeletal remains or faraminifera (Mesri et al. 1975; Najjar et al. 2007). Most of these soils exhibit high friction angle and small or no difference between the drained peak shear strength and the drained residual shear strength regardless of their plasticity (Saldivar and Jardine 2005).

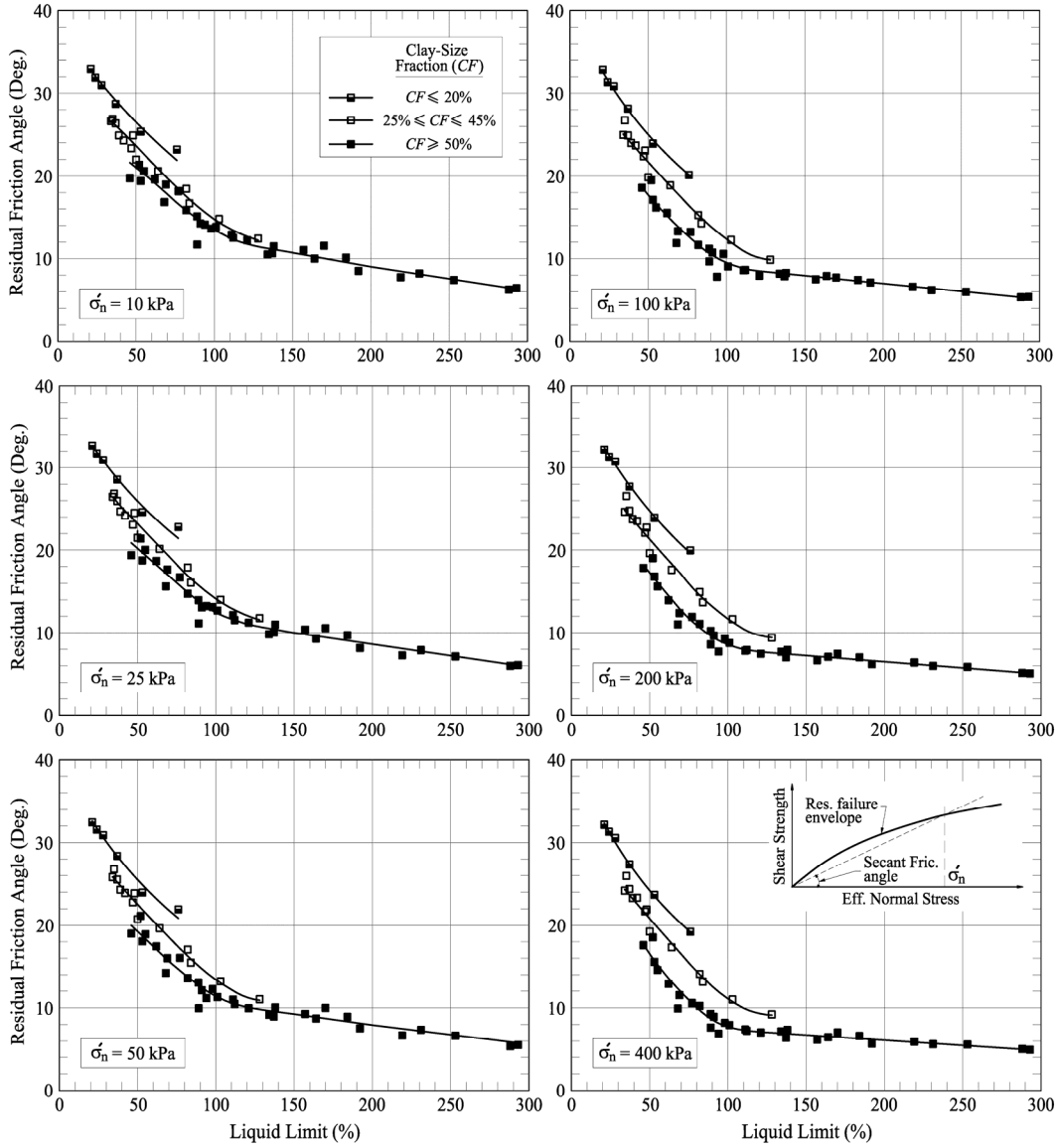

Figure 4.4 Secant residual friction angle relationships with liquid limit and clay-size fraction (sources of data as indicated in Table 4.1)

Fig. 4.4 shows that the secant residual friction angle of soil decreases considerably and almost linearly up to a liquid limit of 80%, higher than which the slope of the relation with liquid limit significantly flattens, especially at high effective normal stresses. Consequently, small errors in measuring the liquid limit

of soils with low to medium plasticity may lead to significant errors in estimated residual shear strengths. The relationships of Fig. 4.4 also show that the influence of the clay-size fraction, as an indication of particle size and shearing mode, on the measured residual friction angles decreases with reducing effective normal stress level. A similar conclusion was made in chapter 3 for residual friction angles of soils at effective normal stresses as low as 3 kPa.

The reduction in the influence of clay-size fraction is clearer for residual friction angles of soils with clay-size fraction equal to or higher than 25% as indicated by the nearness of the clay-fraction trend lines for $\sigma'_n \leq 25$ kPa (Fig. 4.4). It should be noted that the distinguished effect of clay-size fraction on developing different residual shear strength modes, and in turn on the measured friction angles, was presented by several researchers for relatively higher effective normal stresses [e.g., Lupini et al. (1981) for effective normal stress of 350 kPa and Skempton (1985) for 100 kPa].

To reinterpret slope failures that were presented in the literature without including information on clay-size fraction, Mesri and Shahien (2003) re-plotted the residual shear strength data from Stark and Eid (1994) and Eid (1996) against the plasticity index; in essence, plasticity index was considered a parameter that would encapsulate the effect of both liquid limit and clay-size fraction. A clear relationship between soil plasticity index and clay-size fraction has also been shown by Kenney (1959) and Nelson (1992). Using a similar line of thinking, the residual shear strength data from this study for six different effective normal stresses were also plotted against the plasticity index as shown in Fig. 4.5. Decreasing trends of the secant residual friction angle with increasing of plasticity

index can be clearly seen from these results. The comparison between the data scattering in Fig. 4.4 and 4.5 shows the importance of incorporating the clay-size fraction into the residual shear strength relationships. Similar conclusion was made by Kaya (2010) through a comprehensive sensitivity analysis based on a database of residual shear strength. The relationships shown in Fig 4.5 can still be useful in case of analyzing shallow slopes or mobilizing low effective normal stresses at which the percentage of clay particles has a small effect on the residual friction angle. Fig. 4.5 also helps in analyzing slopes with difficulties in determining the clay-size fraction as measured by the sedimentation method due to interaction and flocculation between soil particles (Bishop et al. 1971; Mesri and Cepeda-Diaz 1986; Wesley 2003).

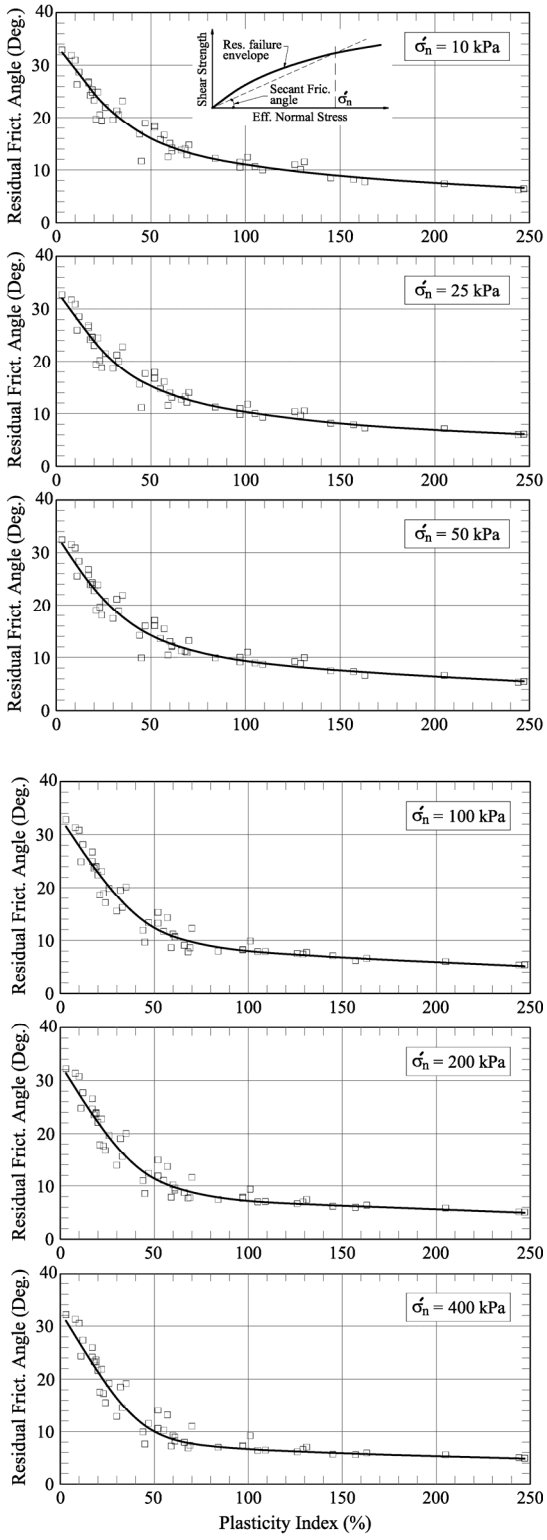

Figure 4.5 Secant residual friction angle relationships with plasticity index (sources of data as indicated in Table 4.1).

4.3.2.1. Effect of Sample Preparation on The Measured Liquid limit, Plasticity Index and Clay-Size Fraction

As explained previously, the liquid limit and clay-size fraction of heavily overconsolidated clays, mudstones, and shales shown in Table 4.1 were determined using ball-milled samples. The commercial laboratories usually utilize the standard sample preparation procedures described in ASTM D422 (1999) and ASTM D4318 (1999) or BS 1377 (1990) for determining Atterberg limits and clay-size fraction. Using these standard-derived indices may lead to overestimating the friction angles of heavily overconsolidated clays, mudstones, and shales (Eid 2006). Consequently, the standard-derived index parameters should be adjusted before estimating the residual friction angles of these indurated materials using the empirical correlations presented in this chapter.

Eid (2001 and 2006) made a comprehensive study on the effect of particle disaggregation, sample size, and rehydration time on the measured classification indices of shales. Liquid limits, plastic limits, and clay-size fractions derived from the standard sample preparation procedure (LL_{ST}, PL_{ST}, and CF_{ST}) and those resulted from using ball-milled samples (LL_{BM}, PL_{BM}, and CF_{BM}) of the same shales were determined. Data presented in these studies are plotted to have a relationship between LL_{ST} and LL_{BM} as shown in Fig. 4.6a. A similar relationship is presented in Fig. 4.6b for the plasticity indices (i.e., PI_{ST} and PI_{BM}). Based on the same database, a relationship between clay-size fraction values derived from the standard sample preparation procedure in terms of the activity, A_{ST} and those derived using ball-milled samples is shown in Fig. 4.6c. Results of a similar sample preparation study presented by Stark et al. (2005) were also superimposed on Fig.

4.6a. Because of the lack of availability of the plastic limits, the results of such study were not represented in parts "b" and "c" of Fig. 4.6. Fig. 4.6 clearly shows the effect of sample preparation procedure on the measured liquid limit, plasticity index and clay-size fraction. For all practical purposes, the nonlinear relationships between the index properties derived from the standard and ball-milling sample preparation techniques shown in Fig. 4.6 can be expressed using the following simple equations

$$LL_{BM} = 1.4 LL_{ST} \tag{4.1}$$

$$PI_{BM} = 1.7 PI_{ST} \tag{4.2}$$

$$CF_{BM} = CF_{ST} + 30 A_{ST}^2 \qquad for\ A_{ST} < 1.0 \tag{4.3a}$$

$$CF_{BM} = CF_{ST} + \frac{30}{A_{ST}^2} \qquad for\ A_{ST} > 1.0 \tag{4.3b}$$

For Red sea shale with LL_{ST} = 57%, PI_{ST} = 32%, CF_{ST} = 25%, and A_{ST} = 1.28, Eid (2006) reported values of LL_{BM} = 84%, PI_{BM} = 57%, CF_{BM} = 44%. These ball-milled derived liquid limit, plasticity index, and clay-size fraction can be estimated using Equations 4.1, 4.2, and 4.3 as 80%, 54%, and 43%, respectively. It should be noted that data scattering around the relationships shown in Fig. 4.6 can be attributed to the variation in the degree of induration of the tested materials. The increase in such scattering for materials with considerably high LL_{BM} and PI_{BM} would not have a significant effect on predicting the residual friction angle using the correlations of Figs. 4.4 and 4.5 due to the flatness of their trend lines in these liquid limit and plasticity index ranges.

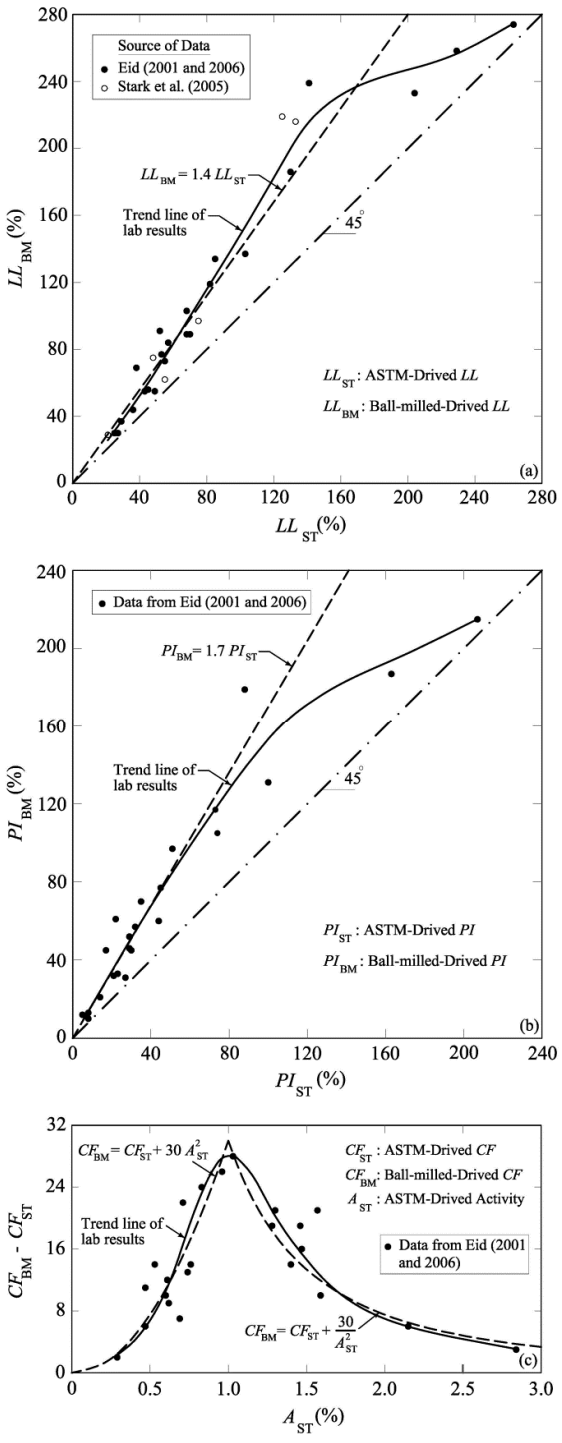

Figure 4.6 Relationships between index parameters of shales, mudstones, and heavily overconsolidated clays disaggregated using the standard and ball milling procedures for: (a) liquid limit; (b) plasticity index; (c) clay-size fraction.

To facilitate the process of estimating the secant residual friction angle as a function of liquid limit, clay-size fraction and effective normal stress, the trend lines of Fig. 4.4 were re-plotted as shown in Fig. 4.7a. The equations needed to adjust the index parameters for estimating the friction angles of indurated materials are also encompassed in the same figure. The test data points were not shown in Fig. 4.7a for clear presentation and better comparison between trend lines of different clay-size fraction groups and effective normal stress levels. The configuration of Fig. 4.7a also helps to make the interpolation needed to estimate the drained friction angle in case of having clay-size fraction or effective normal stress different from those shown in the figure. The presentation technique used in Fig. 4.7a was used to develop residual shear strength correlation as a function of the plasticity index and effective normal stress (Fig 4.7b).

The residual shear strength presented in the current study at relatively low effective normal stresses (i.e., 10 and 25 kPa) and correlated to soil index properties can be utilized in different geotechnical engineering applications rather than the slope stability analyses. Such applications include stability assessment of earth reinforcement, anchor rods, near-shore pipelines placed on seabed, and driven piles supporting shallow-water platforms.

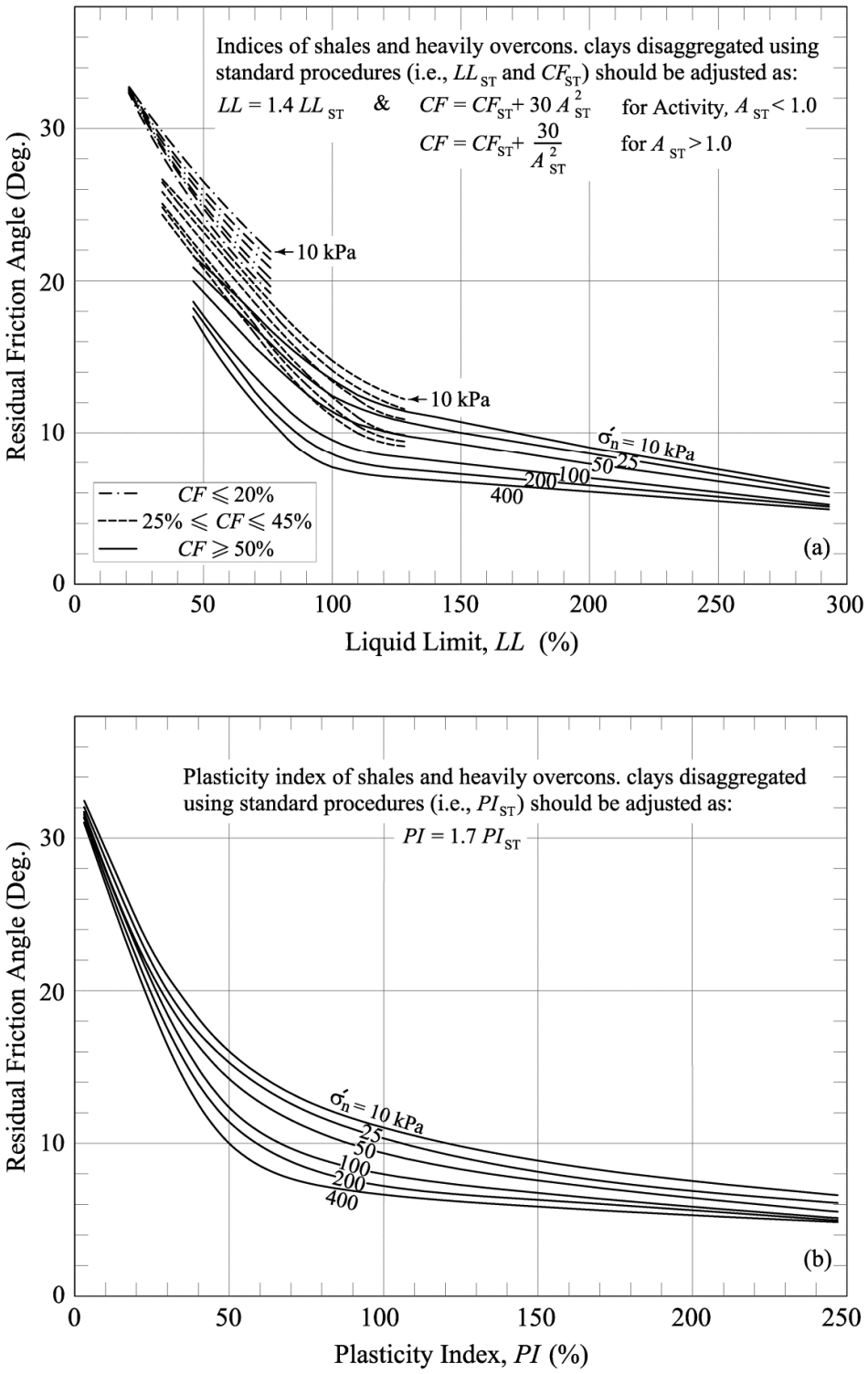

Figure 4.7 Drained secant residual friction angle correlation as a function of: (a) liquid limit, clay-size fraction and effective normal stress; (b) plasticity index and effective normal stress.

4.4. Suitability of the Correlations

The suitability of using the correlations presented in this chapter to estimate soil drained residual shear strength at effective normal stresses relevant to slope stability analyses is illustrated in this section. This was done through checking the back-calculated residual friction angles reported for different case histories of reactivated landslides $[\phi'_r]_{BC}$ against those predicted, $[\phi'_r]_{PR}$, using these correlations and other residual shear strength correlations available in the literature. Fifty four landslides through sedimentary fine-grained materials (i.e., clays, marls, mudstones, and shales) were used for such checking. These case histories (Table 4.2) were chosen from the large number of reactivated landslides reported in the literature considering the need to have the following good reported data/information required for a worthy comparison: (1) a well-defined slip surface passing mostly through one material of a type similar to that of the materials tested in the current study (i.e., soils with mostly plate-like clay particles or minerals); (2) measured the pore-water pressures; (3) plasticity limits and clay-size fraction (defined as the quantity of particles smaller than 0.002 mm); (4) geometric configurations and unit weights that would allow accurate calculation of the average effective normal stress acting on the slip surface; and (5) drained residual friction angle back-calculated using a zero cohesion intercept in the effective stress space. For each considered case history, the reported data needed for the comparison are listed in Table 4.2.

Table 4.2 Reactivated landslides and reported soil indices and parameters used to calibrate the residual shear strength correlations

No.	Site	Stratum	*LL* (%)	*PL* (%)	*CF* [a] (%)	*A*	σ_n' [b] (kPa)	$[\phi_r']_{BC}$ [c] (deg.)	Reference
1-5	Chiusi della Verna (5 slides), Tuscany, Italy	Clay shale	40[d]	19[d]	46[d]	0. 45[d]	166-588 (av.=378)	11.7-15.6 (av.=13.2)	Canuti et al. (1994)
6	River Beas Valley, India	Siwalik rock	41	25	32	0.5	200	18-20	Henkel and Yudhbir (1966); Skempton and Hutchinson (1969)
7	Jackfield, Shropshire, UK	Carboniferous mudstone	45	20	42	0.6	62.3	17.1	Henkel and Skempton (1955); Skempton (1964)
8	St. Martino Valley, Italy	Weathered marl	46[d]	23[d]	38[d]	0.5[d]	228	17	Bertini et al. (1984)
9	Weirton,West Virginia, USA	Colluvium[e]	51	26	55	0.46	140	16	D'Appolonia et al. (1967)
10	St. Cristoforo, Italy	Lugagnano clay	53[d]	27[d]	38[d]	0.7[d]	115	11.5	Cancelli (1981)
11	Mam Tor, Berbyshire, UK	Edale shale	53	28	35	0.7	170-210 (av.=188)	14	Skempton et al. (1989)
12-19	Seattle Freeway (8 slides), Seattle, USA	Lawton clay	55[d]	24[d]	55-60	0.54	85-185 (av.=127)	13.6-16.5 (av.=15.3)	Palladino and Peck (1972)
20	Walton's Wood, Staffordshire, UK	Carboniferous mudstone	57	27	70	0.43	54	13.5-15.5	Early and Skempton (1972)
21	Lyme Regis, UK	Lower Lias clay	57	28	60	0.48	125	11.2	James (1970)
22	Bury Hill, Staffordshire, UK	Etruria marl	60	27	52	0.64	97	12	Hutchinson et al. (1973); Skempton (1985)
23	Burderop Wood, Swindon, UK	Gault clay	64[d]	29[d]	47[d]	0.75[d]	31	13.3	Skempton (1972, 1985)
24	Hodson, Swindon, UK	Gault clay	64[d]	29[d]	47[d]	0.75[d]	42	14	Skempton (1972, 1985)
25	Folkestone Warren, slip W4, Kent, UK	Gault clay	64[d]	29[d]	47[d]	0.75[d]	608-749	7.7-9.4	Hutchinson (1969); Hutchinson et al. (1980); Skempton (1985)
26	Barnsdale, Leicestershire, UK	Upper Lias clay	64[d]	28[d]	52[d]	0.7[d]	92	10.4	Chandler (1976, 1982)
27	Hambleton, Leicestershire, UK	Upper Lias clay	64[d]	28[d]	52[d]	0.7[d]	107	10.3	Chandler (1976, 1982)
28	Uppingham, Leicestershire, UK	Upper Lias clay	64[d]	28[d]	52[d]	0.7[d]	12	16.2	Chandler (1970, 1976)
29	Gretton, Northamptonshire, UK	Upper Lias clay	64[d]	28[d]	52[d]	0.7[d]	38	13.5	Chandler et al. (1973); Chandler (1982)
30	Daventry, Northamptonshire, UK	Upper Lias clay	64[d]	28[d]	52[d]	0.7[d]	45	13	Biczysko and Starzewski (1977a,b); Chandler (1982)
31	Rockingham, Northamptonshire, UK	Upper Lias clay	64[d]	28[d]	52[d]	0.7[d]	34	13.9	Chandler (1971, 1976)
32	Weedon, Northamptonshire, UK	Upper Lias clay	64[d]	28[d]	52[d]	0.7[d]	20	14.2	Chandler et al. (1973); Chandler (1982)
33	Wansford, Cambs, UK	Upper Lias clay	64[d]	28[d]	52[d]	0.7[d]	120	9.8	Chandler (1979, 1982)
34	Wardley, Leicestershire,UK	Upper Lias clay	64[d]	28[d]	52[d]	0.7[d]	18	14.9	Chandler (1982)
35	Endcombe, UK	Atherfield clay	66[d]	25[d]	28[d]	1.46[d]	220	13.7	James (1970)
36	Patney-Chirton, UK	Gault clay	68	25	47[d]	0.92	33	11.9	James (1970); Skempton (1985)
37	Petrofka, Saskatchewan, Canada	Bedrock clay	69	27	42	1.0	830	5.7	Eckel et al. (1987)
38	Spinney Hill, Saskatchewan, Canada	Clay shale	70[d]	26[d]	>50%	NA	183	8.7	Sauer (1984)
39	Denholm, Saskatchewan, Canada	Bedrock clay	78	31	50	0.94	408	6.7	Christiansen (1983); Sauer (1983); Sauer and Christiansen (1987)
40	Hadleigh, (slip surf. 2&3), Essex, UK	Brown London clay	80[d]	29[d]	55[d]	0.9[d]	35	13.2	Hutchinson and Gostelow (1976)
41	Hadleigh, (slip surf. 5), Essex, UK	Brown London clay	80[d]	29[d]	55[d]	0.9[d]	45	13.3	Hutchinson and Gostelow (1976)
42	Hadleigh, (slip surf. 8), Essex, UK	Brown London clay	80[d]	29[d]	55[d]	0.9[d]	49	13.5	Hutchinson and Gostelow (1976)
43	Hadleigh, (slip surf. 12), Essex, UK	Brown London clay	80[d]	29[d]	55[d]	0.9[d]	67	13.2	Hutchinson and Gostelow (1976)
44	Guildford, Surrey, UK	Brown London clay	80[d]	29[d]	55[d]	0.9[d]	69	10.9	Skempton and Petley (1967); Chandler (1982)
45	Beacon Hill, Herne Bay, Kent, UK	Brown and Blue London clay	80[d]	29[d]	55[d]	0.9[d]	108	14.1-14.8	Wise (1957); Hutchinson (1965b); Bayley (1972); Bromhead (1978)
46–47	Queen's Avenue, (1966,1970), Herne Bay, Kent, UK	Brown and Blue London clay	80[d]	29[d]	55[d]	0.9[d]	103-113	12.3-12.5	Hutchinson (1965b); Bromhead (1978)
48–51	Miramar, (1953, 1956, 1966, 1970), Hern Bay, Kent, UK	Brown and Blue London clay	80[d]	29[d]	55[d]	0.9[d]	123-154	10.8-12.3	Hutchinson (1965a,b); Bayley (1972); Bromhead (1972,1978)
52	San Diego, California, USA	Santiago claystone	89[f]	44[f]	57[f]	0.79[f]	288	7.5	Stark and Eid (1992, 1998)
53	Portuguese Bend, California, USA	Altamira bentonitic tuff	98[f]	37[f]	68[f]	0.90[f]	500	6.5	Stark and Eid (1994); Eid (1996)
54	Gardiner Dam, Saskatchewan, Canada	Bearpaw Shale	128[f]	27[f]	43[f]	2.35[f]	95	9.8	Jasper and Peters (1979); Mesri and Capeda-Diaz (1986); Stark and Eid (1994)

[a] Quantity of particles < 0.002 mm; [b]Average effective normal stress on the slip surface; [c]Back-calculated residual friction angle reported for c' = 0; [d]Average value; [e]Not indurated; [f]Indices for ball-milled materials.

4.4.1. Predicted and Back-Calculated Residual Shear Strength Angles

To predict the residual friction angle for a case history using each of the correlations of Fig. 4.7, a residual shear strength failure envelope of the concerned material was first developed by drawing a smooth curve connecting the shear strengths estimated at different effective normal stresses utilizing the reported liquid limit and clay-size fraction, or plasticity index (note that the index parameters were adjusted in case of sliding through indurated materials). The predicted residual friction angle was then determined as the inclination angle of a secant of the developed envelope at the reported average effective normal stress acting on the slip surface. Comparison between the back-calculated residual friction angles and those predicted using the correlations presented in this study is shown in Fig. 4.8. To evaluate the performance of the residual shear strength correlations presented in this chapter compared with those of similar correlations available in the literature, the back-calculated friction angles reported for the case histories listed in Table 4.2 were also checked against the friction angles predicted using twenty four of the residual shear strength correlations existing in the literature (Table 4.3). The back-calculated friction angles and the corresponding angles predicted using a representative set of these correlations as well as the correlation of Fig. 4.7a are shown in Fig. 4.9 for graphical comparison. All of the graphical correlations used in the comparison as well as their associated predicted angles plotted against the corresponding back-calculated residual friction angles are shown in Appendix A.

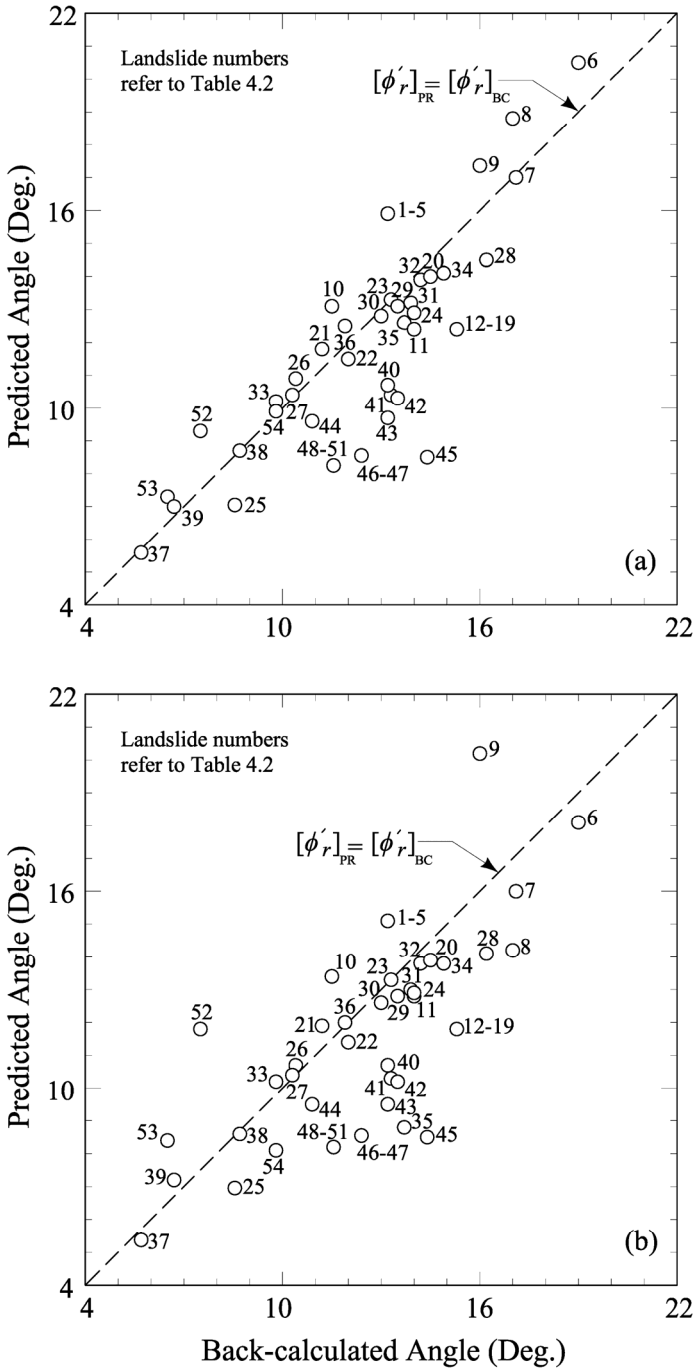

Figure 4.8 Comparison between the back-calculated secant residual friction angles and those predicted using the correlations developed in this study as a function of: (a) liquid limit, clay-size fraction, and effective normal stress [Fig. 4.7a]; (b) plasticity index and effective normal stress [Fig. 4.7b].

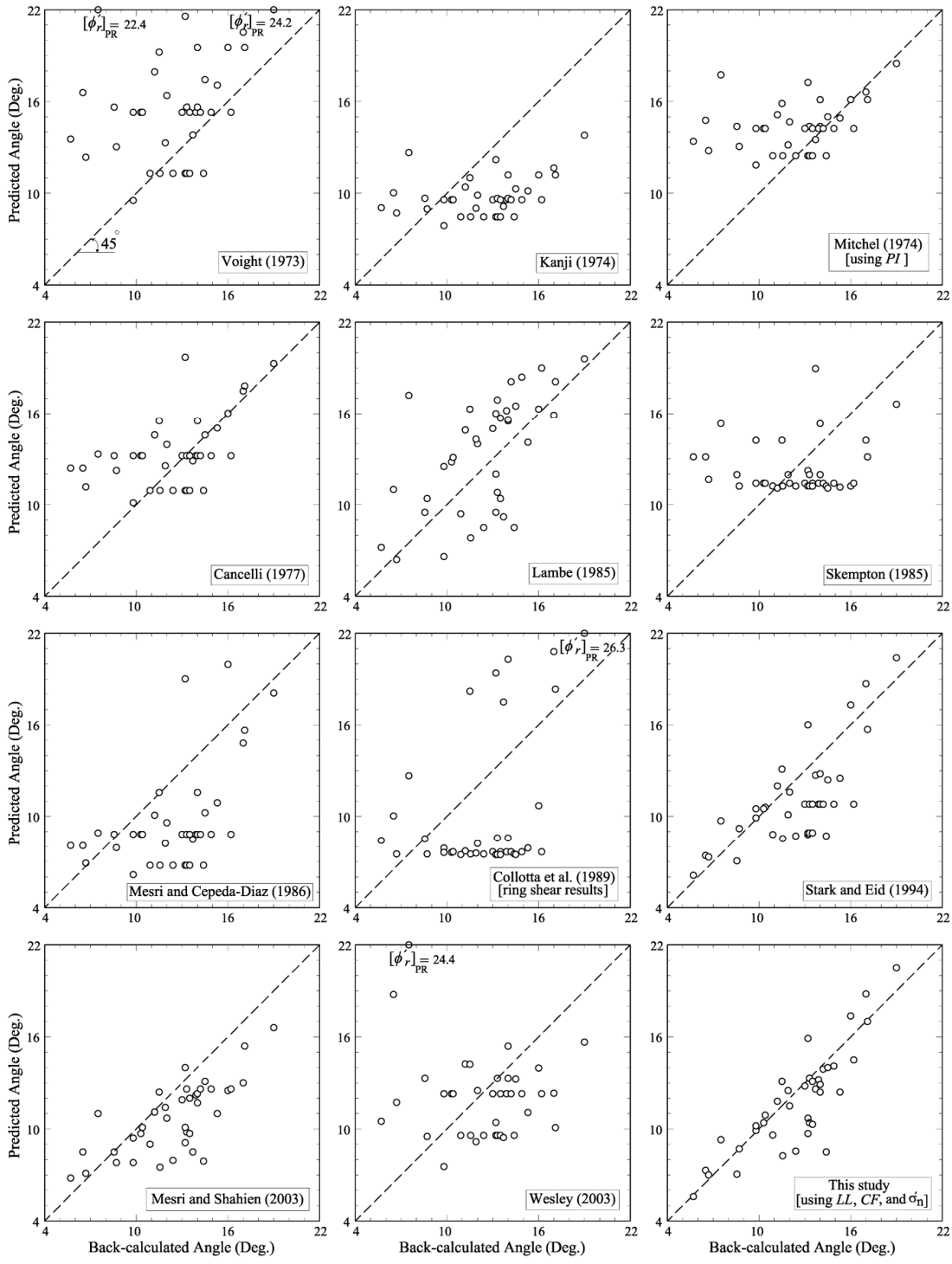

Figure 4.9 Comparison between the back-calculated secant residual friction angles and those predicted using different empirical correlations.

4.4.2. Calibration of Residual Shear Strength Correlations Through Statistical Analysis

In an attempt to quantify statistically the performance of the correlations developed in this study (in predicting the residual friction angles back-calculated from the reactivated landslides) compared with those of the other correlations listed in Table 4.3, the coefficient of determination (R^2) of the regression equation defined by $[\phi'_r]_{PR} = [\phi'_r]_{BC}$, as well as the mean ($\mu$) standard deviation ($S$), and coefficient of variation (COV) of the ratio $[\phi'_r]_{PR} / [\phi'_r]_{BC}$ were calculated for each correlation. The correlations developed in this study seem to yield the highest R^2, closest μ to 1.0, and the lowest S and COV (Table 4.3) compared to other correlations – thus, suggesting the suitability of the correlations proposed in the current study in terms of their accuracies and precisions. This can be attributed to well accounting for the effects of clay mineralogy, soil texture, sample preparation techniques, and effective normal stress in ranges that are relevant to slope stability analyses.

The work undertaken in this study confirms that considering the effect of normal stress is important for better prediction of the residual friction angle as most of the correlations that incorporate the effective normal stress yield fair agreement between the prediction and back-calculated angles indicated by having values close to 1.0 for μ, and relatively low S and COV (Table 4.3). However, the relative performance of these correlations would be governed by the levels of effective stress, soil index parameters and their range, method of sample preparation and testing, and number of data points used in presenting each correlation. For example, in spite of having trend lines that represent effective

normal stresses as low as 19.6 kPa, the correlation presented by Lambe (1985) as a function of the plasticity index was developed based on a relatively few number of tests on Amuay soils only. On the other hand, Stark and Eid (1994) developed their correlation based on a considerable number of test results of several soil and shale types. However, they only covered the high level of effective normal stresses relevant to slope stability analyses. By adding more ring shear test results to those presented in Stark and Eid (1994), Stark et al. (2005) introduced a revisited residual strength correlation that has the same limitation in addition to those related to utilizing index parameters of claystones and shales derived from different sample preparation procedures, miss plotting some of the Stark and Eid (1994) data points (e.g., those of Bearpaw shale, Saskatchewan, Canada), and using some results collected from commercial sources. Kaya (2009) noted that the revised correlation by Stark et al. (2005) shows a larger data scatter up to *LL* of 100%. This may be the reason for the lower R^2 value observed in Table 4.3 for the Stark et al. (2005) correlation compared with that of Stark and Eid (1994) in predicting the back-calculated friction angles. The correlation of Stark and Hussain (2013) inherited the same limitations but exhibits a performance better than that of Stark et al. (2005) correlation due to extending the covered level of effective normal stress down to 50 kPa.

Table 4.3 Results of statistical analysis and calibration of residual shear strength correlations used in predicting the back-calculated friction angles reported for reactivated landslides considered in this study.

Correlation reference	Source of test data	Test device and σ_n' used	Parameters used for prediction	R^2 for $[\phi_r']_{PR} = [\phi_r']_{BC}$	Statistical parameters for the ratio $[\phi_r']_{PR} / [\phi_r']_{BC}$		
					μ	S	COV
Skempton (1964)[a]	Skempton (1964)	Direct shear, σ_n' = 35 to 280 kPa	*CF*	—[f]	1.41	0.53	0.38
Voight (1973)	Kenney (1967); Nonveiller (1967); Skempton and Petley (1967); D'Appolonia et al. (1967); Skempton et al. (1969); Hutchinson (1967, 1969); Chandler (1969, 1970); Hamel (1970)	Direct shear, σ_n' = 10 to 885 kPa	*PI*	—[f]	1.32	0.48	0.36
Kanji (1974)	Bishop et al. (1971); Tulinov and Molokov (1971); Kanji (1970, 1972); Townsend and Gilbert (1973)	Direct shear and Ring shear, σ_n' = 6.9 to 1177 kPa	*PI*	—[f]	0.84	0.27	0.33
Mitchel (1976)[a]	Deere (1974)	—[b]	*LL*	—[f]	1.28	0.37	0.29
Mitchel (1976)[a]	Deere (1974)	—[b]	*PI*	—[f]	1.23	0.39	0.32
Cancelli (1977)	Jamiolkowski and Pasqualini (1976)	—[b]	*LL*	—[f]	1.14	0.33	0.29
Lupini et al. (1981)	Lupini et al. (1981)	Ring shear, σ_n' = 177 to 352 kPa	*PI*	—[f]	1.85	0.65	0.35
Lambe (1985)[e]	Lambe (1985)	Direct shear, σ_n' = 19.6, 48, 98, and 196 kPa	*PI,* and σ_n'	0.27	1.10	0.31	0.28
Skempton (1985)[a]	Skempton (1985)	Ring shear, $\sigma_n' \simeq$ 100 kPa	*CF*	—[f]	1.06	0.39	0.36
Mesri and Cepeda-Diaz (1986)	Kenney (1967); Mesri and Cepeda-Diaz (1986)	Direct shear, σ_n' = 19.6 to 785 kPa	*LL*[c]	—[f]	0.79	0.26	0.32
Collotta et al. (1989)[a]	Collotta et al. (1989)	Direct shear, σ_n' = 100 to 700 kPa	$CALIP = (CF)^2 \times LL \times PI \times 10^{-5}$	—[f]	0.96	0.54	0.56
Collotta et al. (1989)[a]	Collotta et al. (1989)	Ring shear, σ_n' = 100 to 700 kPa	$CALIP = (CF)^2 \times LL \times PI \times 10^{-5}$	—[f]	0.85	0.37	0.44
Nelson (1992)	Nelson (1992)	Direct shear, σ_n' = 96, 192, 383, and 479 kPa	*LL*	0.26	1.03	0.35	0.34
Nelson (1992)	Nelson (1992)	Direct shear, σ_n' = 96, 192, 383, and 479 kPa	*PI*	0.05	1.04	0.52	0.50
Nelson (1992)	Nelson (1992)	Direct shear, σ_n' = 96, 192, 383, and 479 kPa	*CF*	—[f]	0.78	0.33	0.42
Stark and Eid (1994)[e]	Stark and Eid (1994)	Ring shear, σ_n' = 100, 400, and 700 kPa	*LL*[c], *CF*[c], and σ_n'	0.23	0.90	0.18	0.20
Mesri and Shahien (2003)[a,e]	Stark and Eid (1994); Eid (1996)	Ring shear, σ_n' = 50, 100, and 400 kPa	*PI* [c], and σ_n'	—[f]	0.88	0.18	0.20
Wesley (2003)[a]	Townsend and Gilbert (1973); Lupini et al. (1981); Wesley (1992)	Ring shear, and Direct shear, σ_n' = 6.9 to 1177 kPa	$\Delta I_p = PI - 0.73\ (LL\text{-}20)$	—[f]	1.06	0.55	0.52
Sridharan and Raghuveer Rao (2004)	Townsend and Gilbert (1973); Lupini et al. (1981); Wesley (1992); Wesley (2003)	Ring shear, and Direct shear, σ_n' = 6.9 to 1177 kPa	*LL*	—[f]	0.99	0.29	0.29
Sridharan and Raghuveer Rao (2004)	Townsend and Gilbert (1973); Lupini et al. (1981); Wesley (1992); Wesley (2003)	Ring shear, and Direct shear, σ_n' = 6.9 to 1177 kPa	*CF*	—[f]	0.93	0.37	0.39
Sridharan and Raghuveer Rao (2004)	Townsend and Gilbert (1973); Lupini et al. (1981); Wesley (1992); Wesley (2003)	Ring shear, and Direct shear, σ_n' = 6.9 to 1177 kPa	*LL,* and ΔI_p	—[f]	1.03	0.33	0.32
Stark et al. (2005)[e]	Stark and Eid (1994); Stark et al. (2005)	Ring shear, σ_n' = 100, 400, and 700 kPa	*LL*[d], *CF*[d], and σ_n'	0.12	0.88	0.21	0.23
White and Randolph (2007)	White and Randolph (2007)	Ring shear, σ_n' = 50 to 300 kPa	σ_n'	0.21	1.09	0.52	0.48
Stark and Hussain (2013)[e]	Eid (1996); Stark et al. (2005); Stark and Hussain (2013)	Ring shear, σ_n' = 50, 100, 400, and 700 kPa	*LL*[d], *CF*[d], and σ_n'	0.26	0.89	0.19	0.21
This study[e,g]	Stark and Eid (1994) ; Eid (1996); This study	Ring shear, σ_n' = 10, 25, 50, 100, 200, and 400 kPa	*LL*[c], *CF*[c], and σ_n'	0.65	0.95	0.14	0.15
This study[e,g]	Stark and Eid (1994) ; Eid (1996); This study	Ring shear, σ_n' = 10, 25, 50, 100, 200, and 400 kPa	*PI* [c], and σ_n'	0.40	0.94	0.19	0.20

[a]Average curve for the correlation upper and lower bounds was used in determining $[\phi_r']_{PR}$

[b]No available information

[c] Reported index properties of shales, mudstones, and overconsolidated clays were adjusted using the relationships of Fig. 4.6 or Eqs 4.1, 4.2, and 4.3 of this study

[d] Reported index properties of shales, mudstones, and overconsolidated clays were adjusted using the relationships presented in the correlation reference

[e]$[\phi_r']_{PR}$ determined as the inclination of a secant of the envelope-developed as a smooth curve connecting shear strengths estimated at σ_n' values utilized in the correlation-at the reported average σ_n' acting on the slip surface

[f]Failure to represent the linear relationship of $[\phi_r']_{PR} = [\phi_r']_{BC}$

[g]Ranked the best based on their ability to predict the back-calculated friction angles for the considered cases (i.e., having highest R^2, closest μ to 1.0, and the lowest S and COV)

As it considers the effect of normal stress only, the correlation presented in White and Randolph (2007) either overestimates or underestimates the back-calculated residual friction angles mobilized at low or high average effective normal stresses, respectively, of the reactivated landslides shown in Table 4.2. This may interpret having a reasonable value of μ, and high values of S and COV for the ratio $[\text{ø'}_r]_{PR}$ / $[\text{ø'}_r]_{BC}$ corresponding to such correlation (Table 4.3). As described earlier, by not considering shear strength data at effective normal stress ranges below 50 kPa and between 100 kPa and 400 kPa, the other existing residual shear strength correlations that incorporate the effect of normal stress underestimate the residual shear strength at these effective normal stress ranges and consequently have the tendency to underestimate the back-calculated residual friction angles (Fig. 4.9).

4.5. Expression to Account for Stress Dependency of Residual Friction Angle

Using residual shear strength correlations shown in Fig. 4.7, it is possible to propose the following expression that would account for the dependence of the residual friction angle on the effective normal stress

$$(\phi_r')_{\sigma_n'} = (\phi_r')_{P_a}\left[\frac{P_a}{\sigma_n'}\right]^{m_r} \tag{4.4}$$

where $(\text{ø'}_r)_{\sigma'n}$ is the secant residual friction angle at any effective normal stress σ'_n, higher than zero and $(\text{ø'}_r)_{Pa}$ is the secant residual friction angle at an effective normal stress equal to the atmospheric pressure "P_a" (i.e., 100 kPa). The parameter m_r is a constant that is practically independent of σ'_n. Values of m_r were

determined as the slopes of ln $[(\text{ø}'_r)_{\sigma'n}/(\text{ø}'_r)_{Pa}]$ versus ln $[P_a/\sigma'_n]$ for soils with several liquid limits and clay-size fractions as well as several plasticity indices. An example of such process is shown in Fig. 4.10. It can be seen that having test results at the wide range of effective normal stress utilized in this study helped in better estimation of the values of m_r. These values are plotted in Fig. 4.11a to be used in case of utilizing the liquid limit and clay-size fraction for estimating the secant residual friction angles. In case of utilizing the plasticity index for such estimation, Fig. 4.11b is to be used for determining the magnitudes of m_r. It should be noted that Equation 4.4 has a form similar to that of the power expressions introduced by Mesri and Shahien (2003) and Lade (2010) for which no continuous relations between the soil index properties and the power parameters were presented. The processes of determining values of m_r needed to develop the relationships of Fig. 4. 11 are shown in Appendix B.

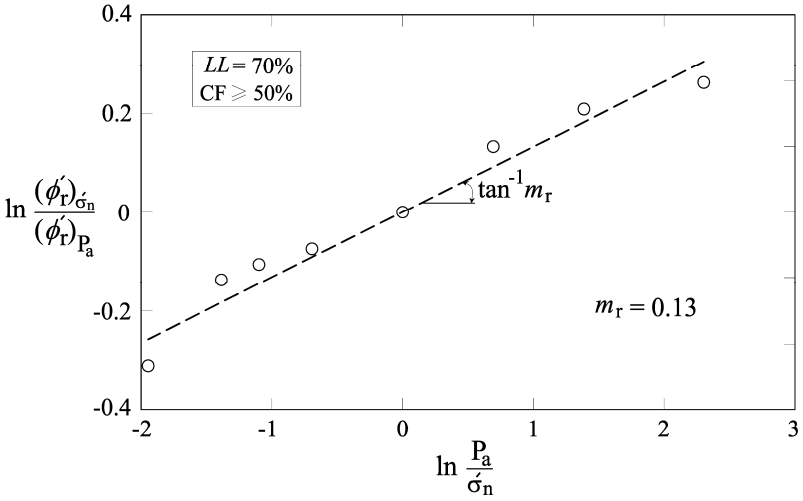

Figure 4.10 Definition of the parameter m_r using trend lines of the residual shear strength correlations developed based on ring shear test results.

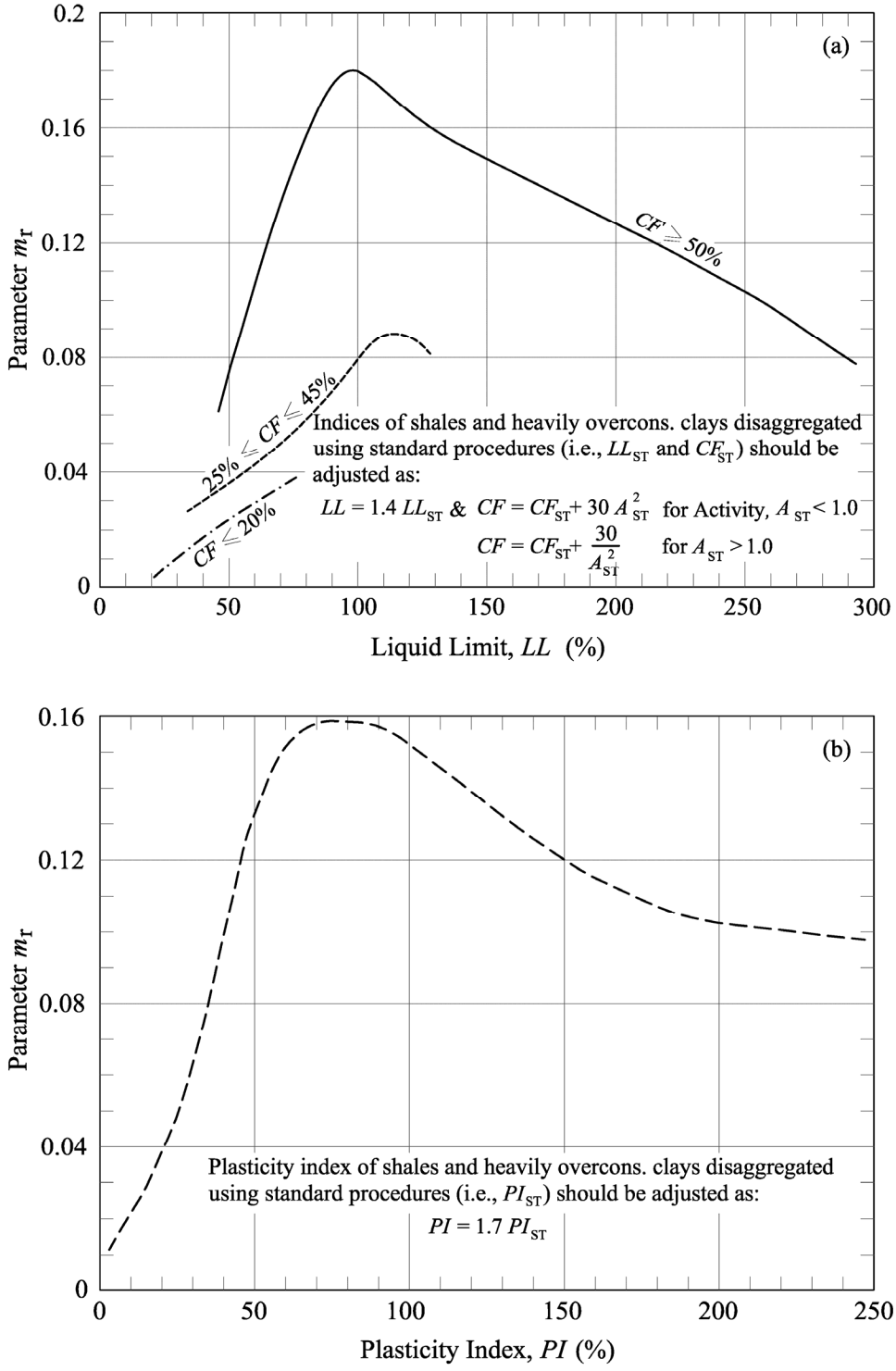

Figure 4.11 Values of parameter m_r for estimating secant residual friction angle in terms of: (a) liquid limit and clay-size fraction; (b) plasticity index.

When $(ø'_r)_{Pa}$ is determined using the trend lines of σ'_n = 100 kPa in the correlations shown in Fig. 4.7, trend lines for other σ'_n values of these correlations can be reproduced through utilizing Equation 4.4. The reproduced trend lines almost coincide with the original lines developed from actual data with maximum deviations limited to ± 0.7°. These deviations are traced at few ranges of soil plasticity and different levels of effective normal stresses (see Figs. 4.12 and 4.13 as an example) Unlike the empirical correlations that are available in graphical form, Equation 4.4 can now be easily incorporated in slope stability software to generate smooth nonlinear residual shear strength failure envelopes. Values of $(ø'_r)_{Pa}$, and m_r would be the only inputs needed to fully describe the drained residual shear strength for slope stability analyses. Values of $(ø'_r)_{Pa}$ can be provided through direct laboratory measurements or estimation using shear strength correlations similar to those given in Fig. 4.7. The magnitudes of the corresponding parameter m_r can then be provided through using Fig 4.11. It should be noticed that having the value of $ø'_r$ at any effective normal stress relevant to slope stability analyses, in addition to the magnitude of m_r, is also enough to fully describe the residual strength envelope using Equation 4.4.

Several expressions are presented in the literature for estimating the residual friction angles as a function of the soil index properties without considering the effective normal stress to yield linear shear strength envelopes (e.g., Kanji 1974; Cancelli 1977; Nelson 1992; Sridharan and Raghuveer Rao 2004) or at specific normal stresses to develop tri-linear or quad-linear shear strength envelopes (e.g., Stark and Hussain 2013). In conducting analyses using slope stability software, utilizing smooth nonlinear envelopes leads to an accurate determination of the

shear strength that corresponds to the effective normal stress acting on the base of each slice of the proposed failure wedge. Errors in determining these strengths may occur when linear envelopes or envelopes with limited number of linear segments are utilized in the analyses.

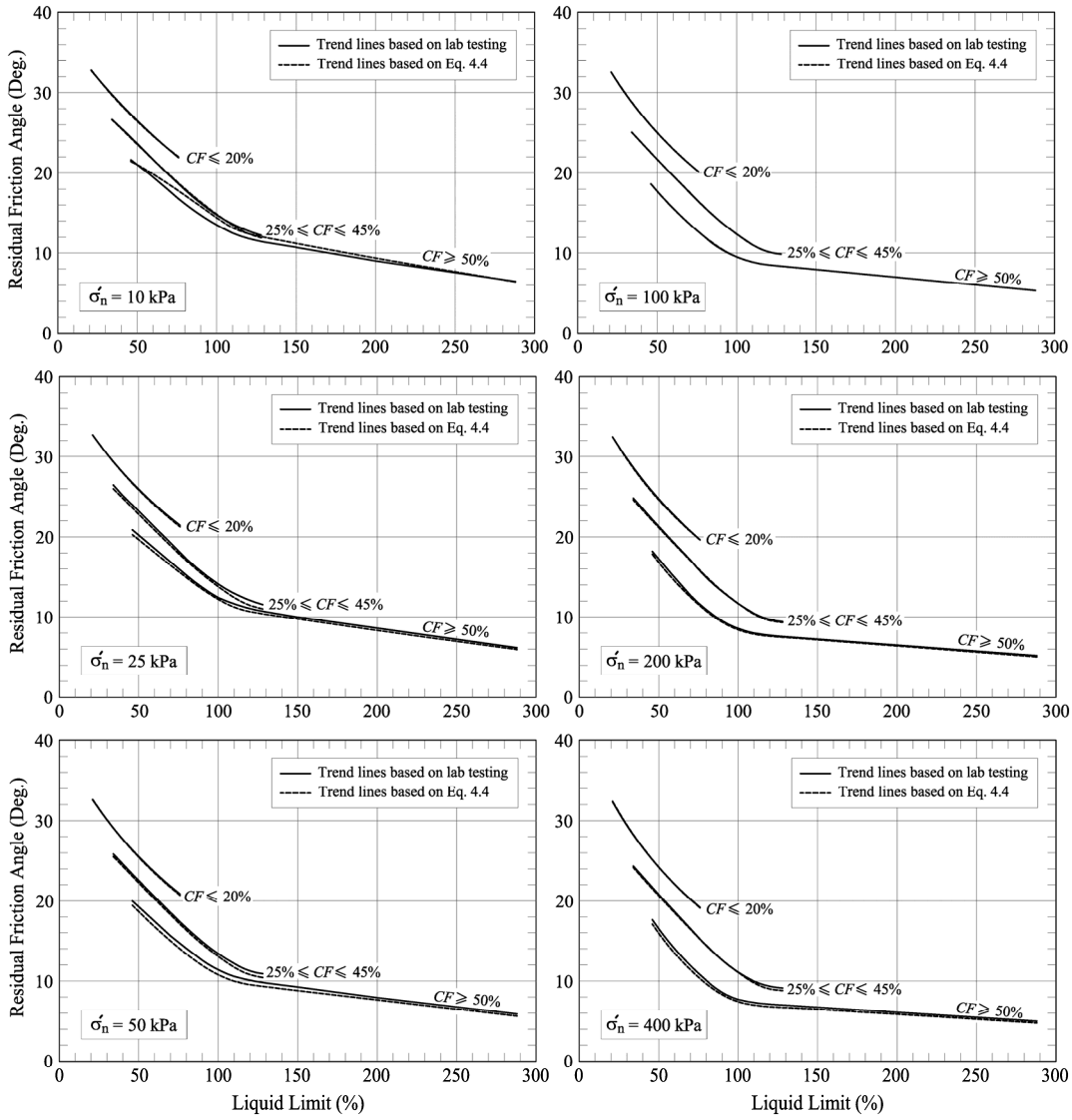

Figure 4.12 Comparison of secant friction angle trend lines developed using different techniques as a function of liquid limit and clay-size fraction for different levels of effective normal stresses

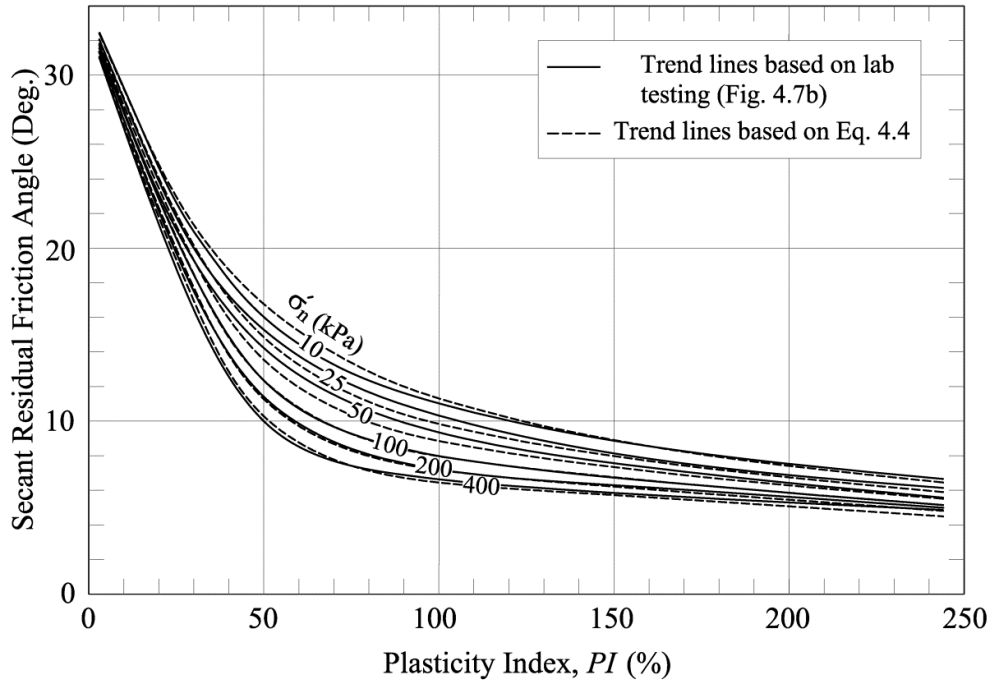

Figure 4.13 Comparison of secant friction angle trend lines developed using different techniques as a function of plasticity index for different levels of effective normal stresses.

4.5.1. Suitability of the New Residual Friction Angle Expression

The suitability of using the newly developed expression (Equation 4.4) to estimate soil residual shear strength at effective normal stresses relevant to slope stability analyses is presented in this subsection. This was done through checking the back-calculated residual friction angles reported for different case histories of reactivated landslides $[\phi'_r]_{BC}$ against those predicted, $[\phi'_r]_{PR}$, using the newly developed expression. The case histories of the fifty four landslides (Table 4.2) were used for such checking. Comparison between the back-calculated residual friction angles and those predicted using (Equation 4.4) presented in this study is shown in Fig. 4.14. Similar to the statistical analysis shown in section (4.4.2), the performance of the newly developed expression (in predicting the residual friction angles back-calculated from the reactivated landslides) was evaluated. The

coefficient of determination (R^2) of the regression equation defined by $[\text{ø}'_r]_{PR} = [\text{ø}'_r]_{BC}$, as well as the mean ($\mu$) standard deviation ($S$), and coefficient of variation (COV) of the ratio $[\text{ø}'_r]_{PR}/[\text{ø}'_r]_{BC}$ were also calculated for this expression as shown in Fig. 4.14 . The newly developed expression seems to yield a relatively good agreement between the prediction and back-calculated angles indicated by having higher R^2, μ close to 1.0, and lower S and COV compared with those calculated for the existing 24 correlations (Table 4.3) – thus, suggesting the suitability of the expression proposed in the current study in terms of their accuracies and precisions.

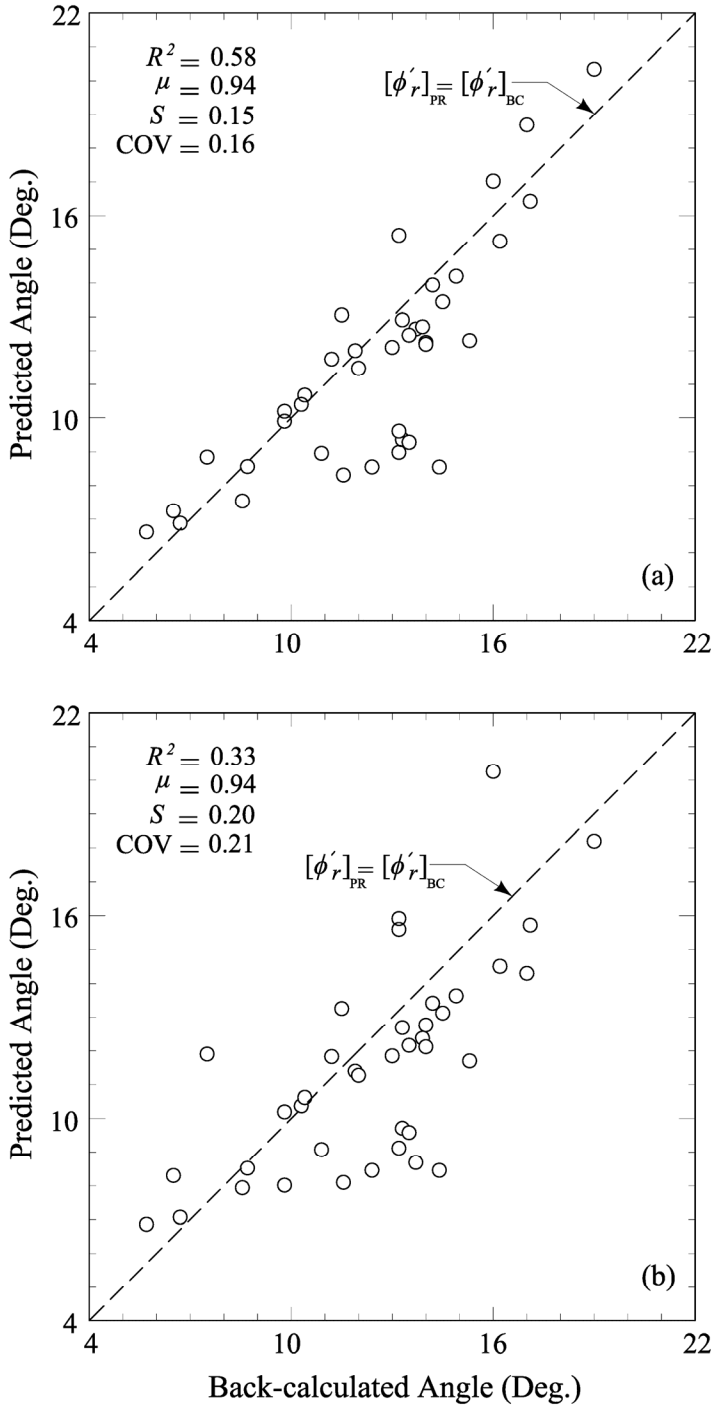

Figure 4.14 Comparison between the back-calculated secant residual friction angles and those predicted using the newly developed expression: (a) parameter m_r in terms of liquid limit, and clay-size fraction [Fig.4.11a]; (b) parameter m_r in terms of plasticity index [Fig.4.11b]

Chapter 5. Conclusions

The following conclusions are drawn based on the results of soil and interface shear testing at low effective normal stresses (between 3 and 6 kPa) as well as an analysis of a provided set of data for soil drained residual shear strength measured at effective normal stresses as low as 10 kPa.

1) The secant residual friction angle of soil decreases with increasing liquid limit and clay-size fraction. These soil parameters have a similar effect on the measured interface residual friction angles that are also lower for smoother surfaces. The change in effective normal stresses within the range of low effective normal stresses (between 3 and 6 kPa) utilized in this study did not show a considerable effect on the measured residual friction angles of soils and interfaces.
2) For low effective normal stresses, the clay-size fraction, as an indication of particle size and shearing mode, has less influence on the measured residual friction angle than the influence of the liquid limit that indicates the clay mineralogy and particle shape.
3) A correlation and a simple equation have been suggested for estimating the interface residual friction between fine-grained soils and solid surfaces sheared at low effective normal stresses as a function of the surface average roughness of the solid surface, R_a, and the soil residual friction angles. The residual interface efficiencies (i.e., the ratio between soil and interface friction angles) determined using the introduced correlation and equation compares well with those reported in the literature for high

effective normal stresses provided that soil and interface residual shear strengths that are estimated at the same effective normal stress range are used for efficiency calculations.

4) Using the normalized roughness, R_a/D_{50}, seems to be not effective in developing a better correlation to estimate the residual interface efficiency for fine-grained soils. It is advocated that the surface roughness alone may not adequately characterize a given surface. Parameters such as hardness, yield strength, the stress-strain behavior of solid material, and compatibility between soil particle size and interface surface roughness are likely to impact the overall interface frictional response observed at soil-solid interfaces. Further studies are warranted to explore these aspects.
5) Nonlinearity of the residual shear strength envelopes is most pronounced at effective normal stresses lower than 50 kPa. For effective stresses equal or higher than 200 kPa that are occasionally mobilized in slope failures, these envelopes can be approximated as straight lines. The influence of clay-size fraction, which is the governing factor in developing different shearing behaviors, on the measured residual friction angle decreased with decreasing the effective normal stress level.
6) Correlations were developed to help in estimating residual shear strength at low effective normal stresses for soil types similar to those utilized in the current study. The correlations describe the secant residual friction angle as a function of soil liquid limit and clay-size fraction as well as the plasticity index. Since the residual shear strength envelope of most fine-grained soils is known to be nonlinear especially at low effective stress

ranges, the newly developed correlations can assist avoiding significant underestimation of residual shear strength angles that would occur when using current correlations that are developed for high effective normal stress ranges. They also avoid overestimating the drained residual friction angles of such soil types when using residual strength expressions, the development of which is influenced by testing soils of distinct contents (i.e., foraminifera, faecal pellets, carbonates, allophane, or halloysite) at low effective normal stresses and consequently do not consider the effect of soil plasticity.

7) The suitability of the new correlations in predicting the residual strength was verified through comparisons with back-calculated shear strength data reported in the literature as well as results yielded from similar existing correlations. It was revealed that accounting for the effect of normal stress is an important consideration in arriving at better predictions using such empirical correlations.
8) New simple formula was generated to express the residual shear strength correlations developed in this study. The formula should facilitate incorporating the nonlinearity of the residual shear strength envelopes in slope stability software. The suitability of the newly developed formula in predicting the residual strength was also verified through comparisons with back-calculated shear strength data reported in the literature.

References

Airo'Farulla, C., and La Rosa, G. (1977). "An analysis of some factors influencing Atterberg limits determination of stiff highly fissured clays." Proceedings of International Symposium on the Geotechnics of Structurally Complex Formations, Capri, Associazione Geotecnica Italiana,Vol. 2, pp. 23-29.

Amarasinghe, R. S. (2013). "Macro-scale direct shear device for studying the large displacement shear strength of soil-structure interfaces under very low effective stresses." MS thesis, University of British Columbia, Vancouver, Canada.

American Society for Testing and Materials (ASTM). (1999a). "Standard test method for particle-size analysis of soils." (D 422), 1999 Annual Book of ASTM Standards, Vol. 04.08, West Conshohocken, Pa, pp. 10-17.

American Society for Testing and Materials (ASTM). (1999b). "Standard test method for liquid limit, plastic limit, and plasticity index of soils." (D 4318), 1999 Annual Book of ASTM Standards, Vol. 04.08, West Conshohocken, Pa, pp. 526-538.

American Society for Testing and Materials (ASTM). (1999c). "Standard test method for torsional ring shaer test to determine drained residual shear strength of cohesive soils." (D 6467) 1999 Annual Book of ASTM Standards, Vol. 04.08, West Conshohocken, Pa, pp. 832-836.

Bayley, M. J. (1972). "Cliff stability at Herne Bay." Civil Engineering and Public Works Review, Vol. 67, pp. 788-792.

Bertini, T., Cugusi, F., D'Elia, B., and Rossi-Doria, M. (1984). "Climatic conditions and slow movements of colluvial covers in Central Italy." Proceedings of the 4th Symposium on Landslides, Toronto, Canada, Canadian Geotechnical Society, Vol. 1, pp. 367-376.

Biczysko, S. J., and Starzewski, K. (1977a). "Daventry bypass landslip." Ground Engineering, Vol. 10, No. 1, pp. 23-25.

Biczysko, S. J., and Starzewski, K. (1977b). "Daventry bypass landslip." Ground Engineering, Vol. 10, No. 3, pp. 6-7.

Bishop, A. W. (1971). "The influence of progressive failure on the choice of the method of stability analysis." Géotechnique, Vol. 21, No. 2, pp. 168-172.

Bishop, A. W., Green, G. E., Garga, V. K., Andresen, A., and Brown, J. D. (1971). "A new ring shear apparatus and its application to the measurement of residual strength." Géotechnique, Vol. 21, No. 4, pp. 273-328.

Bishop, A. W., Webb, D. L., and Lewin, P. I. (1965). "Undisturbed samples of London clay from the Ashford common shaft." Géotechnique, Vol. 15, No. 1, pp. 1-31.

Bromhead, E. N. (1972). "A large coastal landslide at Herne Bay, Kent." Arup Journal, Vol. 7, pp. 12-14.

Bromhead, E. N. (1978). "Large landslides in London Clay at Herne Bay, Kent." Quarterly Journal of Engineering Geology, Vol. 11, pp. 291-304.

Bromhead, E. N. (1979). "A Simple Ring Shear Apparatus." Ground Engineering, Vol. 12, No. 5, pp. 40-44.

British Standards Institute (BSI). (1990). “Methods of Test for Soils for Civil Engineering Purposes.” (BS 1377: Parts 1 to 9), British Standard, London, 406 p.

Bruton, D.A.S., White, D.J., Langford, T., and Hill, A.J. (2009). “Techniques for the assessment of pipe-soil interaction forces for future deepwater developments.” Proceedings of The Offshore Technology Conference (OTC), Paper No. OCT 20096, Houston, TX.

Cancelli, A. (1977). “Residual shear strength and stability analysis of a landslide in fissured overconsolidated clays.” Bulletin of the International Association of Engineering Geology, No. 16, pp. 193-197.

Cancelli, A. (1981). "Evaluation of slopes in overconsolidated clays." Proceedings of the 10th International Conference on Soil Mechanics and Foundation Engineering, Stockholm, Vol. 3, pp. 377-380.

Canuti, P., Casagli, N., and Garzonio, C. A. (1994). “Large-scale mudslides in structurally complex clay shales in the Northern Apennines (Italy)” Proceedings of the 13th Conference on Soil Mechanics and Foundation Engineering, New Delhi, India, Vol. 2, pp. 1111-1114.

Chandler, R. J. (1969). “The effect of weathering on the shear strength properties of Keuper Marl.” Géotechnique, Vol. 19, No. 3, pp. 321-334.

Chandler, R. J. (1970). “A shallow slab slide in the Lias clay near Uppingham, Rutland.” Géotechnique, Vol. 20, No. 3, pp. 253-260.

Chandler, R. J. (1971). “Landsliding on the Jurassic escarpment near Rockingham, Northampton.” Slopes: form and process, International Bulletin of Geology, Special Publication No. 3, pp. 111-128.

Chandler, R. J. (1972). “Lias clay: weathering process and their effect on shear strength.” Géotechnique, Vol. 22, No. 3, pp. 403-431.

Chandler, R. J. (1974). “Lias clay: the long-term stability of cutting slopes.” Géotechnique, Vol. 24, No. 1, pp. 21-38.

Chandler, R. J. (1976). “The history and stability of two Lias clay slopes in the upper Gwash valley, Rutland.” Philosophical Transactions of the Royal Society of London, Vol. 283, No. 1315, pp. 463-491.

Chandler, R. J. (1977). “Back analysis techniques for slope stabilization works: a case record.” Géotechnique, Vol. 27, No. 4, pp. 479-495.

Chandler, R. J. (1979). “Stability of a structure constructed in a landslide: selection of soil strength parameters.” Proceedings of the 7th European Conference on Soil Mechanics and Foundation Engineering, Vol. 3, pp. 175-181.

Chandler, R. J. (1982). “Lias clay slope sections and their implications for the prediction of limiting or threshold slope angles.” Earth Surface Processes and Landforms, Vol. 7, pp. 427-438.

Chandler, R. J. (1984). "Recent European Experience of Landslides in Overconsolidated Clays and Soft Rocks." Proceedings of the 4th International Symposium on Landslides, Toronto, Vol. 1, pp. 61-81.

Chandler, R. J., Pachakis, M., Mercer, J., and Wrightman, J. (1973). “Four long-term failures of embankments founded on areas of landslip.” Quarterly Journal of Engineering Geology, Vol. 6, pp. 405-422.

Chandler, R. J. and Skempton, A. W. (1974). "The Design of permanent cutting slopes in stiff fissured clays." Géotechnique, Vol. 24, No. 4, pp. 457-466.

Charles, J. A., and Soares, M. M. (1984). “The stability of slopes in soils with nonlinear failure envelopes.” Canadian Geotechnical Journal, Vol. 21, No. 3, pp. 397-406.

Christiansen, E. A. (1983). The Denholm landslide, Saskatchewan. Part I: Geology.” Canadian Geotechnical Journal, Vol. 20, pp. 197-207.

Colliat, J.-L., Dendani, H., Puech, A., and Nauroy, J.-F. (2011). “Gulf of Guinea deepwater sediments: Geotechnical properties, design issues and installation experiences.” Proceedings of the 2nd International Symposium on Frontiers in Offshore Geotechnics (ISFOG), Perth, Australia, pp. 59-86.

Collotta, T., Cantoni, R., Pavesi, U., Ruberl, E., and Moretti, P. C. (1989). "A correlation between residual friction angle, gradation and the index properties of cohesive soils." Géotechnique, Vol. 39, No.2, pp. 343-346.

Dagnall, M.A. (1986). “Exploring surface texture.” Rank Taylor Hobson Ltd, Leicester, UK. 178 p.

D’Appolonia, E., Alperstein, R., and D’Appolonia, D. J. (1967). “Behavior of a colluvial slope.” Journal of Soil Mechanics and Foundations Division, ASCE, SM4, pp. 447-473.

Day, R. W., and Axten, G. W. (1989). "Surficial stability of compacted clay slopes." Journal of Geotechnical Engineering, ASCE, Vol. 115, No. 4, pp. 577-580.

Deere, D. U. (1974), Reported by Mitchell, J. K. (1976).

Dove, J.E., and Harpring, J.C. (1999). "Geometric and spatial parameters for analysis of geomembrane/soil interface behavior." Proceedings of Geosynthetics '99, Industrial Fabrics Association International, Boston, Massachusetts, Vol. 1, pp. 575-588.

Early, K. R., and Skempton, A. W. (1972). "Investigations of the landslide at Walton's Wood, Staffordshire." Quarterly Journal of Engineering Geology, Vol. **5**, pp. 19-41.

Eckel, B. F., Sauer, E. K., Christiansen, E. A. (1987). "The Petrofka landslide, Saskatchewan." Canadian Geotechnical Journal, Vol. 24, No. 1, pp. 81-99.

Eid, H. T. (1996). "Drained shear strength of stiff clays for slope stability analyses." Ph.D. thesis, University of Illinois at Urbana-Champaign, Urbana, Illinois.

Eid, H. T. (2001). "Correlation between shale index properties derived from different sample preparation procedures." Proceedings of the 15th International Conference on Soil Mechanics and Geotechnical Engineering, Istanbul, Vol. 1, pp. 77-80.

Eid, H. T. (2006). "Factors influencing determination of shale classification indices and their correlation to mechanical properties." Geotechnical and Geological Engineering Journal, Vol. 24, No. 6, pp. 1695-1713.

Eid, H. T. (2014). Personal Communication.

Esterhuizen, J.J.B., Filz, G.M., and Duncan, J.M. (2001). "Constitutive behavior of geosynthetic interfaces." ASCE Journal of Geotechnical and Geoenvironmental Engineering, Vol. 127, No. 10, pp. 834-840.

Farshad, F.F., Pesacreta, T.C., Garber, J.D., and Bikki, S.R. (2001). "A comparison of surface roughness of pipes as measured by two profilometers and atomic force microscopy." Scanning, Vol. 23, No. 4, pp. 241-248.

Fang, Y. S., Chen, T. J., Holtz, R. D., and Lee, W. F. (2004). "Reduction of boundary friction in model tests." Geotech. Test. J., 27(1), 1–10.

Fishman, K.L., and Pal, S. (1994). "Further study of geomembrane/cohesive soil interface shear behavior." Geotextile and Geomembrane, Vol. 13, No. 9, pp. 571-590.

Fleming, I.R., Sharma, J.S., and Jogi, M.B. (2006). "Shear strength of geomembrane-soil interface under unsaturated conditions." Geotextiles and Geomembranes, Vol. 24, No. 5, pp. 274-284.

Ganesan, S., Kuo, M., and Bolton, M. (2014). "Influence on pipeline interface friction measured in direct shear tests." Geotechnical Testing Journal, ASTM, Vol. 37, No.1, pp. 94-106

Gibson, R. and Henkel, D. (1954). "Influence of duration of tests at constant rate of strain on measured drained strength." Géotechnique, 4(1):6-15.

Hamel, J. V. (1970). Stability of slopes in soft, altered tocks. Ph.D. thesis, University of Pittsburgh.

Hammoud, F, and Boumekik, A. (2006). “Experimental study of the behaviour of interfacial shearing between cohesive soils and solid materials at large displacement.” Asian Journal of Civil Engineering, Vol. 7, No. 1, pp. 63-80.

Hawkins, A. B., and Privett, K. D. (1985). "Measurement and use of residual shear strength of cohesive soils." Ground Engineering, Vol. 18, No. 8, pp. 22-29.

Henkel, D. J., and Skempton, A. W. (1955). “A landslide at Jackfield, Shropshire, in a heavely over-consolidated clay.” Géotechnique, Vol. 5, No. 2, pp. 131-137.

Henkel, D. J., and Yudhbir. (1966). “The stability of slopes in the Siwalik rocks in India.” Proceedings of the 1st International Congress on Rock Mechanics, Laboratorio Nacional de Engenharia Civil, Lisbon, Potugal, Vol. 2, pp. 161-165.

Hill, A.J., Jacob, H. (2008). “In-situ measurement of pipe-soil interaction in deep water.” Proceedings of The Offshore Technology Conference (OTC), Paper No. OCT 19528, Houston, TX.

Hill, A.J, White, D.J., Bruton, D.A.S., Langford, T., Meyer, V., Jewell, R., and Ballard, J-C. (2012). “A new framework for axial pipe-soil resistance, illustrated by a range of marine clay datasets.” Proceedings of the 7th International Offshore Site Investigation and Geotechnics Conference, Society for Underwater Technology (SUT), London, UK, pp. 367-377.

Hutchinson, J. N. (1965a). "The stability of cliffs composed of soft rocks with particular reference to the coast of SE England." Ph.D. thesis, University of Cambridge, England.

Hutchinson, J. N. (1965b). "A survey of the coastal landslides of Kent." Building Research Station, Note EN/35/65.

Hutchinson, J. N. (1967). Written discussion. Proceedings of the Geotechnical Conference on Shear Strength Properties of Natural Soils and Rocks, NGI, Oslo, Norway, Vol. 2, pp. 183-184.

Hutchinson, J. N. (1969). "A reconsideration of the coastal landslides at Folkestone Warren, Kent." Géotechnique, Vol. 19, No. 1, pp. 6-38.

Hutchinson, J. N., Bromhead, E. N., and Lupini, J. F. (1980). "Additional observations on the Folkestone Warren landslides." Quarterly Journal of Engineering Geology, Vol. 13, pp. 1-31.

Hutchinson, J. N., and Gostelow, T. P. (1976). "The development of an abandoned cliff in London Clay at Hadleigh, Essex." Philosophical Transactions of the Royal Society of London, A 283, pp. 557-604.

Hutchinson, J. N., Somerville, S. H. and Petley, D. J. (1973). “A landslide in periglacially disturbed Etruria Marl at Bury Hill, Staffordshire.” Quarterly Journal of Engineering Geology, Vol. 6, pp. 377-404.

ISO4287-ISO/TC5 (1997). *Geometrical Product Specifications (GPS). Surface Texture: Profile Method. Terms, Definitions and Surface Texture Parameters*. International Organization for Standardization, 1997.

James, P. M. (1970). “Time effects and progressive failure in clay slopes.” Ph.D. thesis, University of London, London.

Jamiolkowski, M., and Pasqualini, E. (1976). "Sulla scelta dei parametric geotecnici che intervengono nelle verifiche di stabilita dei pendii natural ed artificiali." (in Italian), 1st di Scienza delle Costruzioni, Politecnico di Torino, no. 319, 53 pp.

Jardine, R., Chow, F., Overy, R., and Standing, J. (2005). ICP design methods for driven piles in sands and clays. Thomas Telford, London, UK, 112 pp.

Jasper, J. L., and Peters, N. (1979). "Foundation performance of Gardiner Dam." Canadian Geotechnical Journal, Vol. 16, pp. 758-788.

Kanji, M. A. (1970). Shear strength of soil-rock interfaces. MS thesis, University of Illinois at Urbana-Champaign.

Kanji, M. A. (1972). Resistência ao cisalhamento de contactos solo-rocha. (in Portuguese). Doctoral dissertation, Universidade de São Paulo.

Kanji, M. A. (1974). "The relationship between drained friction angles and Atterberg limits of natural soils." Géotechnique, Vol. 24, No. 4, pp. 671-674.

Kaya, A. (2009). "Slope residual and fully-softened shear strength evaluation using artificial neural networks." Geotechnical and Geological Engineering, Vol. 27, No. 2, pp. 281-289.

Kaya, A. (2010). "Revisiting correlations between index properties and residual friction angle of natural soils using artificial neural networks." Geomechanics and Geoengineering, Vol. 5, No. 2, pp. 109-116.

Kenney, T. C. (1967). "The influence of mineral composition on the residual strength of natural soils." Proceedings of the Geotechnical Conference on Shear Strength Properties of Natural Soils and Rocks, NGI, Oslo, Norway, Vol. 1, pp. 123-129.

Kuo, M., Y-H., and Bolton, M.D. (2013). “The nature and origin of deep ocean caly crust from the Gulf of Guinea.” Géotechnique, Vol. 63, No. 6, pp 500-509.

Kuo, M., Y-H., and Bolton, M.D. (2014). “Shear tests on deep-ocean clay crust from the Gulf of Guinea.” Géotechnique, Vol. 64, No. 4, pp 249-259.

Kuo, M. Y-H., Bolton, M.D., Hill, A.J., and Rattley, M. (2010). “New evidence for the origin and behaviour of deep ocean ‘crust’.” Proceedings of the 2nd International Symposium on Frontiers in Offshore Geotechnics (ISFOG), Perth, Australia, pp. 365-370.

Kuo, M., Bolton, M., and Puech, A. (2012). “Interface shear testing of Gulf of Guinea sediments implications for the design of hot-oil pipelines and suction caissons.” Proceedings of the 7th International Offshore Site Investigation and Geotechnics Conference, Society for Underwater Technology (SUT), London, UK, pp. 297-305.

La Gatta, D. P. (1970). “Residual strength of clays and clay-shales by rotation shear test.” PhD thesis, Harvard University, MA.

Lambe, T. W. (1985). “Amuay landslides.” Proceedings of the 11th International Conference on Soil Mechanics and Foundation Engineering, A.A. Balkema, Golden Jubilee Volume, pp. 137-158.

Lehane, B. M., and Jardine, R. J. (1992). “Residual strength characteristics of Bothkennar clay.” Géotechnique, 42(2), 363–367.

Lemos, L. J. L., and Vaughan, P. R. (2000). “Clay-interface shear resistance.” Géotechnique, 50(1), 55–64.

Lupini, J. F., Skinner, A. E. and Vaughan, P. R. (1981). "The drained residual strength of cohesive soils." Géotechnique, Vol. 31, No. 2, pp. 181-213.

Maksimovic, M. (1989). “Nonlinear failure envelope for soils.” Journal of Geotechnical Engineering, ASCE, Vol. 115, No. 4, pp. 581-586.

Maksimovic, M. (1996). “A family of nonlinear failure envelopes for non-cemented soils and rock discontinuities.” The Electronic Journal of Geotechnical Engineering, Vol. 1.

Meehan, C.L., Brandon, T.L., and Duncan, J.M. (2007). “Measuring drained residual strengths in the Bromhead ring shear.” Geotechnical Testing Journal, Vol. 30, No. 6, pp. 1-8.

Mesri, G., and Cepeda-Diaz, A. F. (1986). “Residual shear strength of clays and shales.” Géotechnique, Vol. 36, No. 2, pp. 269-274.

Mesri, G., and Shahien M. (2003). “Residual shear strength mobilized in first-time slope.” Journal of Geotechnical and Geoenvironmental Engineering, ASCE, Vol. 129, No. 1, pp. 12-31.

Mesri, G., Rokhsar, A., and Bohor, B.F. (1975). “Composition and compressibility of typical samples of Mexico City clay.” Géotechnique, Vol. 25, No. 3, pp. 527-554.

Mitchell, J. K. (1976). Fundamentals of Soil Behavior, John Wiley and Sons, Inc., New York, 422 pp.

Najjar, S. S., Gilbert, R. B., Liedtke, E. A., McCarron, B.. (2003). “Tilt table test for interface shear resistance between flowlines and soils.” Proceedings of the 22nd International Conference on Offshore Mechanics and Arctic Engineering-OMAE, Vol. 3, ASME, Cancun, Mexico, pp 859-866.

Najjar, S. S., Gilbert, R. B., Liedtke, E., McCarron, B., and Young, A. G. (2007). "Residual Shear Strength for Interfaces between Pipelines and Clays at Low Effective Normal Stresses," *Journal of Geotechnical and Geoenvironmental Engineering*, 133(6), 695–706.

Nash, K. L. (1953). "The shearing resistance of a fine closely graded sand." Proceedings of the 3rd International Conference on Soil Mechanics and Foundation Engineering, Zurich, Vol. 1, pp. 160-164.

Nelson, J. L. (1992). "Clay mineralogy and residual shear strength of the Santa Clara formation claystone, Saratoga Foothills, California." Bulletin of the Association of Engineering Geologists, Vol. 29, No. 3, pp. 299-310.

Nonveiler, E. (1967). "Shear strength of bedded and jointed rock as determined from the Zalesina and Vajont slides." Proceedings of the Geotechnical Conference on Shear Strength Properties of Natural Soils and Rocks, NGI, Oslo, Norway, Vol. 1, pp. 289-294.

Oliphant, J., and Maconochie, A. (2007). "The axial resistance of buried and unburied pipelines." Proceedings of the 6th International Offshore Site Investigation and Geotechnics Conference, Society for Underwater Technology (SUT), London, UK, pp. 125-132.

Paikowsky, S.G., Player, C.M., and Connors, P.J. (1995). "A dual interface apparatus for testing unrestricted friction of soil along solid surfaces." Geotechnical Testing Journal, ASTM, Vol. 18, No. 2, pp. 168-193.

Palladino, D. J., and Peck, R. B. (1972). "Slope failures in an overconsolidated clay, Seattle, Washington." Géotechnique, Vol. 22, No. 4, pp. 563-595.

Penman, A. (1953). “Shear characteristics of saturated silt measured in triaxial compression.” Géotechnique, Vol. 3, No. 8, pp. 312-328.

Ponce, V. M., and Bell, J. M. (1971). “Shear strength of sand at extremely low pressures.” Journal of the Soil Mechanics and Foundations Division, ASCE, Vol. 97, No. 4, pp. 625-638.

Potts, D. M., Kovacevic, N., and Vaughan, P. R. (1997). “Delayed collapse of cut slopes in stiff clay.” Géotechnique,Vol. 47, No. 5, pp. 953-982.

Ramsey, N., Jardine, R.J., Lehane, B.M., and Ridley, A.M. (1998). “A review of soil-steel interface testing with the ring-shear apparatus.” Proceedings of the Offshore Site Investigation and Behaviour Conference, Society for Underwater Technology (SUT), London, UK, pp. 237-258.

Rowe, P. W. (1969). "The relation between the shear strength of sands in triaxial compression, plane strain, and direct shear." Géotechnique, Vol. 19, No. 1, pp. 75-86.

Saldivar, E.E., and Jardine, R.J. (2005). “Application of an effective stress design method to concrete pile driven in Mexico City clay.” Canadian Geotechnical Journal, Vol. 42, No. 6, pp. 1495-1508.

Sauer, E. K. (1983). “The Denholm landslide, Saskatchewan. Part II: analysis.” Canadian Geotechnical Journal, Vol. 20, No. 2, pp. 208-220.

Sauer, E. K. (1984). “A landslide in clay shale in the North Saskatchewan river valley, Canada.” Vol. 20, No. 4, pp. 279-300.

Sauer, E. K., and Christiansen, E. A. (1987). The Denholm landslide, Saskatchewan, Canada, an update.” Canadian Geotechnical Journal, Vol. 24, pp. 163-168.

Skempton, A. W. (1964). "Long-term stability of clay slopes." Géotechnique, Vol. 14, No. 2, pp. 77-101.

Skempton, A. W. (1970). "First-time slides in over-consolidated clays." Géotechnique, Vol. 20, No. 3, pp. 320-324.

Skempton, A. W. (1972). "Investigations and remedial works at Burderop Wood and Hodson landslides on the M4 Mororway near Swindon." Report to Sir Alexander Gibb & Partners.

Skempton, A. W. (1977). "Slope stability of cuttings in brown London clay." Proceedings of the 9th International Conference on Soil Mechanics and Foundation Engineering, Japanese Society of Soil Mechanics and Foundation Engineering, Tokyo, Japan, Vol. 3, pp. 261-270.

Skempton, A. W. (1985). "Residual strength of clays in landslides, folded strata and the laboratory." Géotechnique, Vol. 35, No. 1, pp. 3-18.

Skempton, A. W., and Hutchinson, J. N. (1969). "Stability of natural slopes." Proceedings of the 7th International Conference on Soil Mechanics and Foundation Engineering, Mexico City, State of the Art Volume, pp. 291-340.

Skempton, A. W., Leadbeater, A. D., and Chandler, R. J. (1989). "The Mam Tor landslide, North Derbyshire." Philosophical Transactions of the Royal Society of London, A 329, pp. 503-547.

Skempton, A. W., and Petley, D. J. (1967). "The strength along structural discontinuities in stiff clays." Proceedings of the Geotechnical Conference, Oslo, Vol. 2, pp. 29-46.

Skempton, A. W., Schuster, R. L., and Petley, D. J. (1969). "Joints and Fissures in the London Clay at Wraysburg and Edgware." Géotechnique, Vol. 19, No. 2, pp. 205-217.

Sridharan, A., and Raghuveer Rao, P. (2004). Discussion on "Residual strength of clays and correlation using Atterberg limits" by Wesley, L. D., Géotechnique, Vol. 54, No. 7, pp. 503-504.

Stark, T. D., and Eid, H. T. (1992). "Comparison of field and laboratory residual shear strengths." Proceedings of the ASCE Specialty Conf on Stability and Performance of Slopes and Embankments-II, Univ. of California, Berkeley, Geotech. Special Tech. Pub. No. 31, Vol. 1, pp. 876-889.

Stark, T. D., and Eid, H. T. (1993). "Modified Bromhead ring shear apparatus." Geotechnical Testing Journal, ASTM, Vol. 16, No. 1, pp. 100-107.

Stark, T. D., and Eid, H. T. (1994). "Drained residual strength of cohesive soils." Journal of Geotechnical Engineering, ASCE, Vol. 120, No. 5, pp. 856-871.

Stark, T. D., and Eid, H. T. (1997). "Slope stability analyses in stiff fissured clays." Journal of Geotechnical and Geoenvironmental Engineering, ASCE, Vol. 123, No. 4, pp.335-343.

Stark, T. D., and Eid, H. T. (1998). "Performance of three-dimensional slope stability methods in practice." Journal of Geotechnical and Geoenvironmental Engineering, ASCE, Vol. 124, No. 11, pp. 1049-1060.

Stark, T. D., and Hussain, M. (2013). "Empirical correlations: drained shear strength for slope stability analyses." Journal of Geotechnical and Geoenvironmental Engineering, ASCE, Vol. 139, No. 6, pp. 853-862.

Stark, T. D., Choi, H., and McCone, S. (2005). "Drained shear strength parameters for analysis of landslides." Journal of Geotechnical and Geoenvironmental Engineering, ASCE, Vol. 131, No. 5, pp. 575-588.

Subba Rao, K.S., Allam, M.M., and Robinson, R.G. (1998). "Interfacial friction between sands and solid surfaces." Proceedings of the Institution of Civil Engineers, Geotechnical Engineering, Vol. 131, No. 2, pp. 75-82.

Subba Rao, K.S., Allam, M.M., and Robinson, R.G. (2000). "Drained shear strength of fine-grained soil-solid surface interfaces." Proceedings of the Institution of Civil Engineers, Geotechnical Engineering, Vol. 143, No. 2, pp. 75-81.

Taylor, D. W. (1939). "A comparison of results of direct shear and cylindrical compression test." Proceedings of the American Society for Testing and Material, ASTM, Philadelphia, pp. 1058-1070.

Terzaghi, K., and Peck, R. B. (1948). Soil mechanics in engineering practice, 1st Edition, John Wiley & Sons, Inc., New York.

Tika-Vassilikos, T. (1991). "The clay-on-steel ring shear tests and their implications for displacement piles." Geotech. Test. J., 14(4), 457–463.

Tiwari, B., and Marui, H. (2005). "A new method for the correlation of residual shear strength of the soil with mineralogical composition." Journal of Geotechnical and Geoenvironmental Engineering, ASCE, Vol. 131, No. 9, pp. 1139-1150.

Townsend, F. C., and Banks, D. C. (1974). "Preparation effects on clay shale classification indexes." Proceedings of National Meeting on Water Resources Engineering, ASCE, Los Angeles, Calif., pp. 21-25.

Townsend, F. C., and Gilbert, P. A. (1973). " Tests to measure residual strengths of some clay shales." Géotechnique, Vol. 23, No. 2, pp. 267-271.

Tsubakihara, Y., and Kishida, H. (1993). "Friction behaviour between normally consolidated clay and steel by two direct shear type apparatuses." Soils and Foundations, Vol. 33, No. 2, pp. 1-13

Tsubakihara, Y., Kishida, H., and Nishiyama, T. (1993). "Friction between cohesive soil and steel." Soils and Foundations, 33(2), 145–156.

Tulinov, R., and Molokov, L. (1971). "Role of joint filling material in shear strength of rocks." International Society of Rock Mechanics, Symposium on Rock Fracture, Nancy, Vol. 2, 13 pp.

Uesugi, M., and Kishida, H. (1986). "Frictional resistance at yield between dry sand and mild steel." Soils and Foundations, Vol. 26, No. 4, pp. 139-149.

Voight, B. (1973). "Correlation between Atterberg plasticity limits and residual shear strength of natural soils." Géotechnique, Vol. 23, No. 2, pp. 265-267.

Wesley, L. D. (1977). "Shear strength properties of halloysite and allophane clays in Java, Indonesia." Géotechnique, Vol. 27, No. 2, pp. 125-136.

Wesley, L. D. (1992). "Some residual strength measurements on New Zealand soils." Proceedings of the 6th Australia-New Zealand Conference on Geomechanics, Christchurch, pp. 381-385.

Wesley, L. D. (2003). "Residual strength of clays and correlations using Atterberg limits." Géotechnique, Vol. 53, No. 7, pp. 669-672.

White, D.J., and Cathie, D.N. (2011). "Geotechnics for subsea piplines." Proceedings of the 2nd International Symposium on Frontiers in Offshore Geotechnics, Perth, Australia, pp. 87-123.

White,D.J., and Randolph, M.F. (2007). "Seabed characterization and models for pipeline-soil interaction." Proceedings of the 17th International Offshore and Polar Engineering Conference, Lisbon, Portugal, pp. 758-769.

White, D.J., and Bolton, M.D., Ganesan, S.A., Bruton, D., Ballard, J-C, and Lanford, T. (2011). "SAFEBUCK JIP: Observations from model testing of axial pipe-soil interaction on soft natural clays." Proceedings of The Offshore Technology Conference (OTC), Paper No. OCT 21249, Houston, TX.

White, D.J., Campbell, M.E., Boylan, N.P., and Bransby, M.F. (2012). "A new framework for axial pipe-soil interaction, illustrated by shear box tests on carbonate soils." Proceedings of the 7th International Offshore Site Investigation and Geotechnics Conference, Society for Underwater Technology (SUT), London, UK, pp. 379-387.

Wijewickreme, D., Amarasinghe, R., and Eid, H. (2014). "Macro-scale test device for assessing soil-solid interface friction under low effective normal stresses." Geotechnical Testing Journal, ASTM, Vol. 37, No.1, pp. 121-138.

Wise, E. V. A. (1957). "The stability of natural slopes in overconsolidated fissured clay." MSc thesis, Imperial College, London University, London.

Wright, S. G. 2005. “Evaluation of Soil Shear Strengths for Slope and Retaining Wall Stability Analyses with Emphasis on High Plasticity Clays.” *Project No. 5-1874-01*, Center for Transportation Research, The University of Texas at Austin, TX.

Appendix A

Comparison Between The Back-Calculated Secant Residual Friction Angles and The Residual Angles Predicted Using Existing Residual Shear Strength Correlations.

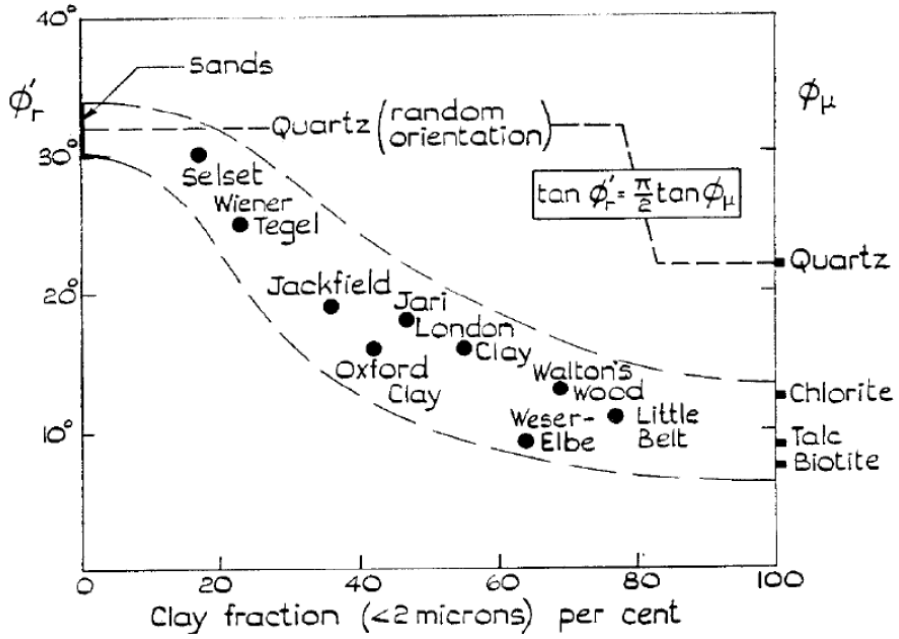

Figure. A-1-a. Drained residual shear strength empirical correlation (after Skempton 1964)

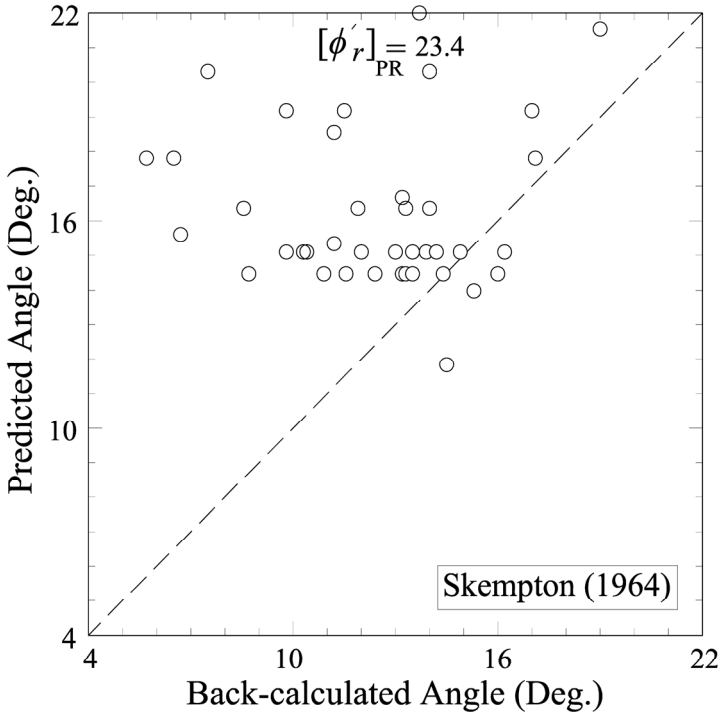

Figure. A-1-b. Comparison between the back-calculated secant residual friction angles and the residual angles predicted using the correlation presented by Skempton (1964)

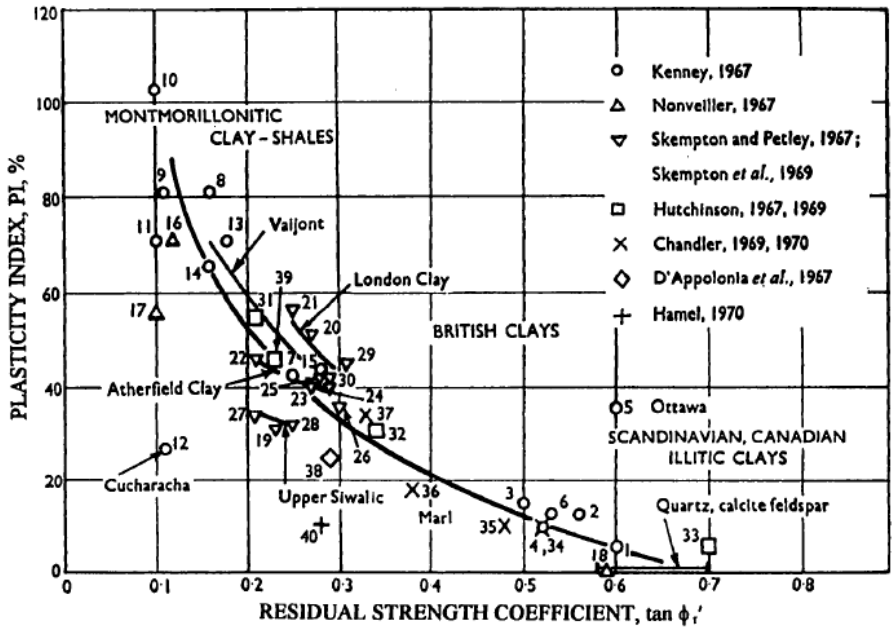

Figure. A-2-a. Drained residual shear strength empirical correlation (after Voight 1973)

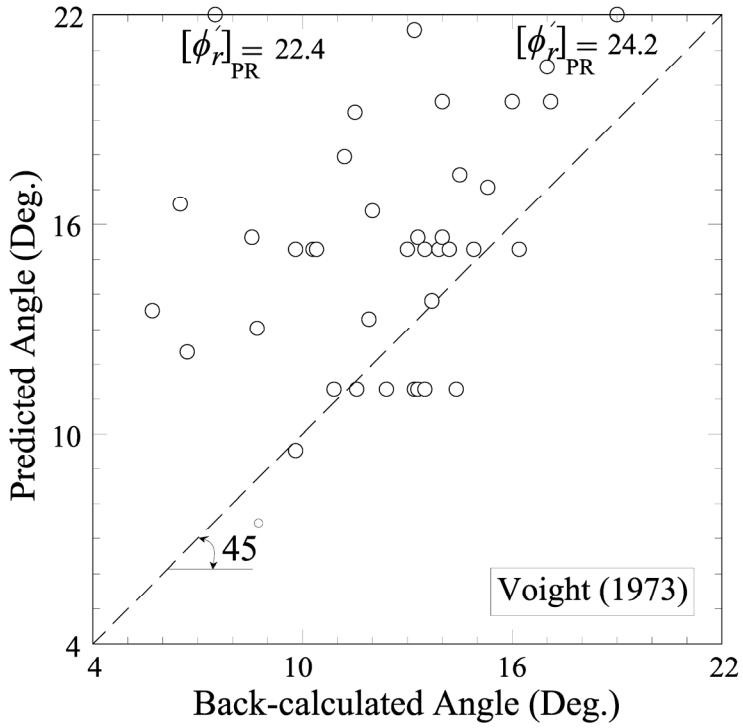

Figure. A-2-b. Comparison between the back-calculated secant residual friction angles and the residual angles predicted using the correlation presented by Voight (1973)

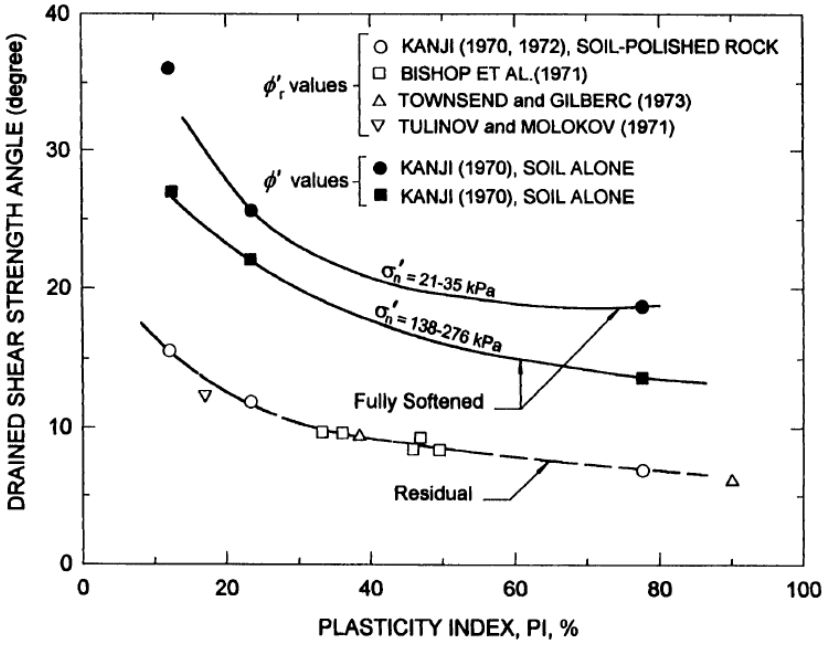

Figure. A-3-a. Drained residual shear strength empirical correlation (after Kanji 1974)

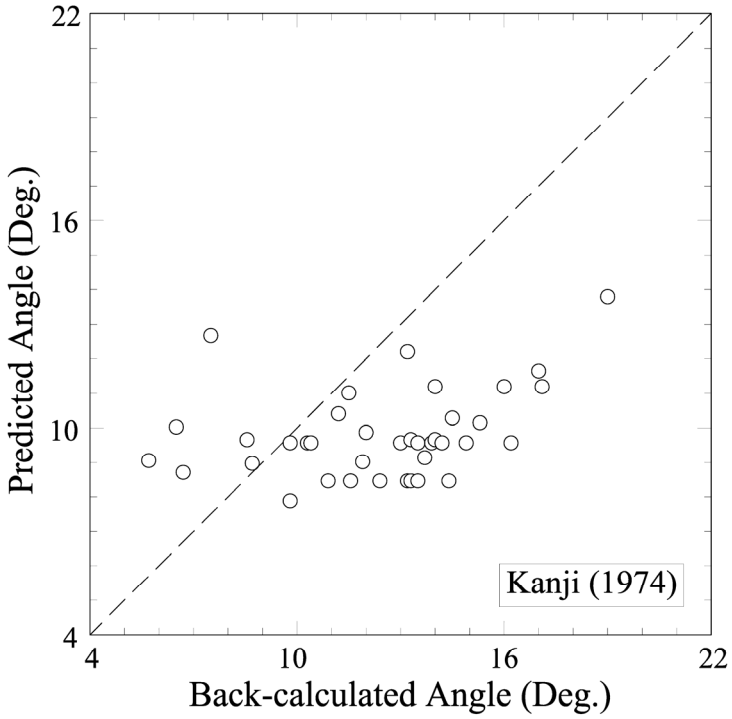

Figure. A-3-b. Comparison between the back-calculated secant residual friction angles and the residual angles predicted using the correlation presented by Kanji (1974)

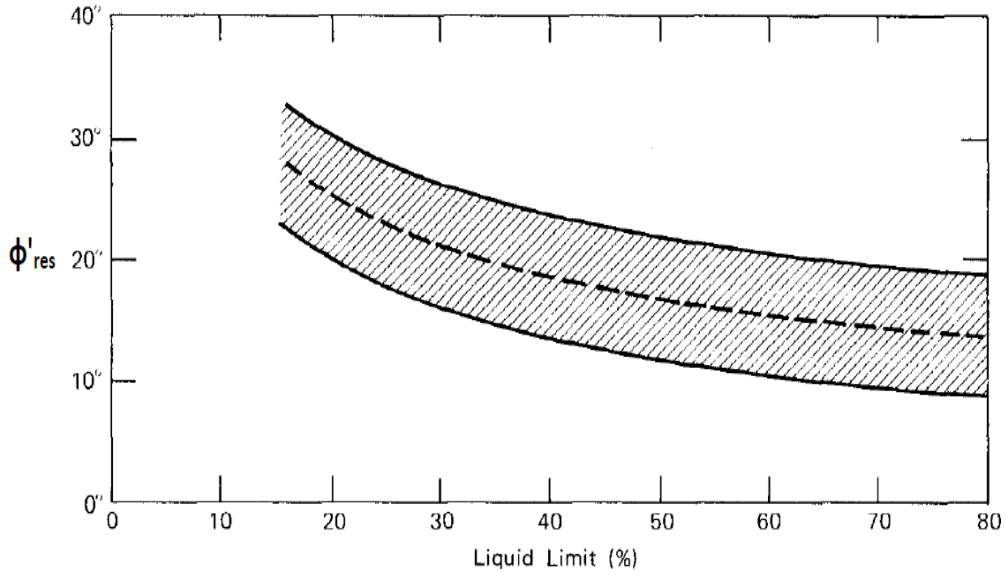

Figure. A-4-a. Drained residual shear strength empirical correlation (after Mitchel 1976)

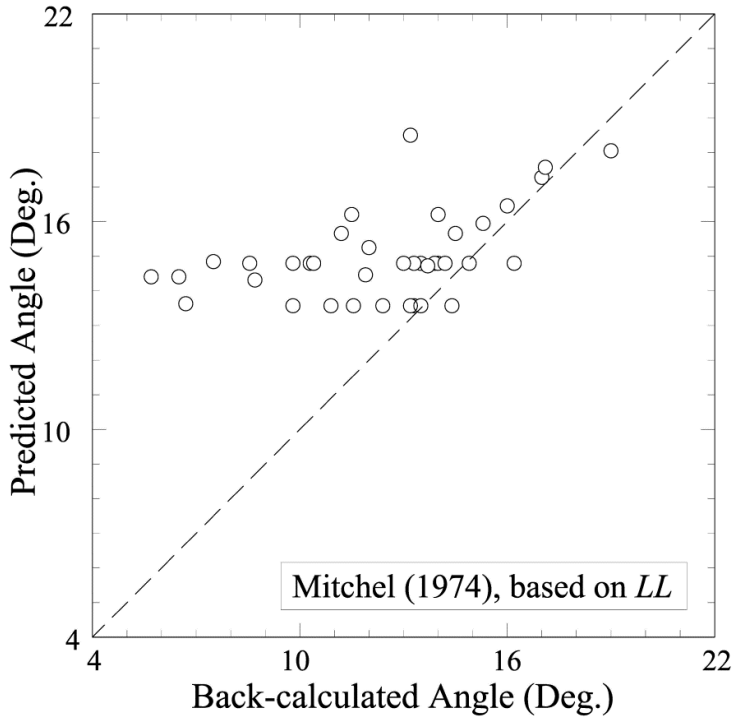

Figure. A-4-b. Comparison between the back-calculated secant residual friction angles and the residual angles predicted using the correlation presented by Mitchel (1976)

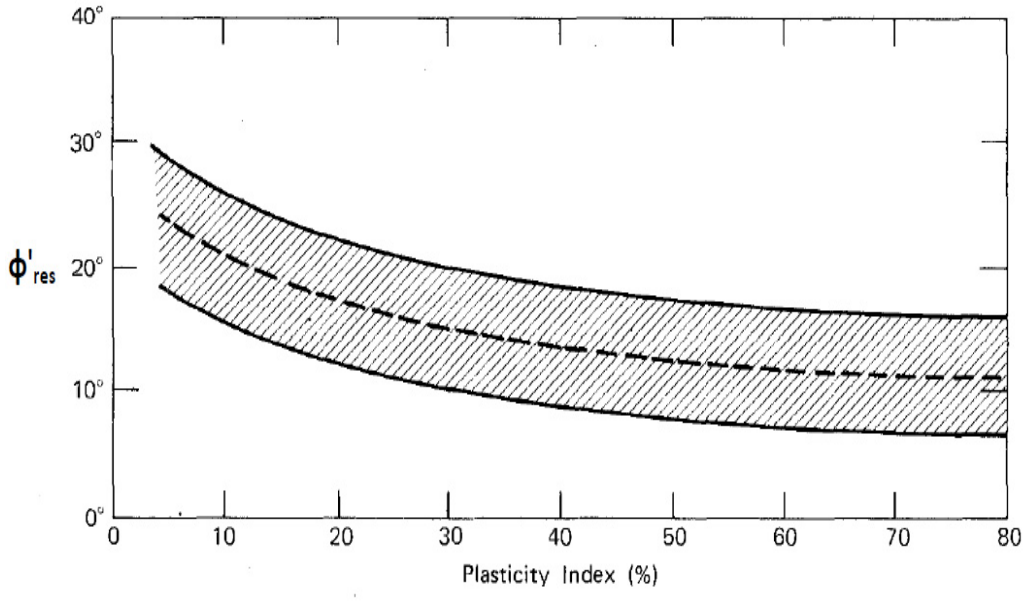

Figure. A-5-a. Drained residual shear strength empirical correlation (after Mitchel 1976)

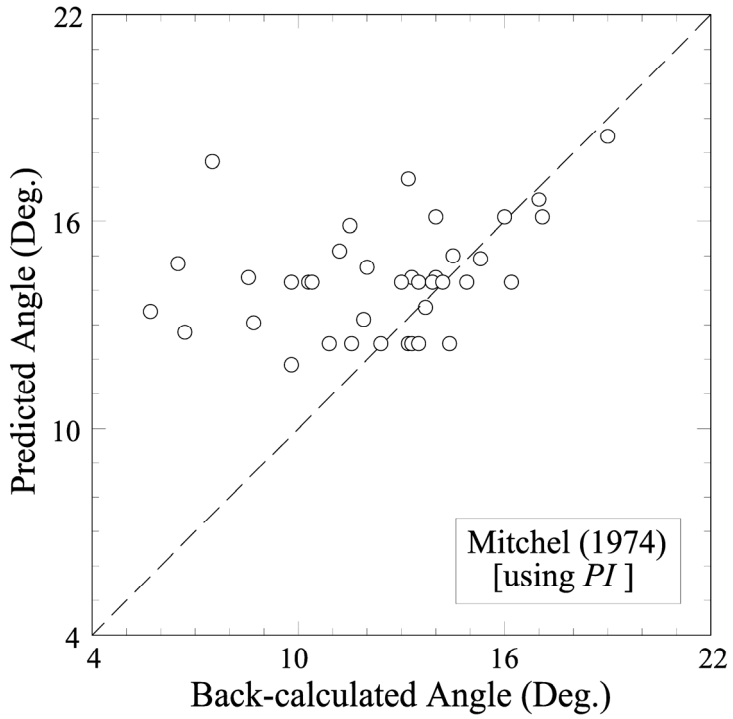

Figure. A-5-b. Comparison between the back-calculated secant residual friction angles and the residual angles predicted using the correlation presented by Mitchel (1976)

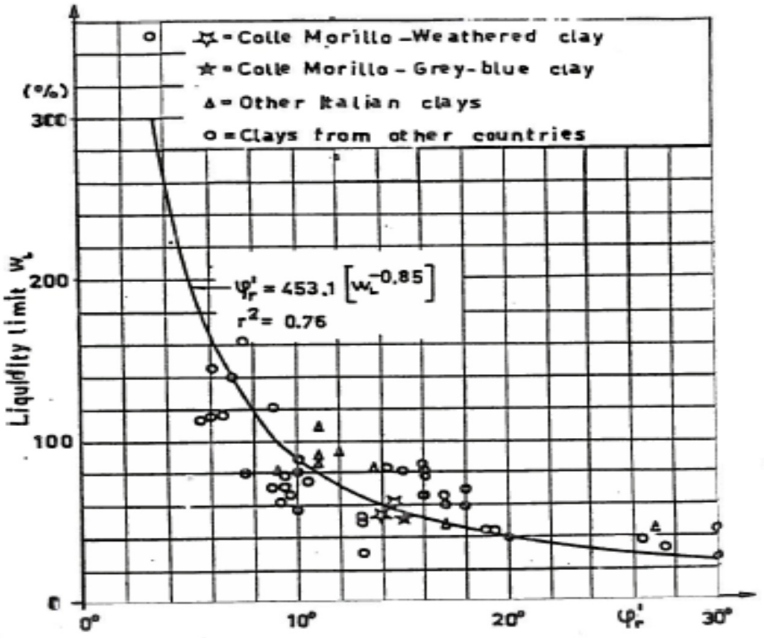

Figure. A-6-a. Drained residual shear strength empirical correlation (after Cancelli 1977)

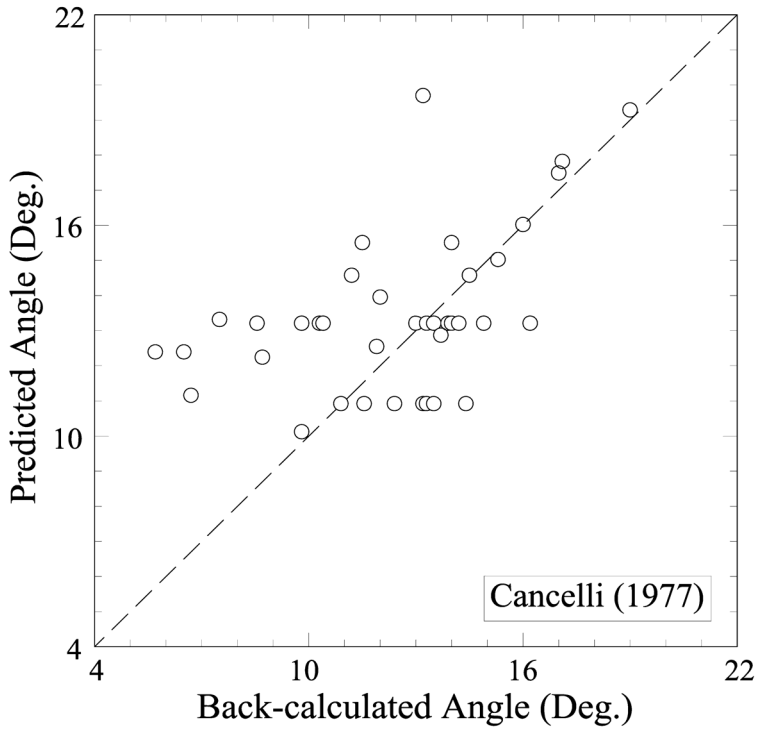

Figure. A-6-b. Comparison between the back-calculated secant residual friction angles and the residual angles predicted using the correlation presented by Cancelli (1976)

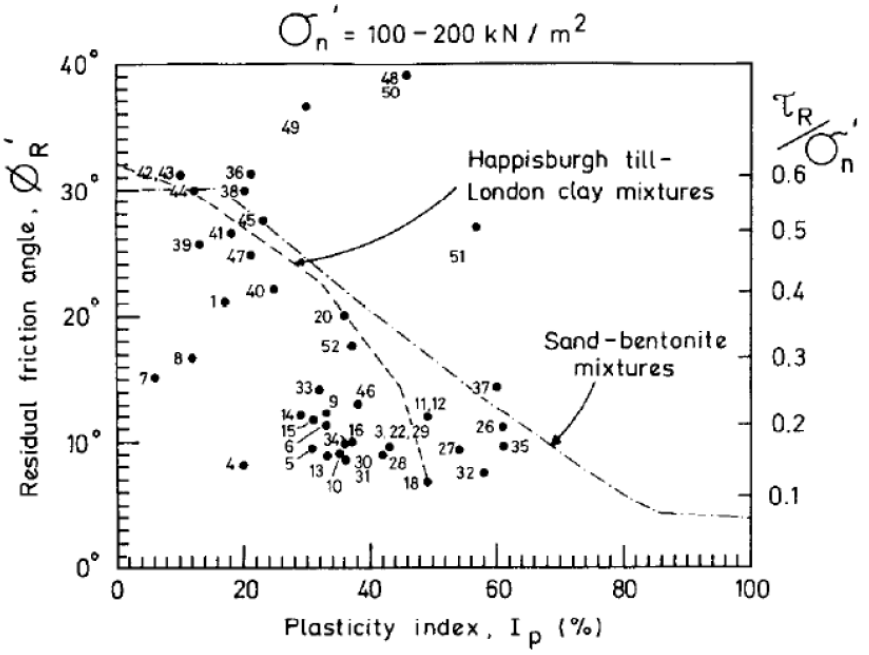

Figure. A-7-a. Drained residual shear strength empirical correlation (after Lupini et al. 1981)

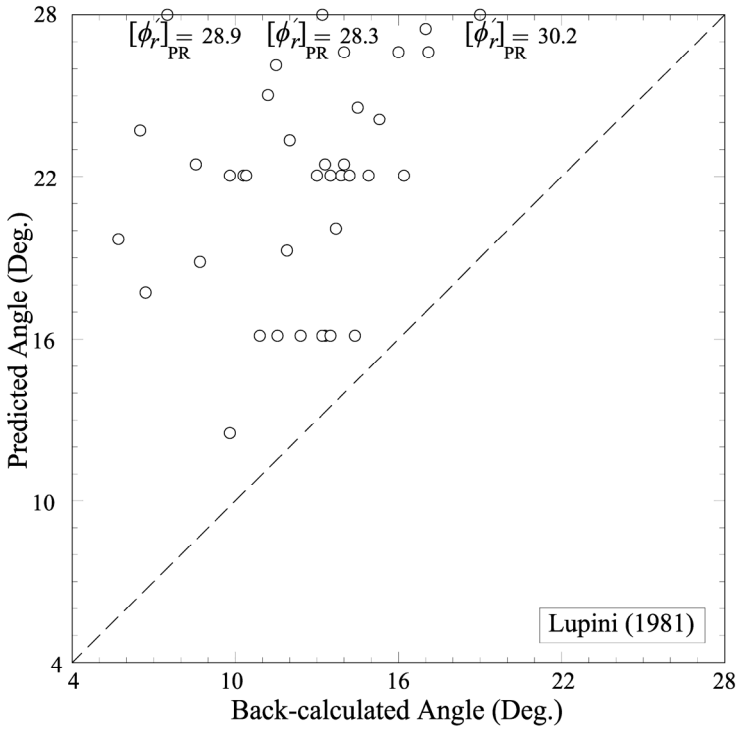

Figure. A-7-b. Comparison between the back-calculated secant residual friction angles and the residual angles predicted using the correlation presented by Lupini et al. (1981)

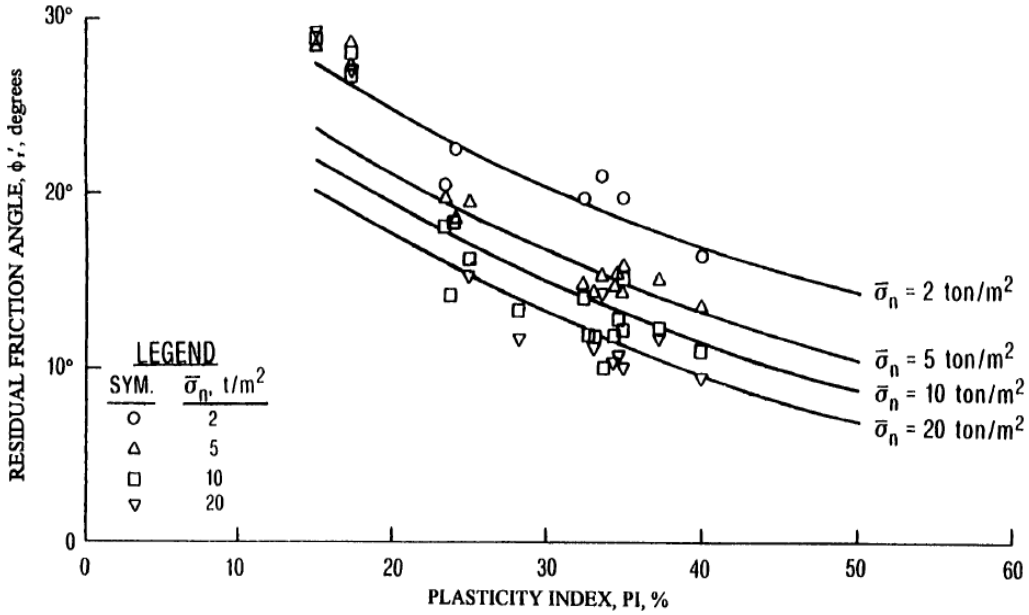

Figure. A-8-a. Drained residual shear strength empirical correlation (after Lambe 1985)

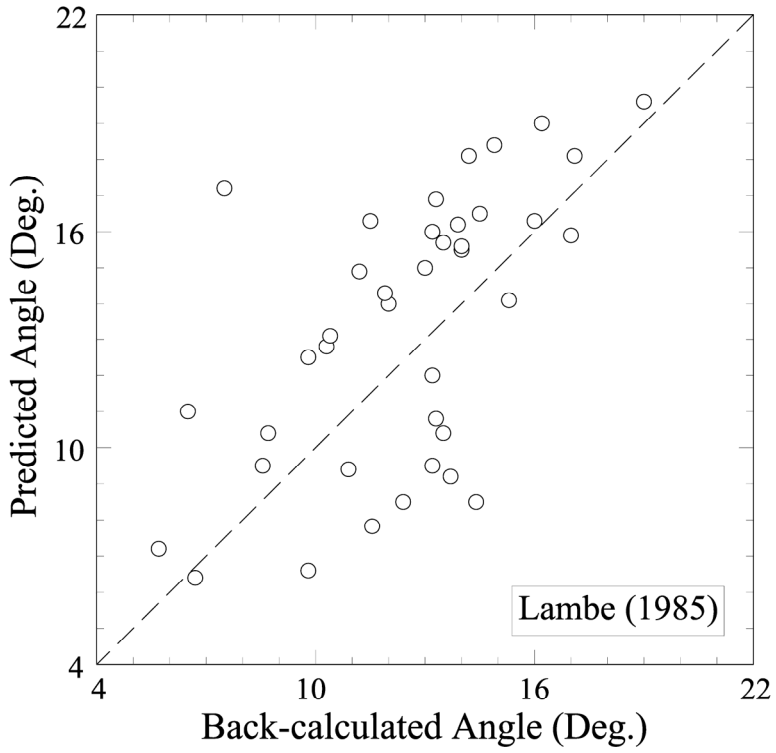

Figure. A-8-b. Comparison between the back-calculated secant residual friction angles and the residual angles predicted using the correlation presented by Lambe (1985)

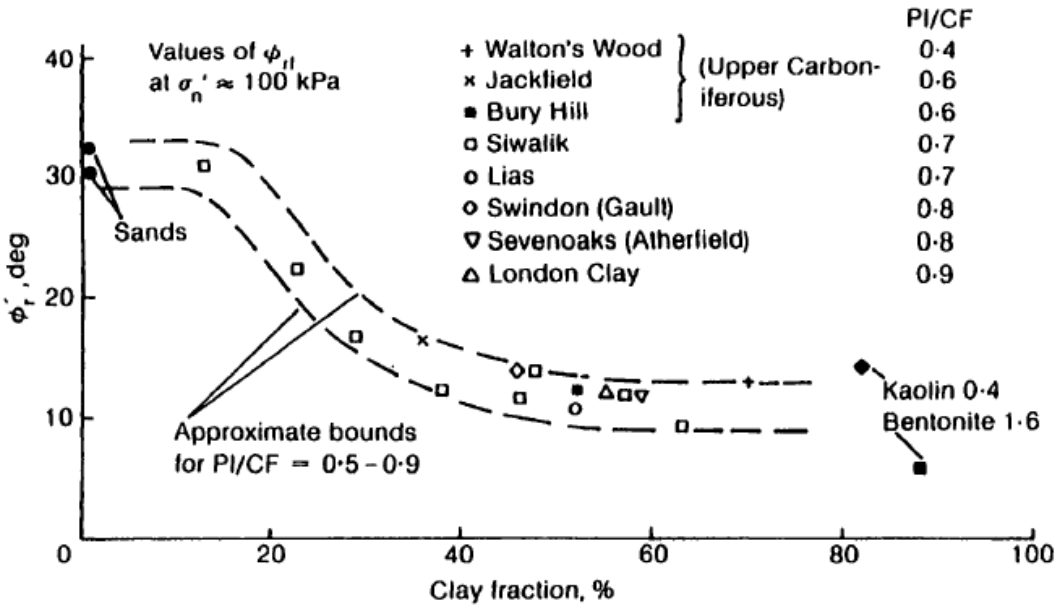

Figure. A-9-a. Drained residual shear strength empirical correlation (after Skempton 1985)

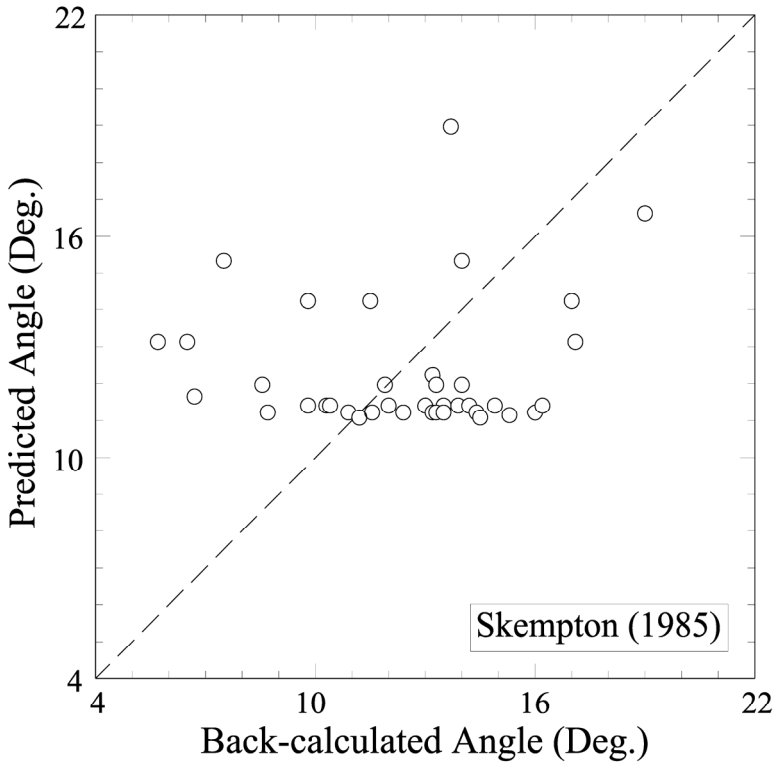

Figure. A-9-b. Comparison between the back-calculated secant residual friction angles and the residual angles predicted using the correlation presented by Skempton (1985)

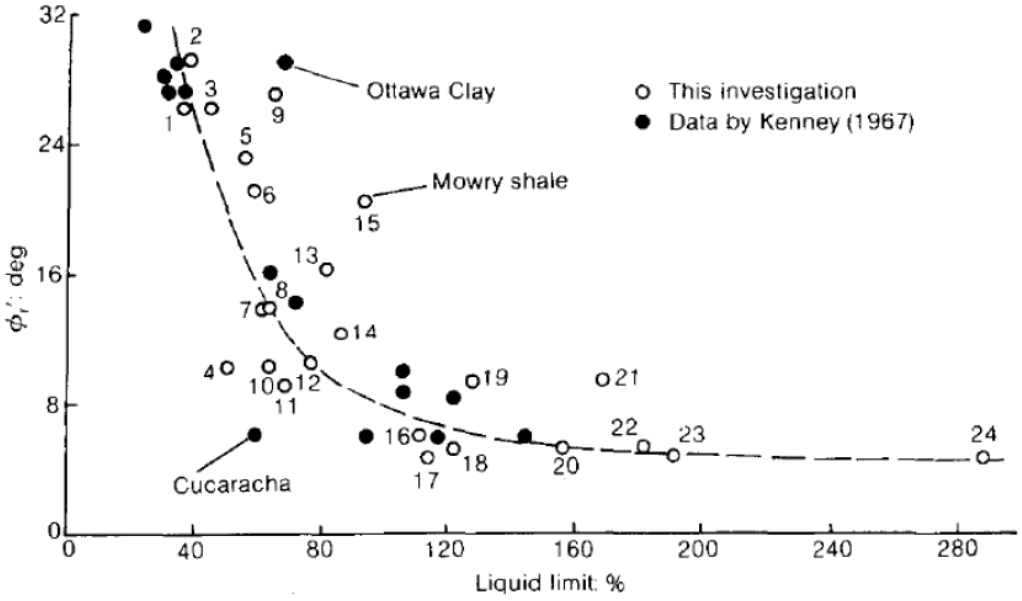

Figure. A-10-a. Drained residual shear strength empirical correlation (after Mesri and Cepeda-Diaz 1986)

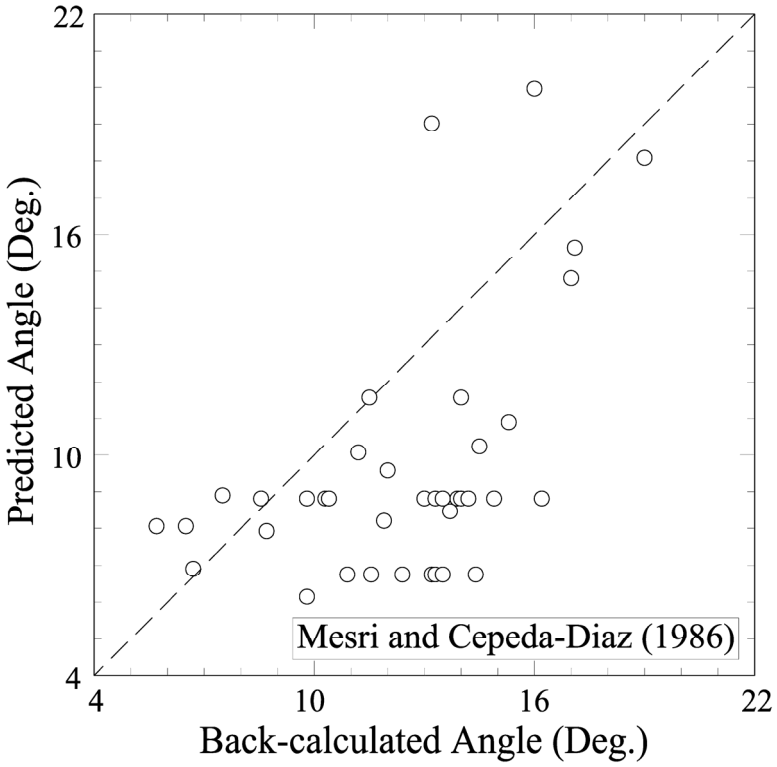

Figure. A-10-b. Comparison between the back-calculated secant residual friction angles and the residual angles predicted using the correlation presented by Mesri and Cepeda-Diaz (1986)

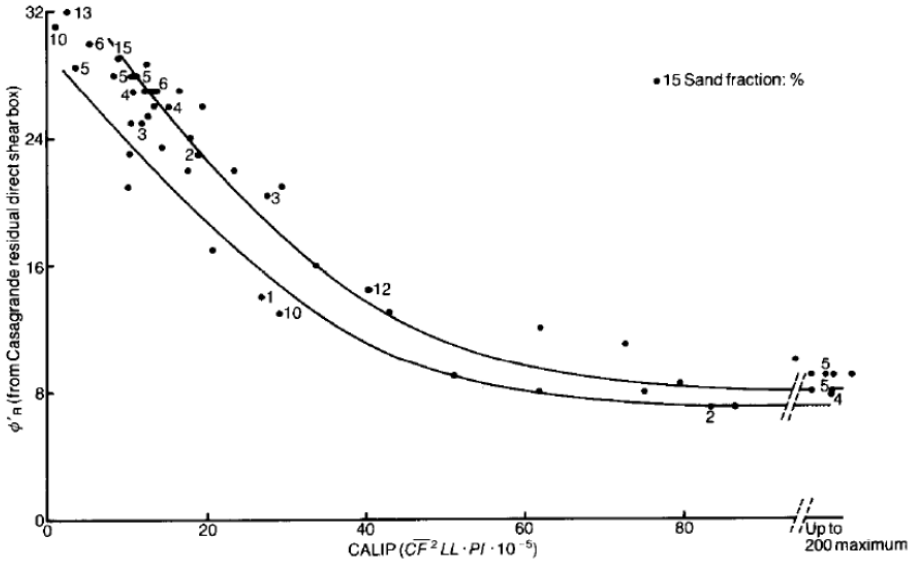

Figure. A-11-a. Drained residual shear strength empirical correlation (after Collotta et al. 1989)

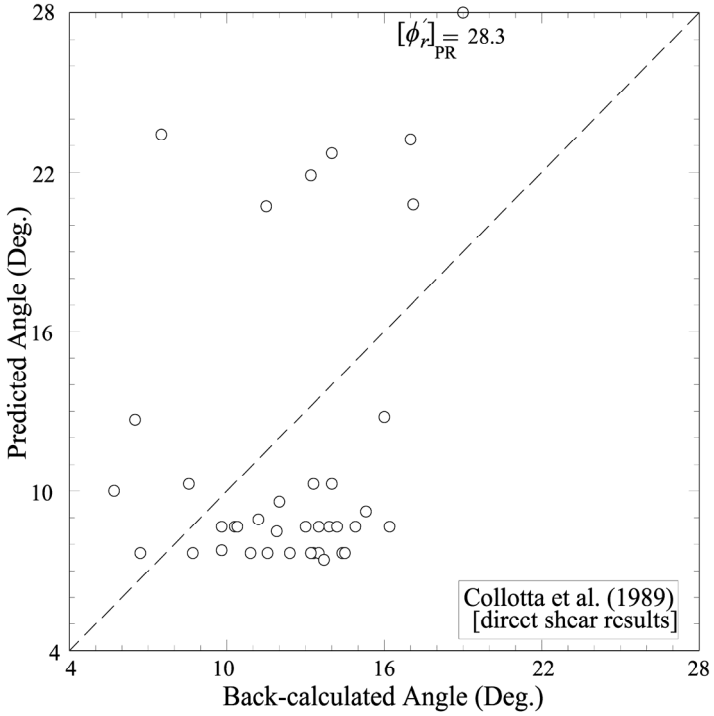

Figure. A-11-b. Comparison between the back-calculated secant residual friction angles and the residual angles predicted using the correlation presented by Collotta et al. 1989)

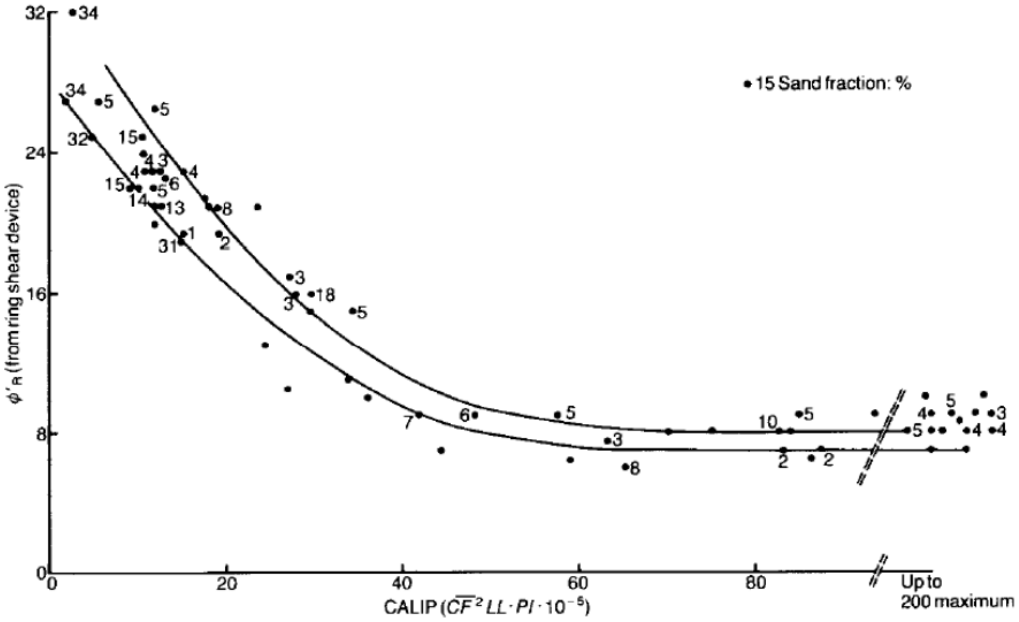

Figure. A-12-a. Drained residual shear strength empirical correlation (after Collotta et al. 1989)

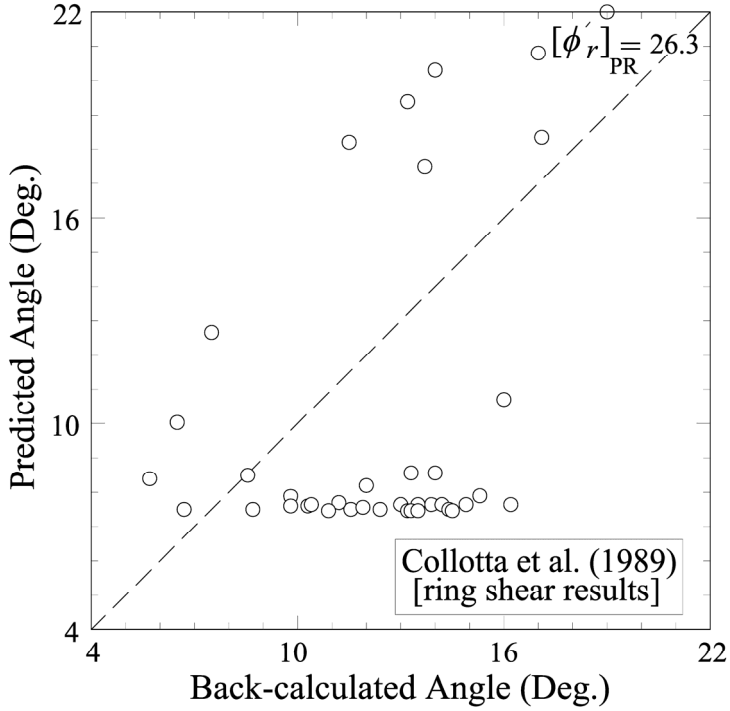

Figure. A-12-b. Comparison between the back-calculated secant residual friction angles and the residual angles predicted using the correlation presented by Collotta et al. 1989)

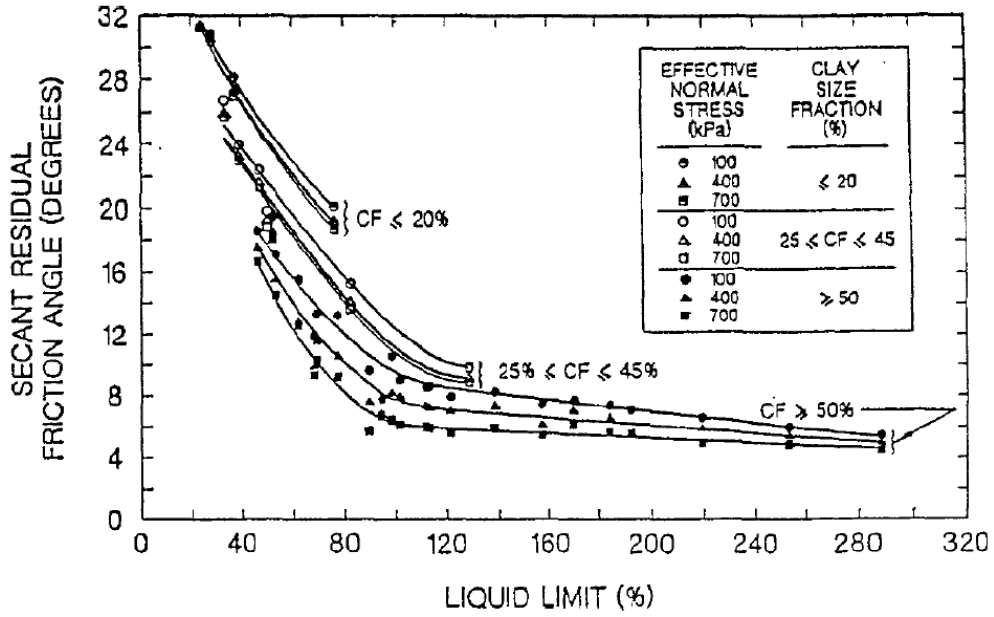

Figure. A-13-a. Drained residual shear strength empirical correlation (after Stark and Eid 1994)

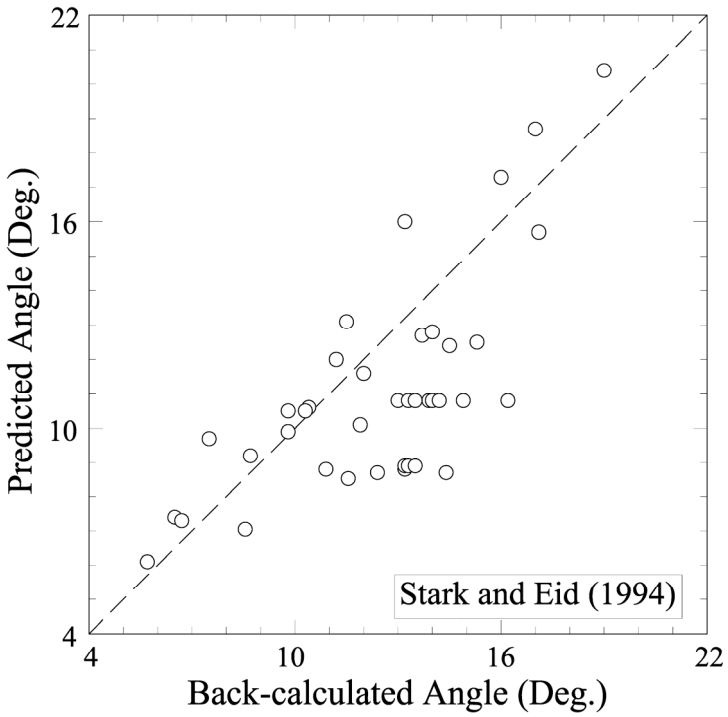

Figure. A-13-b. Comparison between the back-calculated secant residual friction angles and the residual angles predicted using the correlation presented by Stark and Eid (1994)

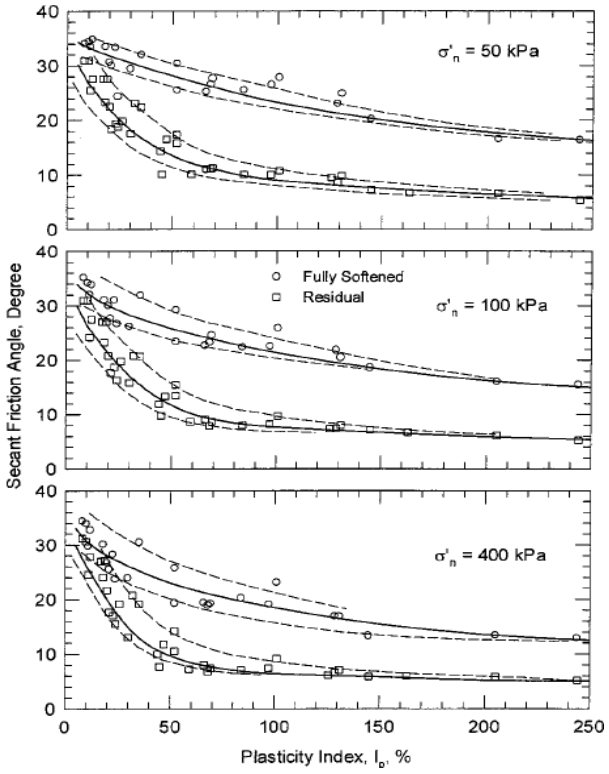

Figure. A-14-a. Drained residual shear strength empirical correlation (after Mesri and Shahien 2003)

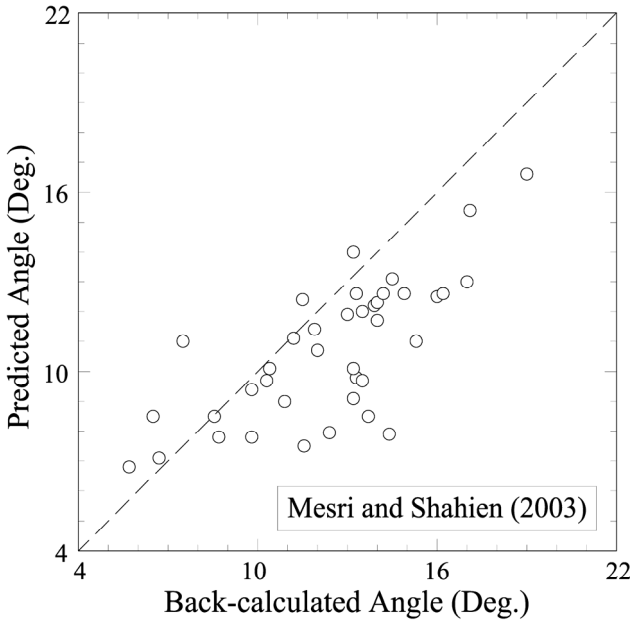

Figure. A-14-b. Comparison between the back-calculated secant residual friction angles and the residual angles predicted using the correlation presented by Mesri and Shahien (2003)

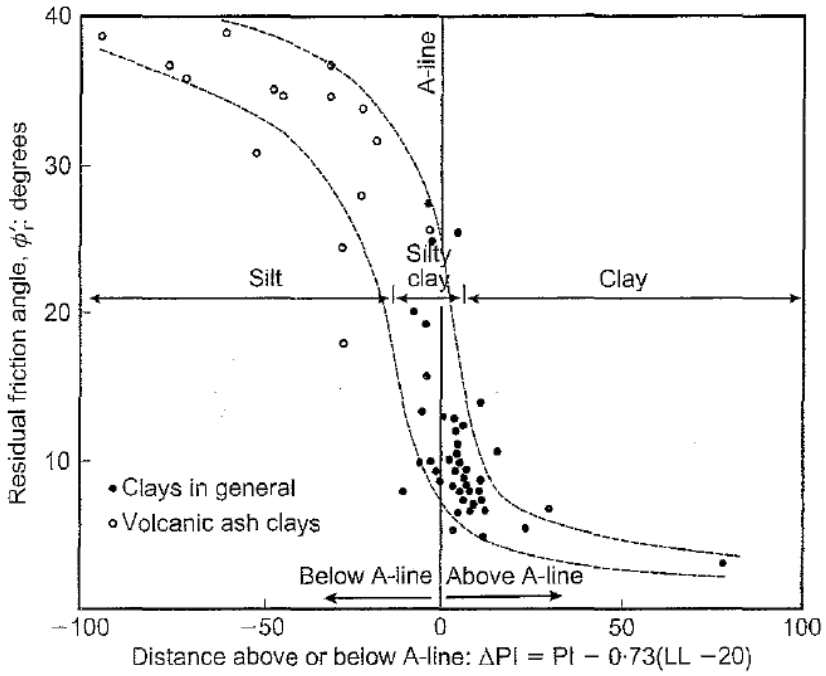

Figure. A-15-a. Drained residual shear strength empirical correlation (after Wesley 2003)

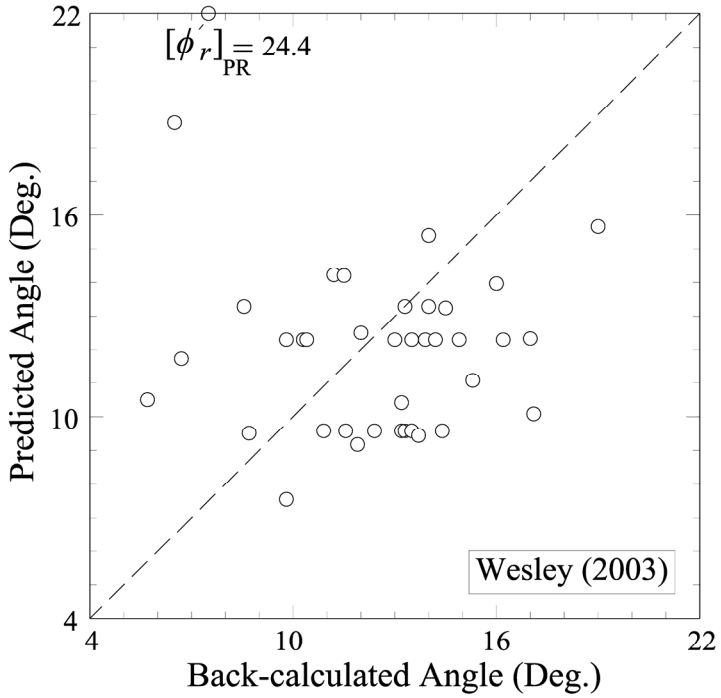

Figure. A-15-b. Comparison between the back-calculated secant residual friction angles and the residual angles predicted using the correlation presented by Wesley (2003)

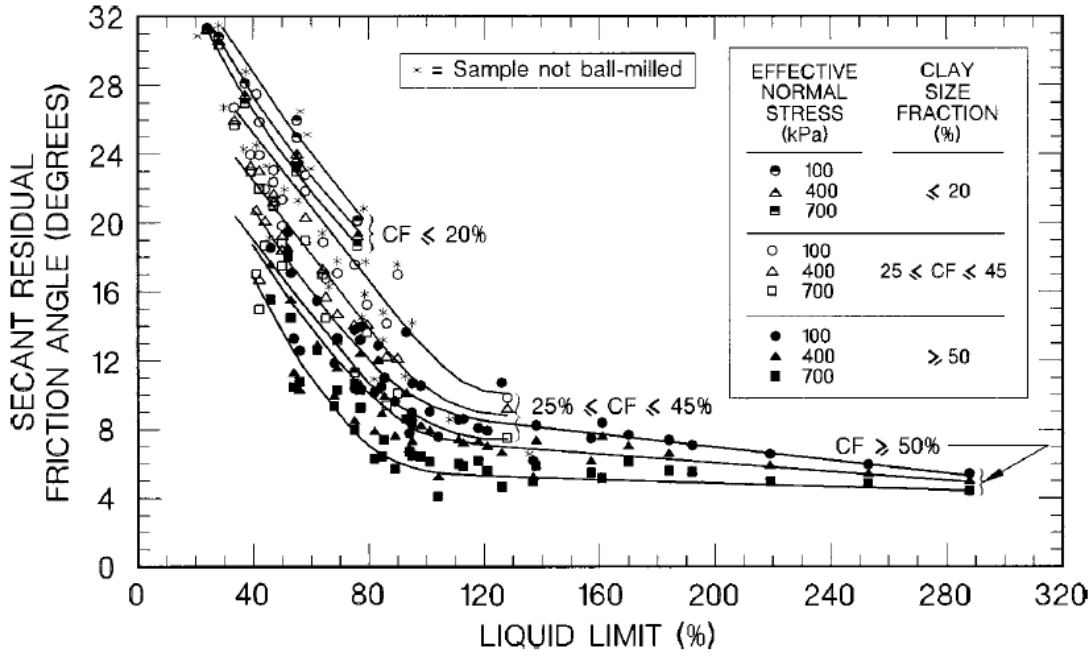

Figure. A-16-a. Drained residual shear strength empirical correlation (after Stark et al. 2005)

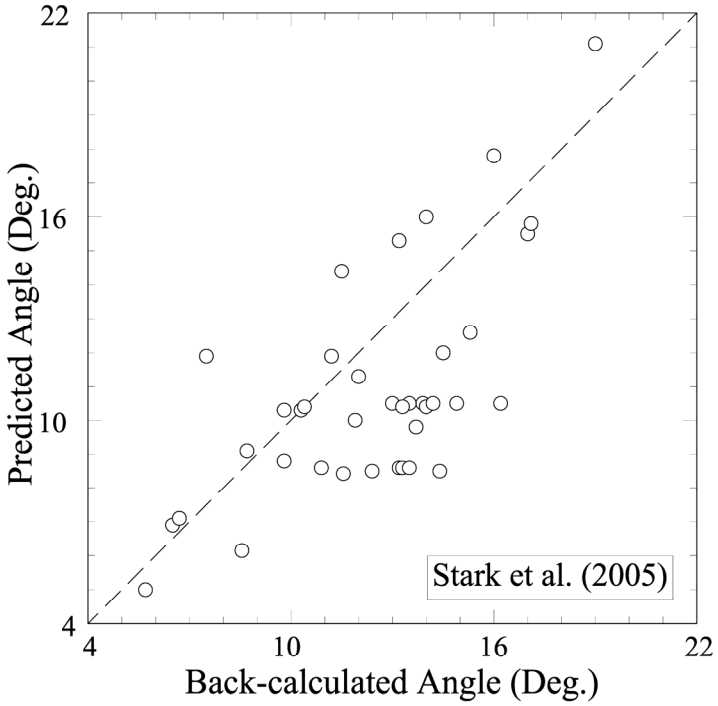

Figure. A-16-b. Comparison between the back-calculated secant residual friction angles and the residual angles predicted using the correlation presented by Stark et al. (2005)

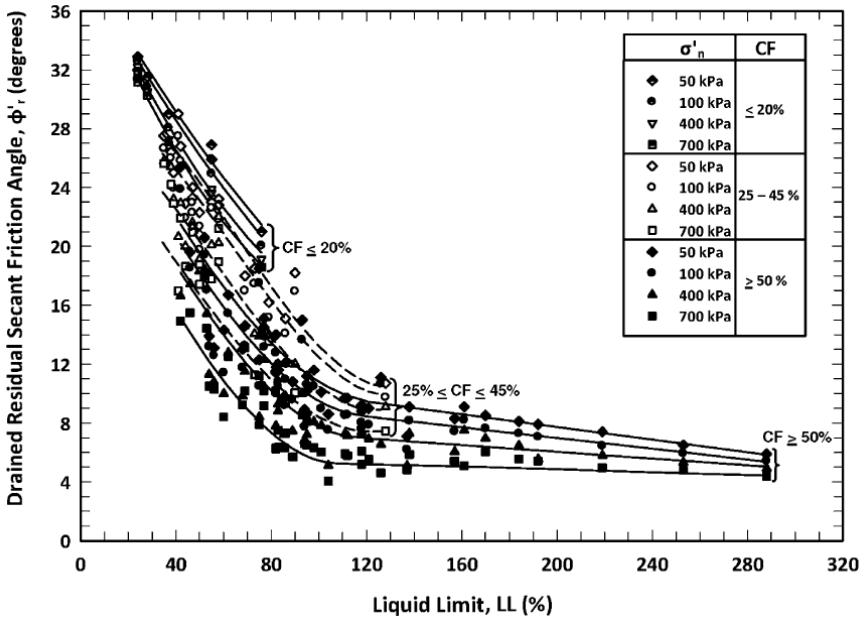

Figure. A-17-a. Drained residual shear strength empirical correlation (after Stark and Hussain 2013)

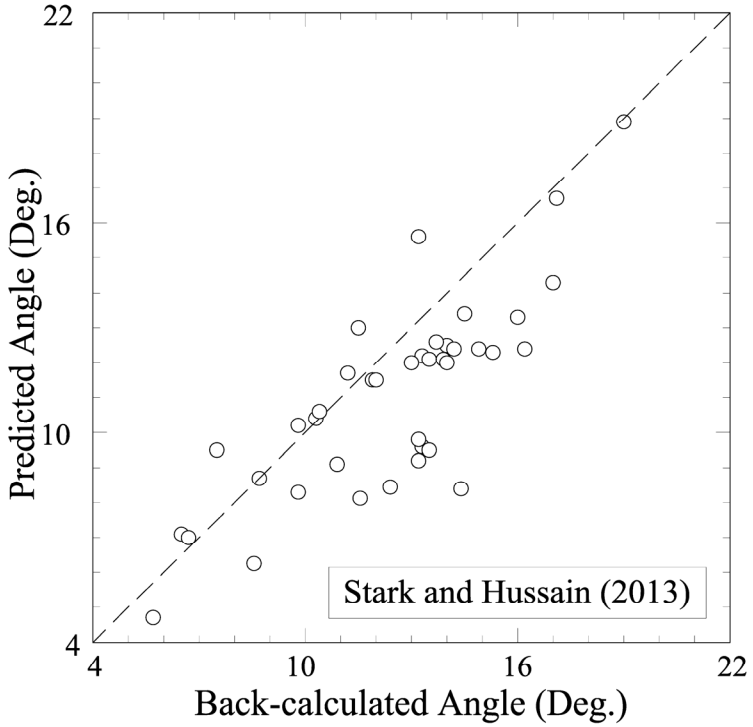

Figure. A-17-b. Comparison between the back-calculated secant residual friction angles and the residual angles predicted using the correlation presented by Stark and Hussain (2013)

Appendix B

Determination of The Value of m_r For an Existing Set of Data.

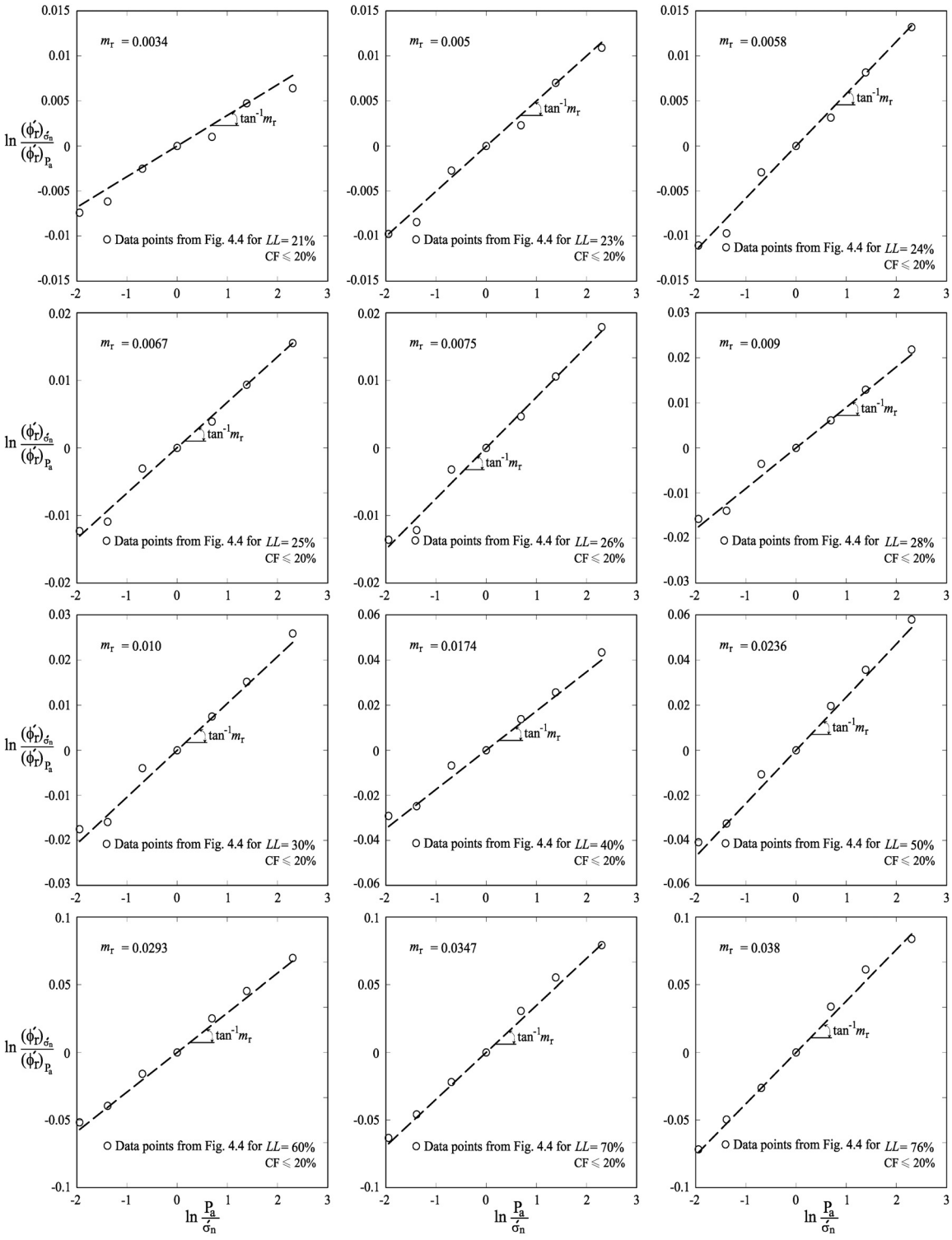

Figure. B-1-a. Determination of the value of m_r based on the liquid limit for soils with clay-size fraction less than or equal to 20%

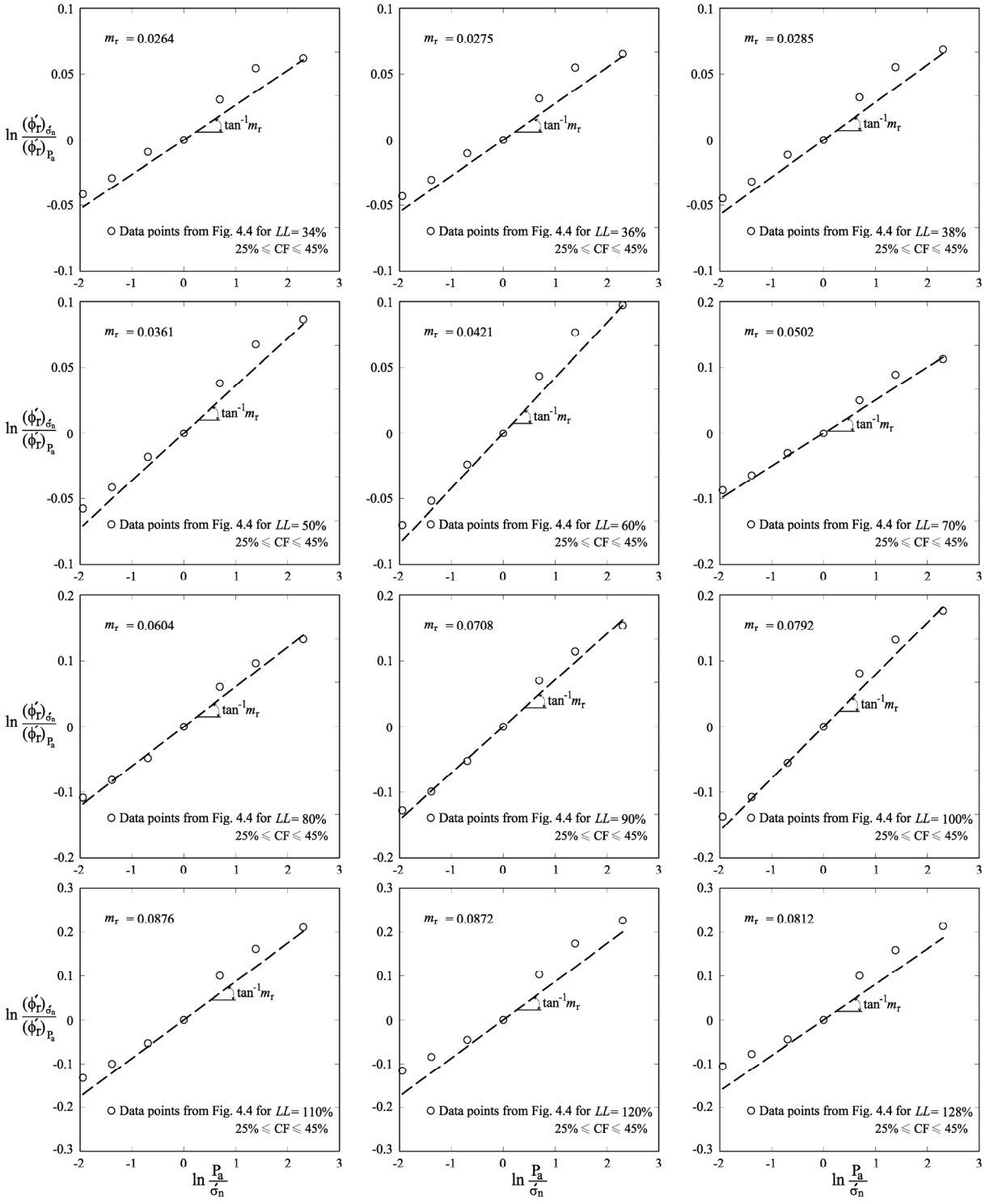

Figure. B-1-b. Determination of the value of m_r based on the liquid limit for soils with clay-size fraction between 25% and 45%.

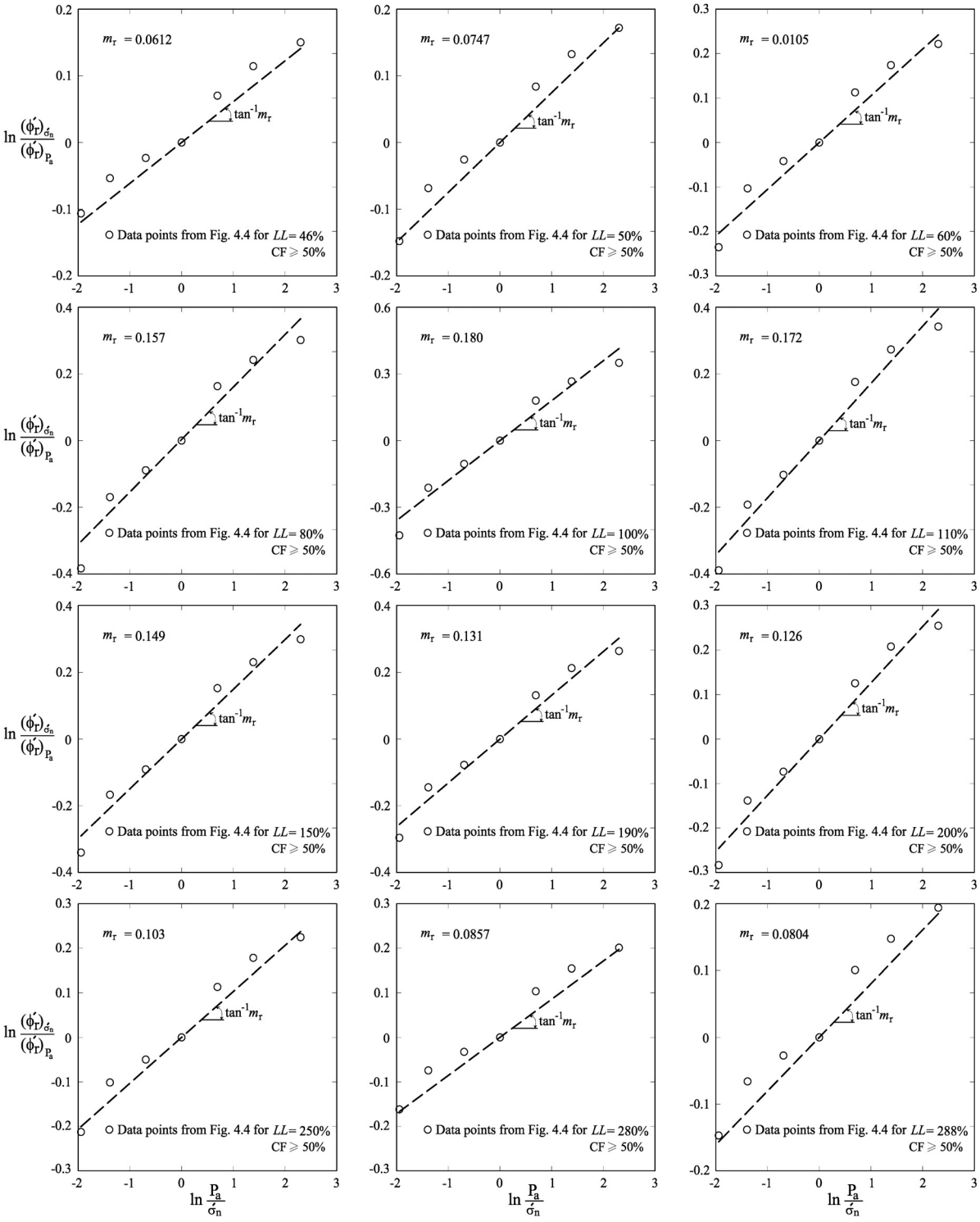

Figure. B-1-c. Determination of the value of m_r based on the liquid limit for soils with clay-size fraction greater than or equal to 50%.

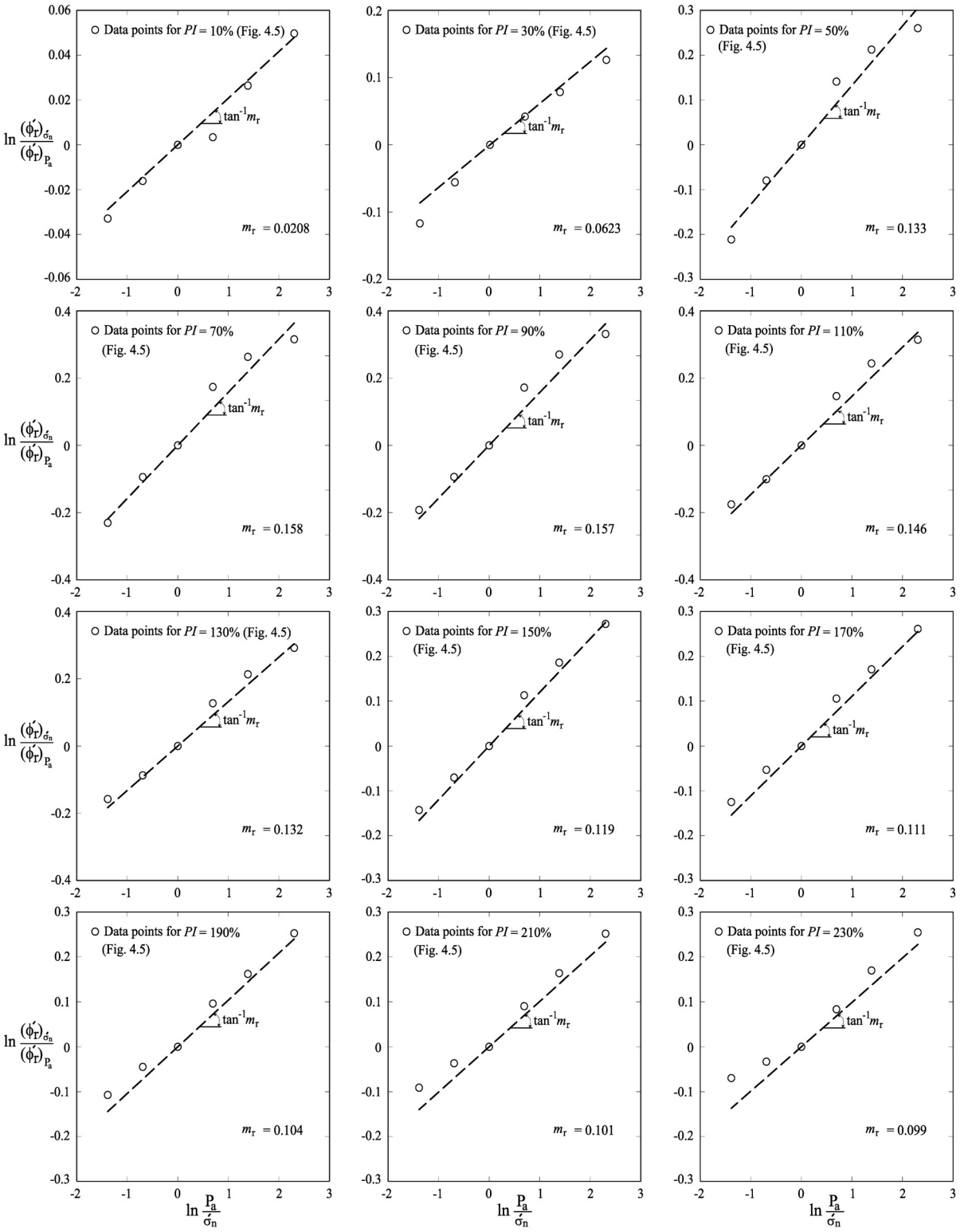

Figure. B-2. Determination of the value of m_r for soils based on the plasticity index.